
GQL-Based Bound-Preserving and Locally Divergence-Free Central Discontinuous Galerkin Schemes for Relativistic Magnetohydrodynamics*

Shengrong Ding^a, Kailiang Wu^{b,a,c,*}

^a*SUSTech International Center for Mathematics, Southern University of Science and Technology, Shenzhen 518055, China*

^b*Department of Mathematics, Southern University of Science and Technology, Shenzhen 518055, China*

^c*National Center for Applied Mathematics Shenzhen (NCAMS), Shenzhen 518055, China*

Abstract

This paper develops novel and robust central discontinuous Galerkin (CDG) schemes of arbitrarily high-order accuracy for special relativistic magnetohydrodynamics (RMHD) with a general equation of state (EOS). These schemes are provably bound-preserving (BP), meaning they consistently preserve the upper bound for subluminal fluid velocity and the positivity of density and pressure, while also (locally) maintaining the divergence-free (DF) constraint for the magnetic field. For 1D RMHD, the standard CDG method is exactly DF, and its BP property is proven under a condition achievable by the BP limiter. For 2D RMHD, we design provably BP and locally DF CDG schemes based on the suitable discretization of a modified RMHD system, which is the relativistic analogue of Godunov's symmetrizable form of the non-relativistic MHD system [S. K. Godunov, *Numerical Methods for Mechanics of Continuum Medium*, 1 (1972) 26–34]. A key novelty in our schemes is the meticulous discretization of additional source terms in the modified RMHD equations, so as to precisely counteract the influence of divergence errors on the BP property across overlapping meshes. Notably, we provide rigorous proofs of the BP property for our CDG schemes and first establish the theoretical connection between BP and discrete DF properties on overlapping meshes for RMHD. Owing to the absence of explicit expressions for primitive variables in terms of conserved variables, the constraints of physical bounds are strongly nonlinear, making the BP proofs highly nontrivial. We overcome these challenges through technical estimates within the geometric quasilinearization (GQL) framework [K. Wu & C.-W. Shu, *SIAM Review*, 65 (2023) 1031–1073], which equivalently converts the nonlinear constraints into linear ones. Furthermore, we introduce a new 2D cell average decomposition on overlapping meshes, which relaxes the theoretical BP CFL constraint and reduces the number of internal nodes, thereby enhancing the efficiency of the 2D BP CDG method. Finally, we implement the proposed CDG schemes for extensive RMHD problems with various EOSs, demonstrating their robustness and effectiveness in challenging scenarios like ultra-relativistic blasts and jets in strongly magnetized environments.

Keywords: Relativistic magnetohydrodynamics; Bound-preserving; Divergence-free; Central discontinuous Galerkin; Cell average decomposition; High-order accuracy; Hyperbolic conservation laws

*This work is partially supported by Shenzhen Science and Technology Program (Grant No. RCJC20221008092757098) and National Natural Science Foundation of China (Grant No. 12171227 and No. 92370108).

*Corresponding author.

e-mail: dingsr@sustech.edu.cn (Shengrong Ding), wukl@sustech.edu.cn (Kailiang Wu)

Affleck-Dine Dirac Leptogenesis

Neil D. Barrie^{1,*} and Chengcheng Han^{2,3,†}

¹*Sydney Consortium for Particle Physics and Cosmology,*

School of Physics, The University of Sydney, NSW 2006, Australia.

²*School of Physics, Sun Yat-Sen University, Guangzhou 510275, China*

³*Asia Pacific Center for Theoretical Physics, Pohang 37673, Korea*

We present a minimal framework that realises successful Dirac Leptogenesis through the Affleck-Dine mechanism. A single right-handed neutrino and a neutrinophilic Higgs doublet are introduced to the Standard Model, which couple via a Yukawa interaction. The inflationary setting is induced by a combination of the two Higgs doublets, with their global symmetry violating interactions leading to a net charge generation via the Affleck-Dine mechanism. This simple Standard Model extension exhibits a unique and connected set of phenomenological implications including the resultant baryon asymmetry, inflationary predictions, cosmological implications, relic right-handed neutrinos, and its low energy phenomenology, while also being able to be embedded in various neutrino mass generating mechanisms.

Introduction - The existence of the matter-antimatter asymmetry in our universe is an essential piece of evidence for physics beyond the Standard Model (SM). One intriguing solution is Leptogenesis, which illuminates this mystery through exploring the current unknowns of the neutrino sector [1–5]. In the standard thermal Leptogenesis scenario, an asymmetry is first generated in the lepton sector through the \mathcal{CP} violating decay of introduced heavy right-handed (RH) neutrinos, before this lepton number is redistributed into baryons by equilibrium sphaleron processes [6]. However, the mass scale of these RH neutrinos is typically required to be higher than 10^7 GeV to be consistent with current observations of the baryon asymmetry [7].¹ The high new physics scales associated with these models render terrestrial experimental tests infeasible for the foreseeable future.

The introduction of a RH neutrino to the SM opens up alternative possibilities for elucidating the origin of the observed baryon asymmetry. One intriguing prospect is Dirac-genesis [10, 11], a scenario in which at least one of the neutrinos exhibits a Dirac nature. In such models, successful Leptogenesis occurs despite the total $B - L$ of the universe being zero. This is achieved by an equal and opposite lepton number being sequestered from the SM sector into a density of decoupled RH neutrinos prior to the Electroweak Phase Transition (EWPT). Subsequently, the residual lepton asymmetry in the SM sector is transferred into a baryon asymmetry via equilibrium sphaleron processes as in usual Leptogenesis.

In this letter, we present a straightforward and simple framework in which to realise Dirac-genesis through the introduction of only one additional Higgs doublet and a single RH neutrino [12–37]. The additional Higgs doublet establishes connections with both the left-handed leptons and the right-handed neutrino through a Yukawa

coupling - while preserving \mathcal{CP} and L conservation in the model [38–45]. An asymmetry in the Higgs sector is generated through the Affleck-Dine mechanism [32, 34, 46], wherein the required initial displaced vacuum value is achieved by configuring the Higgs fields to be the inflaton that drives inflation [47–58].

The possibility of Affleck-Dine Dirac Leptogenesis has been suggested in previous literature [38]. However, a complete renormalizable model that satisfies the necessary conditions for a viable Affleck-Dine mechanism has not been presented. Typically, the Affleck-Dine mechanism is applied within the framework of supersymmetry, benefiting from the existence of a flat direction in the potential through which a large field vacuum can be achieved during inflation. The challenge in the non-supersymmetric Affleck-Dine mechanism lies in the absence of such flat directions for the new scalar field. One solution is to consider the Affleck-Dine field as the Nambu pseudo-goldstone boson of a spontaneously global $U(1)$ symmetry, ensuring the flatness of the potential through its inherent shift symmetry [59, 60]. Another approach involves considering the Affleck-Dine field as the inflaton triggering inflation [12–31], requiring a non-minimal coupling of the Affleck-Dine field to gravity. In this paper, we pursue this approach and present a simple extension of the SM in which the Affleck-Dine mechanism is realised [32, 34].

The Affleck-Dine Mechanism - The observed baryon asymmetry of the universe has been measured to be,

$$\eta_B = \frac{n_B}{s} \simeq 8.5 \times 10^{-11}, \quad (1)$$

where n_B and s are the baryon number and entropy densities of the universe, respectively [61]. The Affleck-Dine mechanism was proposed to explain this asymmetry through the generation of angular motion in the phase of a complex scalar field ϕ , which is charged under a global $U(1)$ symmetry [46]. The ϕ must acquire a large initial

¹ If the masses of two lightest RH neutrinos are nearly degenerate, the required mass scale can be reduced [8, 9].

A study of the Inspiral-Merger-Ringdown Consistency Test with gravitational-wave signals from compact binaries in eccentric orbits

Md Arif Shaikh,^{1,2,3,*} Sajad A. Bhat,^{4,5,†} and Shasvath J. Kapadia^{4,‡}

¹*Department of Physics, Vivekananda Satavarshiki Mahavidyalaya (affiliated to Vidyasagar University), Manikpara 721513, West Bengal, India*

²*Department of Physics and Astronomy, Seoul National University, Seoul 08826, Korea*

³*International Centre for Theoretical Sciences, Tata Institute of Fundamental Research, Bangalore 560089, India*

⁴*The Inter-University Centre for Astronomy and Astrophysics, Post Bag 4, Ganeshkhind, Pune 411007, India*

⁵*Chennai Mathematical Institute, Plot H1 SIPCOT IT Park, Siruseri 603103, India.*

(Dated: February 26, 2024)

The Inspiral Merger Ringdown Consistency Test (IMRCT) is one among a battery of tests of general relativity (GR) employed by the LIGO-Virgo-KAGRA (LVK) collaboration. It is used to search for deviations from GR in detected gravitational waves (GWs) from compact binary coalescences (CBCs) in a model-agnostic way. The test compares source parameter estimates extracted independently from the inspiral and post-inspiral portions of the CBC signals and, therefore, crucially relies on the accurate modeling of the waveform. Current implementations of the IMRCT routinely use quasicircular waveforms, under the assumption that the residual eccentricity of the binary when the emitted GWs enter the frequency band of the LVK detector network will be negligible. In this work, we perform a detailed study to investigate the typical magnitudes of this residual eccentricity that could potentially lead to spurious violations of the IMRCT. To that end, we conduct injection campaigns for a range of eccentricities and recover with both quasicircular and eccentric waveforms. We find that an eccentric GW signal from a GW150914-like system with $e_{\text{gw}} \gtrsim 0.04$ at an orbit averaged frequency $\langle f_{\text{ref}} \rangle = 25$ Hz breaks the IMRCT if recovered with quasicircular waveforms at $\gtrsim 68\%$ confidence. The violation becomes more severe ($\gtrsim 90\%$ confidence) for $e_{\text{gw}} = 0.055$ at $\langle f_{\text{ref}} \rangle = 25$ Hz. On the other hand, when eccentric waveforms are used, the IMRCT remains intact for all eccentricities considered. We also briefly investigate the effect of the magnitude and orientation (aligned/antialigned) of the component spins of the binary on the extent of the spurious violations of the IMRCT. Our work, therefore, demonstrates the need for accurate eccentric waveform models in the context of tests of GR.

I. INTRODUCTION

The LIGO-Virgo [1, 2] network of ground-based interferometric gravitational-wave (GW) detectors has detected ~ 90 compact binary coalescence (CBC) events in its first three observing runs (O1, O2, O3) [3]. The majority of these are binary black hole (BBH) mergers, although binary neutron star (BNS) [4, 5] and neutron star-black hole (NSBH) coalescences [6] have also been observed.

The detected GW signals, especially those pertaining to BBH mergers, come from the last few orbits of the inspiral, as well as the merger and ringdown phases (see, e.g., [7]). These GWs are well-suited to probe general relativity (GR) in the strong-field regime, unlike most tests of GR that use electromagnetic waves, which typically probe the weak field regime¹.

The LIGO-Virgo-KAGRA (LVK) collaboration [1, 2, 10] has conducted a suite of tests of GR across O1, O2, and O3 [11]. This includes² a model-agnostic residuals test, which subtracts out the best-matched GR-modeled CBC waveform from the data containing the GW signal, and checks if the

statistical properties of the residual are consistent with noise [12–14]; a test that probes the inspiral evolution of the CBC by searching for deviations in Post-Newtonian (PN) parameters of the GW signal [15–22]; an inspiral-merger-ringdown consistency test (IMRCT) that compares and assesses the consistency between the low and high-frequency portions of the CBC signals [23, 24]; and propagation tests of GWs that compare their speed with respect to the speed of light [25] as well as any modulations in the waveform due to finite-graviton-mass-driven velocity dispersion [26].

In this work, we restrict our attention to the IMRCT. The IMRCT compares the two-dimensional joint posterior on the final mass and spin of the merged binary estimated independently from the inspiral (low-frequency) and post-inspiral (high-frequency) portions of the waveform [23, 24]. A sufficiently large deviation from GR should result in the difference distribution evaluated from these 2D posteriors to deviate from the origin (zero). However, it is conceivable that waveforms that do not accurately capture the physics of the CBC could lead to biased posteriors. We propose to study the resulting systematics in the IMRCT. In particular, we investigate how the neglect of eccentricity in the waveform models could cause spurious violations of this test.

It is well-known that, as GWs carry away energy and angular momentum of a CBC, it reduces the binary orbit's eccentricity [27, 28]. The prevalent expectation is that by the time GWs from the CBC enter the frequency band of the LVK network, any initial eccentricity that the binary may have had at the time of formation would have been reduced to a negligibly small value. Indeed, current constraints on the rate of eccentric merg-

* arifshaikh.astro@gmail.com

† sajad.bhat@iucaa.in; The first two authors contributed equally

‡ shasvath.kapadia@iucaa.in

¹ A notable exception to this are the results of the Event Horizon Telescope (EHT) [8], which imaged the shadow of the supermassive black hole at the center of the M31 galaxy and enabled EM-based strong-field tests of GR [9].

² but is not limited to

Spin Doctors: How to diagnose a hierarchical merger origin

ETHAN PAYNE,^{1,2} KYLE KREMER,^{3,*} AND MICHAEL ZEVIN^{4,5}

¹*Department of Physics, California Institute of Technology, Pasadena, CA 91125, USA*

²*LIGO Laboratory, California Institute of Technology, Pasadena, CA 91125, USA*

³*TAPIR, California Institute of Technology, Pasadena, CA 91125, USA*

⁴*Adler Planetarium, 1300 South DuSable Lake Shore Drive, Chicago, IL, 60605, USA*

⁵*Center for Interdisciplinary Exploration and Research in Astrophysics (CIERA), Northwestern University, Evanston, IL, 60201, USA*

ABSTRACT

Gravitational-wave observations provide the unique opportunity of studying black hole formation channels and histories — but only if we can identify their origin. One such formation mechanism is the dynamical synthesis of black hole binaries in dense stellar systems. Given the expected isotropic distribution of component spins of binary black hole in gas-free dynamical environments, the presence of anti-aligned or in-plane spins with respect to the orbital angular momentum is considered a tell-tale sign of a merger’s dynamical origin. Even in the scenario where birth spins of black holes are low, hierarchical mergers attain large component spins due to the orbital angular momentum of the prior merger. However, measuring such spin configurations is difficult. Here, we quantify the efficacy of the spin parameters encoding aligned-spin (χ_{eff}) and in-plane spin (χ_p) at classifying such hierarchical systems. Using Monte Carlo cluster simulations to generate a realistic distribution of hierarchical merger parameters from globular clusters, we can infer mergers’ χ_{eff} and χ_p . The cluster populations are simulated using Advanced LIGO–Virgo sensitivity during the detector network’s third observing period and projections for design sensitivity. Using a “likelihood-ratio”-based statistic, we find that $\sim 2\%$ of the recovered population by the current gravitational-wave detector network has a statistically significant χ_p measurement, whereas no χ_{eff} measurement was capable of confidently determining a system to be anti-aligned with the orbital angular momentum at current detector sensitivities. These results indicate that measuring spin-precession through χ_p is a more detectable signature of a hierarchical mergers and dynamical formation than anti-aligned spins.

Keywords: Stellar mass black hole (1611) — Gravitational waves (678) — Star clusters (1567) — Bayesian statistics (1900)

1. INTRODUCTION

Following the first handful of observations of binary black hole (BBH) mergers through their gravitational wave (GW) emission (Abbott et al. 2016, 2019, 2021), many studies predicted that the dominant formation channel of BBHs would be determined after $\mathcal{O}(10-100)$ observations (Zevin et al. 2017; Stevenson et al. 2015; Stevenson et al. 2017; Fishbach & Holz 2017; Vitale et al. 2017; Arca Sedda & Benacquista 2019; Safarzadeh 2020). However, despite the LIGO–Virgo–KAGRA Collaboration (LVK) detector network accumulating nearly 100 confident BBH observations (Abbott et al. 2023a),

prominent formation pathways for BBH mergers remains an open question in GW astrophysics. The incongruity between prior expectation and reality can be attributed to a number of factors:

1. The diversity in the gravitational-wave events detected thus far does not show a strong preference for any one formation channel, with observations spanning a broad range of masses and mass ratios (e.g. Abbott et al. 2019, 2021, 2023a; Olsen et al. 2022; Mehta et al. 2023).
2. Additional potential formation channels have been proposed in addition to the canonical “dynamical-versus-isolated” distinction (see e.g. Mandel & Farmer 2022, for a review), as well as subchannels to these canonical birth environments, which

epayne@caltech.edu

* NASA Hubble Fellow

The imitation game reloaded: effective shadows of dynamically robust spinning Proca stars

Ivo Sengo^{*1}, Pedro V.P. Cunha^{†1}, Carlos A. R. Herdeiro^{‡1}, and Eugen Radu^{§1}

¹Departamento de Matemática da Universidade de Aveiro and Centre for Research and Development in Mathematics and Applications (CIDMA), Campus de Santiago, 3810-183 Aveiro, Portugal

February 2024

Abstract

We analyse the lensing images by dynamically robust rotating (mini-)Proca stars surrounded by thin accretion disks. Due to their peculiar geodesic structure we show that these images exhibit striking similarities with the ones of BHs, for appropriately chosen disk intensity profile, when imposing a GRMHD-motivated emission cut off. Additionally, and unlike the non-rotating case, these similarities prevail even when considering equatorial observations. This example illustrates how a horizonless compact object without light rings, with a plausible formation mechanism and dynamically robust, could mimic detailed features of black hole imagiology.

arXiv:2402.14919v1 [gr-qc] 22 Feb 2024

*sengo@ua.pt

†pvcunha@ua.pt

‡herdeiro@ua.pt

§eugen.radu@ua.pt

Consistent particle physics in metric-affine gravity from extended projective symmetry

Will Barker^{1,2,*} and Sebastian Zell^{3,†}

¹*Astrophysics Group, Cavendish Laboratory, JJ Thomson Avenue, Cambridge CB3 0HE, UK*

²*Kavli Institute for Cosmology, Madingley Road, Cambridge CB3 0HA, UK*

³*Centre for Cosmology, Particle Physics and Phenomenology – CP3, Université catholique de Louvain, B-1348 Louvain-la-Neuve, Belgium*

It is well-known that the Einstein-Hilbert action exhibits a projective invariance in metric-affine gravity, generated by a single vector (just like diffeomorphisms). However, this symmetry offers no protection against formulating inconsistent models, e.g., with ghost and strong coupling problems. In this letter, we observe that non-minimal kinetic terms of Dirac spinors point to a new *extended projective* (EP) symmetry generated by a pair of vectors. We prove that the most general EP-invariant theory (at most quadratic in field strengths) is naturally free from all pathologies. Its spectrum only features the massless graviton and a single additional scalar field arising from the square of the Holst curvature. The scalar potential is suitable for inflation and our model moreover contains effective 4-Fermi interactions capable of producing fermionic dark matter. Finally, we point out an alternative double-vector symmetry that similarly leads to a healthy theory with a propagating vector field.

Fundamental forces from symmetries — Among the greatest achievements of fundamental science is a description of our world in terms of as few as four basic forces. Three of them – the strong, weak, and electromagnetic interactions – are at the heart of the Standard Model (SM) of particle physics and are crucial for understanding phenomena on microscopic scales. The fourth force, gravity, is carried in by the theory of General Relativity (GR) and shapes the macroscopic structure of our Universe. All four forces are fundamentally defined in terms of symmetries. On the particle physics side, the essence of the SM is captured by the internal gauge groups SU(3), SU(2), and U(1) corresponding to the strong, weak, and electromagnetic interactions, respectively. In gravity, invariance under external spacetime diffeomorphisms allows local observers to choose their own coordinate systems.

Constraints on possible theories — One can understand the key role of symmetries as constraints on possible theories. Since only invariant terms (operators) are admissible in the action, the theory space is severely reduced. Famously, the symmetries of the SM forbid the existence of explicit mass terms. This led to the seminal theoretical prediction of the Brout-Englert-Higgs mechanism [1, 2], which, decades later, was confirmed with the discovery of the Higgs boson [3, 4]. Compared to the SM, the situation in GR is more ambiguous. This is because diffeomorphism invariance does not uniquely determine the fundamental geometry of spacetime: the presence of the three geometric properties curvature, torsion and non-metricity define various equivalent formulations of GR [5–29]; see [30–33] for overviews. Might this ambiguity indicate that more symmetries of gravity are yet to be discovered?

Metric-affine gravity — Without ad hoc assumptions about the geometry of spacetime, the field content of GR comprises a metric $g_{\mu\nu}$ and an independent affine connection $\Gamma^\mu_{\nu\rho}$. The latter can be field-reparameterised into torsion and non-

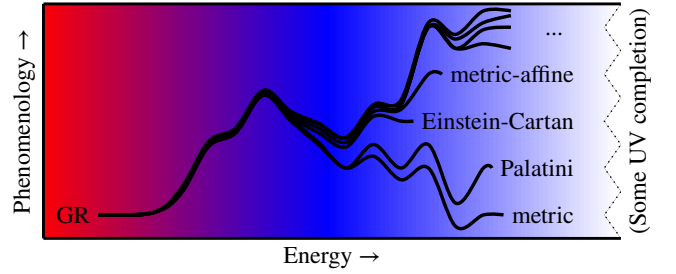


FIG. 1. As a low-energy effective theory, Einstein’s GR has many equivalent geometrical formulations that will only be distinguishable by experimental bounds on their high-energy phenomenology, in particular observational constraints from the very early Universe.

metricity tensors (see conventions in Appendix A)

$$T^\alpha_{\mu\nu} \equiv 2\Gamma^\alpha_{[\mu\nu]}, \quad Q_{\lambda\mu\nu} \equiv \nabla_\lambda g_{\mu\nu}, \quad (1)$$

where $\nabla_\lambda g_{\mu\nu} \equiv \partial_\lambda g_{\mu\nu} - 2\Gamma^\alpha_{\lambda(\mu} g_{\nu)\alpha}$. The curvature is

$$R^\rho_{\sigma\mu\nu} \equiv 2 \left(\partial_{[\mu} \Gamma^\rho_{|\nu]\sigma} + \Gamma^\rho_{[\mu|\alpha} \Gamma^\alpha_{|\nu]\sigma} \right), \quad (2)$$

and Eqs. (1) and (2) determine the effects of parallel transport. Allowing for $R^\rho_{\sigma\mu\nu}$, $T^\alpha_{\mu\nu}$ and $Q_{\alpha\mu\nu}$ leads to the *metric-affine* formulation [34–38], while the a priori restriction $Q_{\alpha\mu\nu} \equiv 0$ yields *Einstein-Cartan* gravity [9, 11–16]. Excluding both $T^\alpha_{\mu\nu} \equiv Q_{\alpha\mu\nu} \equiv 0$ results in the most-commonly used *metric* formulation of GR [5], in which the connection loses its independence from the metric and is fixed by the Christoffel formula $\Gamma^\mu_{\nu\rho} \equiv \overset{\circ}{\Gamma}^\mu_{\nu\rho} \equiv g^{\mu\lambda} (\partial_{(\nu} g_{\rho)\lambda} - \frac{1}{2} \partial_\lambda g_{\nu\rho})$. There are many more options [5–29], and even interpolations [34, 39–51] between them: full metric affine geometry is completely unrestricted, and will be our focus. For the simplest action only consisting of the Ricci scalar $R \equiv R^{\mu\nu}_{\mu\nu}$, the different formulations of GR are fully equivalent in pure gravity as $T^\alpha_{\mu\nu} \approx Q_{\alpha\mu\nu} \approx 0$ dynamically on the shell. As illustrated in Fig. 1, when SM matter fields are included, formulations start to deviate at high energies, e.g., due to effective

* wb263@cam.ac.uk

† sebastian.zell@uclouvain.be

The Karzas-Latter-Seiler Model of a High-Altitude Electromagnetic Pulse: A New Numerical Code for an Old Model

Gavin S. Hartnett*
RAND Corporation

1776 Main St, Santa Monica, CA 90401

A high-altitude nuclear blast can produce an electromagnetic pulse (EMP) capable of disrupting electronics on Earth. The basic phenomenology of the initial (E1) phase of the EMP was initially worked out in the 1960s by Longmire, Karzas, and Latter, and although more accurate and sophisticated EMP models have since been devised, the Karzas-Latter model is particularly simple and amenable to implementation as a numerical code. This paper accompanies the release of a new software implementation of an approximation of the Karzas-Latter model due to Seiler. This is, as far as we are aware, the only such publicly available numerical EMP code. After reviewing the physics and assumptions of the model, the numerical results for EMP simulations under a range of conditions are presented. It is shown how the results from multiple line of sight integrations of the field equations can be assembled to form a map of the EMP intensity across a broad geographic region. The model predictions are at least qualitatively correct and in general agreement with other simulation results, including the characteristic “smile” pattern in the spatial variation of the EMP intensity.

I. INTRODUCTION

There is value to the public in developing open-source, transparent, and easily accessible models of the many Nuclear Weapons Effects (NWEs), such as the blast wave, radiation, fall-out, and the electromagnetic pulse (EMP). These models may be used to inform public discourse concerning the risk of nuclear war and can help in civil defense planning. For these purposes, it is not necessary to have particularly accurate models; even rough, order-of-magnitude estimates can be useful in educating the public and scenario planning. Fortunately, there are many simple and unclassified mathematical models of NWEs that could be developed into software tools.

The present work accompanies the public release of a Python implementation of the Karzas-Latter [1, 2] model for high-altitude electromagnetic pulse (HEMP).¹ This model treats the early E1 phase of the phenomenon and uses a series of rather crude approximations and simplifying assumptions. Nonetheless, we are not aware of any other public implementations of this model and believe that there is value in releasing it, provided its many limitations are well documented and communicated. In this work, we review the Karzas-Latter model of HEMP, as well as an extension of the model provided by Seiler [3] that greatly simplifies the calculation. We also discuss how this model, which was initially designed to compute the electric field strength along a line of sight from the burst to a target, may be extended to produce the characteristic “smile diagrams” showing the magnitude of the EMP across a large region of the Earth’s surface (Figure 1).

This paper is organized as follows. In Section II the Karzas-Latter model is briefly reviewed. Section III presents the results from the numerical code, and Section IV concludes with a discussion of the limitations of this model. Additional details are relegated to two appendices; Appendix A reviews the Seiler approximation to the Karzas-Latter model, and Appendix B contains details on the coordinate systems used as well as how the geomagnetic field has been modeled.

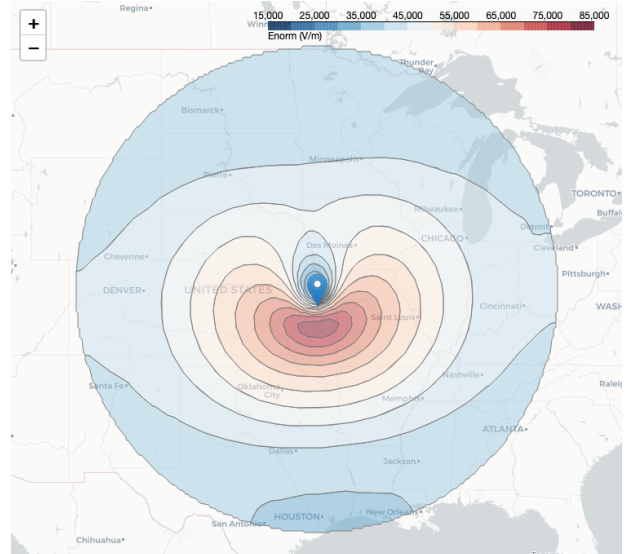


Figure 1. Contour plot of the maximum (over time) EMP intensity for a 5 kiloton nuclear detonation 100 km directly overhead Topeka, Kansas, USA.

* hartnett@rand.org

¹ The code is available here: <https://github.com/gshartnett/karzas-latter-seiler>.

A Model for the Redshift-Space Galaxy 4-Point Correlation Function

William Ortolá Leonard,^{1,3} Zachary Slepian^{2,3} and Jiamin Hou^{2,4}

¹Department of Physics, University of Florida,
2001 Museum Rd., Gainesville, FL 32611, USA

²Department of Astronomy, University of Florida,
211 Bryant Space Science Center, Gainesville, FL 32611, USA

³Lawrence Berkeley National Laboratory,
1 Cyclotron Road, Berkeley, CA 94720, USA

⁴Max-Planck-Institut für Extraterrestrische Physik,
Postfach 1312, Giessenbachstrasse 1, 85748 Garching bei München, Germany

E-mail: wortola@ufl.edu, zslepian@ufl.edu, jiamin.hou@ufl.edu

Abstract. The field of cosmology is entering an epoch of unparalleled wealth of observational data thanks to galaxy surveys such as DESI, Euclid, and Roman. Therefore, it is essential to have a firm theoretical basis that allows the effective analysis of the data. With this purpose, we compute the nonlinear, gravitationally-induced connected galaxy 4-point correlation function (4PCF) at the tree level in Standard Perturbation Theory (SPT), including redshift-space distortions (RSD). We begin from the trispectrum and take its inverse Fourier transform into configuration space, exploiting the isotropic basis functions of [76]. We ultimately reduce the configuration-space expression to low-dimensional radial integrals of the power spectrum. This model will enable the use of the BAO feature in the connected 4PCF to sharpen our constraints on the expansion history of the Universe. It will also offer an additional avenue for determining the galaxy bias parameters, and thus tighten our cosmological constraints by breaking degeneracies. Survey geometry can be corrected in the 4PCF, and many systematics are localized, which is an advantage over data analysis with the trispectrum. Finally, this work is a first step in using the parity-even 4PCF to calibrate out any possible systematics in the parity-odd 4PCF; comparing our model to the measurement will offer a consistency test that can serve as a “canary in the coal mine” for systematics in the odd sector.

The α -element enrichment of gas in distant galaxies

Anna Velichko^{1,2}, Annalisa De Cia^{3,1}, Christina Konstantopoulou¹, Cédric Ledoux⁴, Jens-Kristian Krogager⁵, and Tanita Ramburuth-Hurt¹

¹ Department of Astronomy, University of Geneva, Chemin Pegasi 51, 1290 Versoix, Switzerland e-mail: anna.velichko@unige.ch

² Institute of Astronomy, Kharkiv National University, Sumska 35, Kharkiv, 61022, Ukraine

³ European Southern Observatory, Karl-Schwarzschild Str. 2, 85748 Garching bei München, Germany

⁴ European Southern Observatory, Alonso de Córdova 3107, Casilla 19001, Vitacura, Santiago, Chile

⁵ Centre de Recherche Astrophysique de Lyon, Univ. Claude Bernard Lyon 1, 9 Av. Charles André, 69230 St Genis Laval, France

Received date / Accepted date

ABSTRACT

Context. The chemical evolution of distant galaxies cannot be assessed from observations of individual stars, in contrast to the case of nearby galaxies. On the other hand, the study of the interstellar medium (ISM) offers an alternative way to reveal important properties of the chemical evolution of distant galaxies. The chemical enrichment of the ISM is produced by all the previous generations of stars and it is possible to precisely determine the metal abundances in the neutral ISM in galaxies. The chemical abundance patterns in the neutral ISM are determined by the gas metallicity, presence of dust (the depletion of metals into dust grains), and possible deviations due to specific nucleosynthesis, for example, α -element enhancements.

Aims. We aim to derive the metallicities, dust depletion, and α -element enhancements in the neutral ISM of gas-rich mostly-metal-poor distant galaxies (Damped Lyman- α absorbers, DLAs). Furthermore, we aim to constrain the distribution of α -element enhancements with metallicity in these galaxies.

Methods. We collected a literature sample of column density measurements of O, Mg, Si, S, Ti, Cr, Fe, Ni, Zn, P, and Mn in the neutral ISM of DLAs at redshifts of $0.60 < z < 3.40$. We used this sample to define a golden sample of DLAs with constrained observations of Ti and at least one other α -element. By studying the abundance patterns, we determined the amount of dust depletion, solely based on the observed relative abundances of the α -elements. We then used the abundances of Fe-peak elements to determine the overall metallicity of each system, after correcting for dust depletion. In addition, we studied the deviations from the basic (linear) abundance patterns. We divided our sample into two groups of galaxies based on the widths of their absorption lines (Δv_{90} above or below 100 km s^{-1}), which may be considered as a proxy for their dynamical mass. We characterised the distribution of the α -element enhancements as a function of metallicity for the galaxy population as a whole, by fitting a piecewise function (plateau, decline, plateau) to the data.

Results. We observed systematic deviations from the basic abundance patterns for O, Mg, Si, S, Ti, and Mn, which we interpreted as α -element enhancements and a Mn underabundance. The distribution of the α -element enhancements with metallicity is different in the high- Δv_{90} and low- Δv_{90} groups of galaxies. We constrained the metallicity of the α -element knee for the high- Δv_{90} and low- Δv_{90} groups of galaxies to be -1.02 ± 0.15 dex and -1.84 ± 0.11 dex, respectively. The average α -element enhancement at the high-plateau is $[\alpha/\text{Fe}] = 0.38 \pm 0.07$ dex. On the other hand, Mn shows an underabundance in all DLAs in the golden sample of -0.36 ± 0.07 dex, on average.

Conclusions. We have constrained, for the first time, the distribution of the α -element enhancement with metallicity in the neutral ISM in distant galaxies. Less massive galaxies show an α -element knee at lower metallicities than more massive galaxies. This can be explained by a lower star formation rate in less massive galaxies. If this collective behaviour can be interpreted in the same way as it is for individual systems, this would suggest that more massive and metal-rich systems evolve to higher metallicities before the contribution of SN-Ia to $[\alpha/\text{Fe}]$ levels out that of core-collapse SNe. This finding may plausibly be supported by different SFRs in galaxies of different masses. Overall, our results offer important clues to the study of chemical evolution in distant galaxies.

Key words. ISM: abundances – dust, extinction – quasars: absorption lines – galaxies: evolution

1. Introduction

The outcome of the evolutionary history of galaxies is recorded in the interstellar abundances of chemical elements. Observations of the interstellar medium (ISM) in galaxies of various types, differing in terms of mass, size, metallicity, and their respective evolutionary stages, may provide a key to understanding the processes taking place in galaxies (Maiolino & Mannucci 2019).

In the Milky Way (MW) and nearby galaxies, one of the ways to trace their evolutionary process is from observations of the detailed abundances of chemical elements in individual stars

(McWilliam 1997; Tolstoy et al. 2009). Although it is impossible to obtain information about individual stars in distant galaxies, the chemical properties of their interstellar medium (ISM) can be analysed in great detail. The chemical abundance patterns in the ISM is the result of enrichment produced by all the previous generations of stars. These patterns make up a snapshot of the evolutionary history of the galaxy.

One of the techniques to determine element abundances in the gas of faint high-redshift galaxies is based on the detection of its imprint on the spectrum of a background sources which may be a quasi-stellar object (QSO) or gamma-ray burst (GRB) after-

Length and Velocity Scales in Protoplanetary Disk Turbulence.

DEBANJAN SENGUPTA,^{1,2} JEFFREY N. CUZZI,³ ORKAN M. UMURHAN,^{4,3,5,6} AND WLADIMIR LYRA¹

¹*Department of Astronomy, New Mexico State University, PO Box 30001, MSC 4500, Las Cruces, NM 88003-8001, USA;
(debanjan@nmsu.edu)*

²*NASA Postdoctoral Program Fellow, Ames Research Center, NASA; Mail Stop 245-3, Moffett Field, CA 94035, USA*

³*NASA Ames Research Center; Mail Stop 245-3, Moffett Field, CA 94035, USA*

⁴*SETI Institute, 389 Bernardo Way, Mountain View, CA 94043, USA*

⁵*Cornell Center for Astrophysics and Planetary Sciences, Cornell University, Ithaca, NY 14853, USA*

⁶*Department of Earth and Planetary Science, University of California Berkeley, Berkeley, CA 94720, USA*

(Received February 26, 2024)

ABSTRACT

In the theory of protoplanetary disk turbulence, a widely adopted *ansatz*, or assumption, is that the turnover frequency of the largest turbulent eddy, Ω_L , is the local Keplerian frequency Ω_K . In terms of the standard dimensionless Shakura-Sunyaev α parameter that quantifies turbulent viscosity or diffusivity, this assumption leads to characteristic length and velocity scales given respectively by $\sqrt{\alpha}H$ and $\sqrt{\alpha}c$, in which H and c are the local gas scale height and sound speed. However, this assumption is not applicable in cases when turbulence is forced numerically or driven by some natural processes such as Vertical Shear Instability. Here we explore the more general case where $\Omega_L \geq \Omega_K$ and show that under these conditions, the characteristic length and velocity scales are respectively $\sqrt{\alpha/R'}H$ and $\sqrt{\alpha R'}c$, where $R' \equiv \Omega_L/\Omega_K$ is twice the Rossby number. It follows that $\alpha = \tilde{\alpha}/R'$, where $\sqrt{\tilde{\alpha}c}$ is the root-mean-square average of the turbulent velocities. Properly allowing for this effect naturally explains the reduced particle scale heights produced in shearing box simulations of particles in forced turbulence, and may help with interpreting recent edge-on disk observations; more general implications for observations are also presented. For $R' > 1$ the effective particle Stokes numbers are increased, which has implications for particle collision dynamics and growth, as well as for planetesimal formation.

1. INTRODUCTION

Protoplanetary disks are increasingly regarded as being moderately turbulent, under a handful of magnetohydrodynamic (Balbus & Hawley 1991; Turner et al. 2014; Lesur et al. 2022) or purely hydrodynamic instabilities (Nelson et al. 2013; Lyra 2014; Marcus et al. 2013). In many applications, such as global models of disk evolution under turbulent viscosity (Estrada et al. 2016; Sengupta et al. 2022), it is impractical to use more than a simple parameterization of the viscous and diffusive effects of turbulence, and by far the most popular one is the so-called “ α -model” (Shakura & Sunyaev 1973; Shakura et al. 1978). In this closure model, the spatial and temporal evolution of turbulent protoplanetary gas and particle disks is determined by the large-scale effective viscosity and diffusivity of the gas, and the particles in it. For many purposes, it is adequate (and indeed necessary given our limited understanding) to simplify the complex effects of real turbulence into a

scalar viscosity ν and diffusivity D . The basic scaling or mixing length approximation for turbulent diffusivity and viscosity is $(D, \nu) \equiv [L][V_L]$, where L and V_L are respectively the characteristic length and velocity scales of the turbulence. In this case, L can be identified with the energy injection scale or the energy containing large spatial scale and V_L is the velocity at that scale. Shakura & Sunyaev (1973) introduced the widely-used mixing length-like closure model $\nu \equiv \alpha cH$ to incorporate our ignorance about the turbulence into the single parameter α , where c is the gas sound speed and H is the gas vertical scale height. In this classic paper¹, it was suggested briefly that $L \sim H$ and thus $V_L \sim \alpha c$, indeed with α often taken to be of order unity (Cameron 1978; Lin & Bodenheimer 1982; Weidenschilling 1984;

¹ We note that the first description and application of mixing length theory to disks may be found in Prendergast & Burbidge (1968), but an explicit mathematical prescription was not given.

The dynamics of self-gravity wakes in the Mimas 5:3 bending wave: modifying the linear theory

DANIEL D. SEGA,¹ GLEN STEWART,¹ JOSHUA E. COLWELL,² GIRISH M. DUVVURI,^{1,3} RICHARD JEROUSEK,²
AND LARRY ESPOSITO¹

¹Laboratory for Atmospheric and Space Physics, University of Colorado at Boulder, Boulder, CO, 80309, USA

²Department of Physics, University of Central Florida, Orlando, FL, 32816, USA

³Center for Astrophysics and Space Astronomy, University of Colorado at Boulder, Boulder, CO, 80309, USA

(Dated: February 26, 2024)

ABSTRACT

The satellite Mimas launches a bending wave—a warping of the rings that propagates radially through self-gravity—at the 5:3 inner vertical resonance with Saturn’s rings. We present a modification of the linear bending wave theory (Shu et al. 1983) which includes the effects of satellite self-gravity wakes on the particles in the wave. We show that, when treated as rigid, these wakes generate an extra layer of particles whose number density is proportional to the magnitude of the slope of the warped ring. Using a ray-tracing code we compare our predictions with those of Shu et al. (1983) and with 60 stellar occultations observed by the Cassini Ultraviolet Imaging Spectrograph (UVIS) and find that the extra layer of particles of our perturbed bending wave model has a considerable explanatory power for the UVIS dataset. Our best model explains the most discrepant and surprising features of the Mimas 5:3 bending wave; the enhancement of the signal for the cases of occultations with high ring opening angle and the bigger-than-expected viscosity, $\nu = 576 \text{ cm}^2/\text{s}$, which is more than double the viscosity computed from density waves (Tiscareno et al. 2007). This shows that self-gravity wakes can be effective at transporting angular momentum in a vertically perturbed disk. Relative to neighboring density waves (Tiscareno et al. 2007), we find a lower-than-expected value for the surface mass density, $\sigma = 36.7 \text{ g/cm}^2$, which suggests that the enhanced viscous interactions may be transporting material into the surrounding regions.

Keywords: Saturn, Planetary Rings, Celestial Mechanics, Stellar Occultation, Saturn Satellites

1. INTRODUCTION

A bending wave (BW) is a warping of a disk (a circular and thin mass plane) caused by perturbations normal to the disk that propagates due to self-gravity. Warped disks are ubiquitous in astrophysics and can be found around young stars (Epstein-Martin et al. 2022), black holes (Thomas et al. 2021), and around planets (Shu et al. 1983), for which we have a vast amount of observations available. While warps are only

Abundant sub-micron grains revealed in newly discovered extreme debris discs

Attila Moór,^{1,2*} Péter Ábrahám,^{1,2,3,4} Kate Y. L. Su,⁵ Thomas Henning,⁶ Sebastian Marino,⁷ Lei Chen,^{1,2} Ágnes Kóspál,^{1,2,6,3} Nicole Pawellek,^{4,1,2} József Varga^{1,2} and Krisztián Vida^{1,2}

¹Konkoly Observatory, Research Centre for Astronomy and Earth Sciences, HUN-REN,

Konkoly-Thege Miklós út 15-17, H-1121 Budapest, Hungary

²CSFK, MTA Centre of Excellence, Budapest, Konkoly Thege Miklós út 15-17., H-1121, Hungary

³ELTE Eötvös Loránd University, Institute of Physics, Pázmány Péter sétány 1/A, H-1117 Budapest, Hungary

⁴Department of Astrophysics, University of Vienna, Türkenschanzstraße 17, 1180, Vienna, Austria

⁵Department of Astronomy/Steward Observatory, The University of Arizona, Tucson, AZ 85721-0009, USA

⁶Max-Planck-Institut für Astronomie, Königstuhl 17, D-69117 Heidelberg, Germany

⁷Department of Physics and Astronomy, University of Exeter, Stocker Road, Exeter EX4 4QL, UK

Accepted XXX. Received YYY; in original form ZZZ

ABSTRACT

Extreme debris discs (EDDs) are bright and warm circumstellar dusty structures around main sequence stars. They may represent the outcome of giant collisions occurring in the terrestrial region between large planetesimals or planetary bodies, and thus provide a rare opportunity to peer into the aftermaths of these events. Here, we report on results of a mini-survey we conducted with the aim to increase the number of known EDDs, investigate the presence of solid-state features around $10\ \mu\text{m}$ in eight EDDs, and classify them into the silica or silicate dominated groups. We identify four new EDDs and derive their fundamental properties. For these, and for four other previously known discs, we study the spectral energy distribution around $10\ \mu\text{m}$ by means of VLT/VISIR photometry in three narrow-band filters and conclude that all eight objects likely exhibit solid-state emission features from sub-micron grains. We find that four discs probably belong to the silicate dominated subgroup. Considering the age distribution of the entire EDD sample, we find that their incidence begins to decrease only after 300 Myr, suggesting that the earlier common picture that these objects are related to the formation of rocky planets may not be exclusive, and that other processes may be involved for older objects (≥ 100 Myr). Because most of the older EDD systems have wide, eccentric companions, we suggest that binarity may play a role in triggering late giant collisions.

Key words: (stars:) circumstellar matter – infrared: planetary systems – stars: individual: TYC 5940-1510-1, TYC 8105-310-1, TYC 4946-1106-1, J060917.00-150808.5, J071206.54-475242.3, J092521.90-673224.8, J104416.70-451613.9, J204315.23+104335.3

1 INTRODUCTION

In recent decades, observations at mid-infrared (mid-IR) wavelengths have led to the identification of a number of main-sequence stars surrounded by warm dust at temperatures of $\sim 200\text{--}600$ K (e.g., Kennedy & Wyatt 2013; Cruz-Saenz de Miera et al. 2014; Cotten & Song 2016). For Sun-like stars with a spectral type between mid F and late K, these temperatures are indicative of dust grains located within a few au, i.e. in a region where the terrestrial planets orbit in the Solar System. The lifetime of such small warm particles is significantly shorter than the age of their host star, as under the influence of stellar radiation and stellar wind they are removed from the system on a timescale of tens of thousands of years at most. So the long-term maintenance of a circumstellar disc requires continuous dust replenishment from erosion of larger bodies. The second gener-

ation debris grains could either be released from an in situ collisional cascade that grinds a ring of planetesimals into (sub)micron-sized particles, from a single large collision, or even from bodies originally located much further away, for example as sublimation or disruption of icy minor bodies transported from a cold, outer reservoir into the inner region (Wyatt 2008; Rigley & Wyatt 2022).

Some warm debris discs contain such large amounts of dust that are clearly not sustainable for the lifetime of the system, implying instead that a recent episodic dust production event has resulted in a strongly elevated dust level for a temporary period (Wyatt et al. 2007). The IR luminosity of the dustiest of these warm transient discs exceeds 1% of the luminosity of their host stars. These so-called extreme debris discs (EDDs), of which we currently know about 20 (Oudmaijer et al. 1992; Gorlova et al. 2004; Song et al. 2005; Gorlova et al. 2007; Rhee et al. 2008; Melis et al. 2010; Zuckerman et al. 2012; de Wit et al. 2013; Tajiri et al. 2020; Melis et al. 2021; Moór et al. 2021; Higashio et al. 2022), are pro-

* E-mail: moor.attila@csfk.org

CON-quest

II. Spatially and spectrally-resolved HCN/HCO⁺ line ratios in local luminous and ultraluminous infrared galaxies

Y. Nishimura^{1,2,3}, S. Aalto⁴, M. D. Gorski⁴, S. König⁴, K. Onishi⁴, C. Wethers⁴, C. Yang⁴, L. Barcos-Muñoz⁵, F. Combes⁶, T. Díaz-Santos^{7,8}, J. S. Gallagher^{9,10}, S. García-Burillo¹¹, E. González-Alfonso¹², T. R. Greve^{13,14}, N. Harada^{3,15}, C. Henkel^{16,17}, M. Imanishi³, K. Kohno², S. T. Linden¹⁸, J. G. Mangum⁵, S. Martín^{19,20}, S. Müller⁴, G. C. Privon^{5,21,22}, C. Ricci^{23,24}, F. Stanley²⁵, P. P. van der Werf²⁶, and S. Viti^{26,27}

(Affiliations can be found after the references)

Received October 20, 2023 / Accepted February 23, 2024

ABSTRACT

Context. Nuclear regions of luminous and ultraluminous infrared galaxies (U/LIRGs) are powered by starbursts and/or active galactic nuclei (AGNs), often obscured by extremely high columns of gas and dust. Molecular lines in the submillimeter windows have potential to determine physical conditions of these compact obscured nuclei (CONs).

Aims. We aim to reveal the distributions of HCN and HCO⁺ emission in local U/LIRGs, and investigate whether and how they are related to galaxy properties.

Methods. Using the Atacama Large Millimeter/submillimeter Array (ALMA), we have conducted sensitive observations of the HCN $J=3-2$ and HCO⁺ $J=3-2$ lines toward 23 U/LIRGs in the local Universe ($z < 0.07$) with a spatial resolution of $\sim 0.3''$ ($\sim 50-400$ pc).

Results. We detected both HCN and HCO⁺ in 21 galaxies, only HCN in one galaxy, and neither in one galaxy. The global HCN/HCO⁺ line ratios, averaged over scales of $\sim 0.5-4$ kpc, range from 0.4 to 2.3, with an unweighted mean of 1.1. These line ratios appear to have no systematic trend with bolometric AGN luminosity or star formation rate. The line ratio varies with position and velocity within each galaxy, with an average interquartile range of 0.38 on a spaxel-by-spaxel basis. In eight out of ten galaxies known to have outflows and/or inflows, we find spatially and kinematically symmetric structures of high line ratios. These structures appear as a collimated bicone/bipole in two galaxies and as a thin spherical shell in six galaxies.

Conclusions. Non-LTE analysis suggests that the high HCN/HCO⁺ line ratio in outflows is predominately influenced by the abundance ratio. Chemical model calculations indicate that the enhancement of HCN abundance in outflows is likely due to high temperature chemistry triggered by shock heating. These results imply that the HCN/HCO⁺ line ratio can aid identifying the outflow geometry when the shock velocity of the outflows is sufficiently high to heat the gas.

Key words. galaxies: evolution – galaxies: nuclei – galaxies: ISM – ISM: molecules – ISM: jets and outflows

1. Introduction

Luminous and ultraluminous infrared galaxies (LIRGs: $L_{\text{IR}}(8-1000\mu\text{m}) = 10^{11}-10^{12}L_{\odot}$, ULIRGs: $L_{\text{IR}} \geq 10^{12}L_{\odot}$, see e.g., Sanders & Mirabel 1996; Pérez-Torres et al. 2021, for reviews) emit most of their energy at infrared wavelengths, powered by nuclear starbursts and/or active galactic nuclei (AGNs) in their central regions. Both observational and theoretical studies proposed that gas-rich galaxy mergers are one of the most important mechanisms to trigger starbursts and fuel supermassive black holes (SMBHs) by funneling large amounts of gas and dust into the nuclei (e.g., Sanders et al. 1988; Hopkins et al. 2006). These studies also pointed out that the central SMBHs are deeply embedded by high columns of obscuring material during the process of mass accretion and that U/LIRGs eventually evolve into optically visible quasars when nuclear feedback (i.e., outflow) disperses the surrounding material. Hence the evolution of U/LIRGs is of key importance to account for the large number of luminous quasars at high redshift, as merger events are considered to be more frequent in the early universe (e.g., Romano et al. 2021).

Now there is mounting evidence that U/LIRGs often host compact ($\lesssim 100$ pc) and highly enshrouded ($N_{\text{H}_2} \gtrsim 10^{24} \text{ cm}^{-2}$) nu-

clei (e.g., Sakamoto et al. 2013; Martín et al. 2016; Aalto et al. 2019; Ricci et al. 2021). These compact obscured nuclei (CONs) exhibit bright emission of rotational transition of HCN, which is vibrationally excited by the mid-infrared continuum emitted from dust (henceforth referred to as HCN-vib; e.g., Sakamoto et al. 2010; Costagliola et al. 2013; Imanishi & Nakanishi 2013; Aalto et al. 2015b, 2019). Using HCN-vib emission, Falstad et al. (2021, hereafter Paper I) conducted a systematic survey of CONs, and revealed that $\sim 50\%$ of the ULIRGs and $\sim 20\%$ of the LIRGs host CONs.

Because of the high obscuration by dust, it is often difficult for observations at many wavelengths to probe the embedded nuclear activities in the center of U/LIRGs (e.g., Lutz et al. 1996). In particular for CON-host galaxies, we need probes free from severe extinction to know the physical properties of the nuclear regions, e.g., if and how much the buried AGNs contribute to the total energy of the source. Molecular lines at (sub)millimeter wavelengths are less affected by dust extinction, and thus have been explored for useful diagnostic methods. As a best practice,

Particle selection from an equilibrium DF

J. A. Sellwood*

Steward Observatory, University of Arizona, 933 N Cherry Ave, Tucson AZ 85722, USA

26 February 2024

ABSTRACT

When starting an N -body simulation of an isolated galaxy, it is desirable to select particles from a distribution function to ensure that the model is in equilibrium. Random sampling from a DF is widely used, but results in a set of particles that differs by shot noise from that intended. This paper presents a method to reduce sampling noise that has been developed by the author in a many collaborations over a number of years. The technique has been partly described in past papers, though the ideas have not previously been gathered together, nor have its advantages been clearly demonstrated in past work. Of course, sampling errors can also be reduced by a brute force increase in the number of particles, but methods to achieve the same effect with fewer particles have obvious advantages. Here we not only describe the method, but also present three sets of simulations to illustrate the practical advantages of reducing sampling error. The improvements are not dramatic, but are clearly worth having.

Key words: galaxies: general — galaxies: kinematics and dynamics — methods: numerical

1 INTRODUCTION

Our understanding of the dynamics of isolated model galaxies has been considerably advanced by N -body simulation, particularly of models that begin from a settled state. Yet creating an equilibrium set of particles from which to start remains one of the most challenging steps. The simplest models are single component disks or spheroids in which all the mass is in the particles, but one may wish to embed the self-gravitating particles in an externally imposed, rigid gravitational field or, in more elaborate models, to represent the disk, bulge and halo as separate components in a combined equilibrium model. Note that the gravitational potential in any model is the total arising from all mass components, whether rigid or composed of mobile particles, but the distribution function (DF) for each component must be an equilibrium function in the total potential.

Sellwood & Athanassoula (1986), Hernquist (1993), Kuijken & Dubinski (1995), Debattista & Sellwood (2000), Holley-Bockelmann, Weinberg & Katz (2005), Widrow *et al.* (2008), Rodionov, Athanassoula & Sotnikova (2009), Yurin & Springel (2014), and others have offered techniques to create single or multi-component models, which achieve something increasingly close to a global equilibrium. Perhaps the most sophisticated are the AGAMA models by Vasiliev (2019), who uses iterative techniques to devise equilibrium distribution functions (DFs) for each component in the combined potential. The DF is generally expressed as a function of integrals $\{\mathbf{I}\}$, such as the classical energy and angular momentum $f(E, \mathbf{L})$ or actions $f(\mathbf{J})$.

However, having found an equilibrium DF, many practi-

tioners simply select N particles at random from the DF. The procedure is to generate candidate particles that are uniformly distributed in each dimension of (\mathbf{x}, \mathbf{v}) -space, and then select only those for which $f(\mathbf{I}) > tf_{\max}$, with t being a random value from a uniform distribution $0 \leq t \leq 1$, and then keep trying until N are accepted. Here, f_{\max} is the largest value of $f(\mathbf{I})$, which is usually for a particle at rest in the center of the component.¹ There are many obvious, and some clever, means to improve efficiency, such as limiting $|\mathbf{x}| \leq r_{\max}$ and \mathbf{v} so that the candidate particle at the selected \mathbf{x} is gravitationally bound, *etc.*, but the vast majority of candidate particles are rejected because $f(\mathbf{I})$ is generally much smaller than its peak value over most of available phase space. Not only is this random sampling method inefficient, but it results in a distribution of \mathbf{I} values that differs by shot noise from the desired $f(\mathbf{I})$. While shot noise declines as $N^{-1/2}$, the benefit from increasing N is painfully slow.

Random sampling works because f specifies the mass in a $2n$ -dimensional volume element of Cartesian phase space $d^n \mathbf{x} d^n \mathbf{v}$ and generating candidate particles that are uniformly distributed in (\mathbf{x}, \mathbf{v}) space leads naturally to the probability of acceptance. We could choose candidate particles in some other system of coordinates, such as a set of integrals $\{\mathbf{I}\}$, which requires knowledge of the mass fraction, $d^m \mathcal{M} / d\mathbf{I}^m$ in an m -dimensional volume element of those integrals. This function is related to the mass in a Cartesian volume element through the Jacobian determinant of the coordinate trans-

¹ The referee pointed out that f_{\max} can be infinite in rare cases, although it must be an integrable singularity, since the mass within any small volume should be finite. However, random selection can still be achieved by transformation of variables, such as we describe in §2.

* E-mail: sellwood@as.arizona.edu

Bubble-wall velocity in local thermal equilibrium: hydrodynamical simulations vs analytical treatment

Tomasz Krajewski¹ Marek Lewicki² Mateusz Zych²

¹*Nicolaus Copernicus Astronomical Center, ul. Bartycka 18, 00-716 Warsaw, Poland*

²*Faculty of Physics, University of Warsaw, ul. Pasteura 5, 02-093 Warsaw, Poland*

E-mail: tkrajewski@camk.edu.pl, marek.lewicki@fuw.edu.pl,
mateusz.zych@fuw.edu.pl

ABSTRACT: We perform real-time hydrodynamical simulations of the growth of bubbles formed during cosmological first-order phase transitions under the assumption of local thermal equilibrium. We confirm that pure hydrodynamic backreaction can lead to steady-state expansion and that bubble-wall velocity in such case agrees very well with the analytical estimates. However, this is not the generic outcome. Instead, it is much more common to observe runaways, as the early-stage dynamics right after the nucleation allow the bubble walls to achieve supersonic velocities before the heated fluid shell in front of the bubble is formed. This effect is not captured by other methods of calculation of the bubble-wall velocity which assume stationary solutions to exist at all times and would have a crucial impact on the possible generation of both baryon asymmetry and gravitational wave signals.

A Universal Method for Solar Filament Detection from $H\alpha$ Observations using Semi-supervised Deep Learning

Andrea Diercke^{1,2,3,4}, Robert Jarolim^{5,6}, Christoph Kuckein^{7,8,3,9}, Sergio J. González Manrique^{1,7,8,10}, Marco Ziener¹¹, Astrid M. Veronig^{5,12}, Carsten Denker³, Werner Pötzi^{5,12}, Tatiana Podladchikova¹³, and Alexei A. Pevtsov²

¹ Institut für Sonnenphysik (KIS), Schöneckstr. 6, 79104 Freiburg, Germany
e-mail: diercke@leibniz-kis.de

² National Solar Observatory (NSO), 3665 Discovery Drive, Boulder, CO, USA, 80303

³ Leibniz-Institut für Astrophysik Potsdam (AIP), An der Sternwarte 16, 14482 Potsdam, Germany

⁴ Universität Potsdam, Institut für Physik und Astronomie, Karl-Liebknecht-Straße 24/25, 14476 Potsdam, Germany

⁵ University of Graz, Institute of Physics, Universitätsplatz 5, 8010 Graz, Austria

⁶ High Altitude Observatory (HAO), 3090 Center Green Drive, Boulder, CO, USA, 80301
e-mail: rjarolim@ucar.edu

⁷ Instituto de Astrofísica de Canarias (IAC), Vía Láctea s/n, 38205 La Laguna, Tenerife, Spain

⁸ Departamento de Astrofísica, Universidad de La Laguna 38205, La Laguna, Tenerife, Spain

⁹ Max-Planck-Institut für Sonnensystemforschung, Justus-von-Liebig-Weg 3, 37077 Göttingen, Germany

¹⁰ Astronomical Institute, Slovak Academy of Sciences, 05960 Tatranská Lomnica, Slovak Republic

¹¹ Applied AI Company Limited (AAICO), C29 - C11-Building 2 Al Khaleej St, Al Muntazah - Zone 1, Abu Dhabi, UAE

¹² University of Graz, Kanzelhöhe Observatory for Solar and Environmental Research, Kanzelhöhe 19, 9521 Treffen am Ossiacher See, Austria

¹³ Skolkovo Institute of Science and Technology, Bolshoy Boulevard 30, bld. 1, Moscow 121205, Russia

Received October 18, 2023; accepted XXXX XX, XXXX

ABSTRACT

Filaments are omnipresent features in the solar atmosphere. Their location, properties and time evolution can provide important information about changes in solar activity and assist the operational space weather forecast. Therefore, filaments have to be identified in full disk images and their properties extracted from these images. Manual extraction is tedious and takes too much time; extraction with morphological image processing tools produces a large number of false-positive detections. Automatic object detection, segmentation, and extraction in a reliable manner allows us to process more data in a shorter time. The Chromospheric Telescope (ChroTel), Tenerife, Spain, the Global Oscillation Network Group (GONG), and the Kanzelhöhe Observatory for Solar and Environmental Research (KSO), Austria, provide regular full-disk observations of the Sun in the core of the chromospheric $H\alpha$ absorption line. We present a deep learning method that provides reliable extractions of solar filaments from $H\alpha$ filtergrams. First, we train the object detection algorithm YOLOv5 with labeled filament data of ChroTel $H\alpha$ filtergrams. We use the trained model to obtain bounding-boxes from the full GONG archive. In a second step, we apply a semi-supervised training approach, where we use the bounding boxes of filaments, to learn a pixel-wise classification of solar filaments with u-net. Here, we make use of the increased data set size which avoids overfitting of spurious artifacts from the generated training masks. Filaments are predicted with an accuracy of 92%. With the resulting filament segmentations, physical parameters such as the area or tilt angle can be easily determined and studied. This we demonstrate in one example, where we determine the rush-to-the pole for Solar Cycle 24 from the segmented GONG images. In a last step, we apply the filament detection to $H\alpha$ observations from KSO which demonstrates the general applicability of our method to $H\alpha$ filtergrams.

Key words. Methods: statistical – Techniques: image processing – Sun: chromosphere – Astronomical data bases – Catalogs

1. Introduction

Solar filaments are structures of dense, cool plasma, which reach from the chromosphere into the corona, stabilized by the magnetic field. They appear above and along the polarity inversion line (PIL), which separates large areas of opposite magnetic polarities (Martin 1998; Mackay et al. 2010). Filaments can be very dynamic objects, which change their appearance in only a few hours. If the magnetic field is destabilized, the filaments can erupt, e.g., as coronal mass ejections (CMEs), and the plasma stored in them is ejected into space (Wang et al. 2020; Kuckein et al. 2020). We differentiate between three kinds of filaments (Bruzek & Durrant 1977): i) active region filaments, which are

smaller, more dynamic, and rooted at large magnetic field concentrations of active regions; ii) quiescent filaments, which appear at all latitudes and are usually larger and more stable; and iii) the category of intermediate filaments, where filaments are subsumed, if they do not fit to the aforementioned classes (Mackay et al. 2010). A special type of quiescent filaments are polar crown filaments, which appear at high-latitudes above 50° (Leroy et al. 1983). Systematic filament studies have been performed across all filament classes mainly utilizing $H\alpha$ full-disk filtergrams (e.g., statistical studies by Hao et al. 2015; Pötzi et al. 2015; Diercke & Denker 2019; Chatzistergos et al. 2023). The key ingredient of all these studies is an effective extraction of

Interstellar detection of O-protonated carbonyl sulfide, HOCS⁺

MIGUEL SANZ-NOVO ^{1,2}, VÍCTOR M. RIVILLA ¹, IZASKUN JIMÉNEZ-SERRA ¹, JESÚS MARTÍN-PINTADO ¹,
LAURA COLZI ¹, SHAOSHAN ZENG ³, ANDRÉS MEGÍAS ¹, ÁLVARO LÓPEZ-GALLIFA ¹,
ANTONIO MARTÍNEZ-HENARES ¹, SARAH MASSALKHI ¹, BELÉN TERCERO ⁴, PABLO DE VICENTE ⁵,
DAVID SAN ANDRÉS ¹, SERGIO MARTÍN ^{6,7} AND MIGUEL A. REQUENA-TORRES ^{8,9}

¹*Centro de Astrobiología (CAB), INTA-CSIC, Carretera de Ajalvir km 4, Torrejón de Ardoz, 28850 Madrid, Spain*

²*Computational Chemistry Group, Departamento de Química Física y Química Inorgánica, Universidad de Valladolid, E-47011 Valladolid, Spain*

³*Star and Planet Formation Laboratory, Cluster for Pioneering Research, RIKEN, 2-1 Hirosawa, Wako, Saitama, 351-0198, Japan*

⁴*Observatorio Astronómico Nacional (OAN-IGN), Calle Alfonso XII, 3, 28014 Madrid, Spain*

⁵*Observatorio de Yebes (OY-IGN), Cerro de la Palera SN, Yebes, Guadalajara, Spain*

⁶*European Southern Observatory, Alonso de Córdova 3107, Vitacura 763 0355, Santiago, Chile*

⁷*Joint ALMA Observatory, Alonso de Córdova 3107, Vitacura 763 0355, Santiago, Chile*

⁸*University of Maryland, College Park, ND 20742-2421 (USA)*

⁹*Department of Physics, Astronomy and Geosciences, Towson University, Towson, MD 21252, USA*

ABSTRACT

We present the first detection in space of O-protonated carbonyl sulfide (HOCS⁺), in the midst of an ultradeep molecular line survey toward the G+0.693-0.027 molecular cloud. From the observation of all $K_a = 0$ transitions ranging from $J_{lo} = 2$ to $J_{lo} = 13$ of HOCS⁺ covered by our survey, we derive a column density of $N = (9 \pm 2) \times 10^{12} \text{ cm}^{-2}$, translating into a fractional abundance relative to H₂ of $\sim 7 \times 10^{-11}$. Conversely, the S-protonated HSCO⁺ isomer remains undetected, and we derive an upper limit to its abundance with respect to H₂ of $\leq 3 \times 10^{-11}$, a factor of ≥ 2.3 less abundant than HOCS⁺. We obtain a HOCS⁺/OCS ratio of $\sim 2.5 \times 10^{-3}$, in good agreement with the prediction of astrochemical models. These models show that one of the main chemical routes to the interstellar formation of HOCS⁺ is likely the protonation of OCS, which appears to be more efficient at the oxygen end. Also, we find that high values of cosmic-ray ionisation rates (10^{-15} - 10^{-14} s^{-1}) are needed to reproduce the observed abundance of HOCS⁺. In addition, we compare the O/S ratio across different interstellar environments. G+0.693-0.027 appears as the source with the lowest O/S ratio. We find a HOCO⁺/HOCS⁺ ratio of ~ 31 , in accordance with other O/S molecular pairs detected toward this region and also close to the O/S solar value (~ 37). This fact indicates that S is not significantly depleted within this cloud due to the action of large-scale shocks, unlike in other sources where S-bearing species remain trapped on icy dust grains.

Keywords: Interstellar molecules(849), Interstellar clouds(834), Galactic center(565), Spectral line identification(2073), Astrochemistry(75)

1. INTRODUCTION

The pursuit of understanding the chemical reservoir of the interstellar medium (ISM) is a cornerstone of modern astrochemistry. At the heart of this quest is the investigation of molecules harboring sulfur (S), which play a key role in diverse aspects, from stellar nucleosynthesis and chemical evolution of galaxies (Perdigon et al. 2021) to atmospheric chemistry in planets (Krasnopolsky 2012; Gómez Martín et al. 2017; Chang et al. 2023), or biological processes (April 1986), and they are consid-

ered essential ingredients for life on Earth (Richardson et al. 2013; Todd 2022).

Starting with the discovery of carbon monosulfide (CS; Penzias et al. 1971), the first S-bearing molecule observed in space, and followed by the detection of carbonyl sulfide (OCS; Jefferts et al. 1971), more than thirty interstellar S-bearing molecules have been identified to date, which corresponds to $\sim 10\%$ of the overall chemical inventory found in the ISM (see McGuire 2022 for a recent molecular census). In this context, recent detections of new S-bearing molecules (e.g.,

Optimisation-based alignment of wideband integrated superconducting spectrometers for sub-mm astronomy

A. Moerman^{*1}, K. Karatsu^{1,2}, S. J. C. Yates³, R. Huiting², F. Steenvoorde⁴, S. O. Dabironezare¹, T. Takekoshi⁵, J. J. A. Baselmans^{1,2}, B. R. Brandl^{6,7}, and A. Endo¹

¹ Faculty of Electrical Engineering, Mathematics and Computer Science, Delft University of Technology, Mekelweg 4, 2628 CD, Delft, The Netherlands

² SRON—Netherlands Institute for Space Research, Niels Bohrweg 4, 2333 CA, Leiden, The Netherlands

³ SRON—Netherlands Institute for Space Research, Landleven 12, 9747 AD, Groningen, The Netherlands

⁴ DEMO: Electronic and Mechanical Support Division, Delft University of Technology, Mekelweg 4, 2628CD, Delft, The Netherlands

⁵ Kitami Institute of Technology, 165 Koen-cho, Kitami, 090-8507 Hokkaido, Japan

⁶ Leiden Observatory, Leiden University, PO Box 9513, 2300 RA, Leiden, The Netherlands

⁷ Faculty of Aerospace Engineering, Delft University of Technology, Kluyverweg 1, 2629 HS, Delft, The Netherlands

Received; accepted

ABSTRACT

Context. Integrated superconducting spectrometers (ISSs) for wideband sub-mm astronomy utilise quasi-optical systems for coupling radiation from the telescope to the instrument. Misalignment in these systems is detrimental to the system performance. The common method of using an optical laser to align the quasi-optical components requires accurate alignment of the laser to the sub-mm beam coming from the instrument, which is not always guaranteed to a sufficient accuracy.

Aims. To develop an alignment strategy for wideband ISSs directly utilising the sub-mm beam of the wideband ISS. The strategy should be applicable in both telescope and laboratory environments. Moreover, the strategy should deliver similar quality of the alignment across the spectral range of the wideband ISS.

Methods. We measure misalignment in a quasi-optical system operating at sub-mm wavelengths using a novel phase and amplitude measurement scheme, capable of simultaneously measuring the complex beam patterns of a direct-detecting ISS across a harmonic range of frequencies. The direct detection nature of the MKID detectors in our device-under-test, DESHIMA 2.0, necessitates the use of this measurement scheme. Using geometrical optics, the measured misalignment, a mechanical hexapod, and an optimisation algorithm, we follow a numerical approach to optimise the positioning of corrective optics with respect to a given cost function. Laboratory measurements of the complex beam patterns are taken across a harmonic range between 205 and 391 GHz and simulated through a model of the ASTE telescope in order to assess the performance of the optimisation at the ASTE telescope.

Results. Laboratory measurements show that the optimised optical setup corrects for tilts and offsets of the sub-mm beam. Moreover, we find that the simulated telescope aperture efficiency is increased across the frequency range of the ISS after the optimisation.

Key words. instrumentation: spectrographs – methods: numerical

1. Introduction

Wideband sub-mm spectroscopy could serve as a powerful tool for studying a wide range of astrophysical phenomena (Stacey 2011). For single-pixel spectroscopy, one such target is the redshifted [CII] emission line, which can be used to probe star formation over cosmic time (Lagache et al. 2018), study the universe at the epoch of reionization (Gong et al. 2011), and study high-redshift dusty star-forming galaxies (Rybak et al. 2022). Multi-pixel spectrometers, also called integral field units (IFUs), can spectroscopically observe wide field-of-views. This allows for studies on larger spatial scales, such as line intensity mapping of the [CII] line (Yue et al. 2015; Yue & Ferrara 2019; Karoumpis et al. 2022) which can be used to study the growth of large-scale structure (LSS) in the early Universe. Also, the extragalactic rotational emission lines of CO can be used in cross-correlation power spectra studies with other LSS tracers such as

the CIB (Maniyar et al. 2023) and the Ly- α forest signal (Qezlou et al. 2023).

State-of-the-art integrated superconducting spectrometers (ISSs) for ground-based wideband sub-mm astronomy, such as Superspec (Karkare et al. 2020), μ -spec (Mirzaei et al. 2020) and DESHIMA (Endo et al. 2019a), rely on superconducting detectors called microwave kinetic inductance detectors (Day et al. 2003; Baselmans 2012) (MKIDs) to detect incoming radiation. Unlike quasi-optical spectrometers such as CONCERTO (Ade et al. 2020), an ISS integrates both the detectors and the dispersive element on a single chip. This includes everything from the antenna capturing the incoming radiation, the filterbank or dispersive element that separates spectral channels, down to the MKID detectors. An obvious advantage of the ISS is the scalability from a single-pixel instrument to a multi-pixel IFU: because the entire device is already fabricated on a single chip, it is possible to fabricate multiple of these devices on a single wafer.

Coupling the broadband single-mode signal from the telescope to the single-pixel ISS requires good alignment of all in-

* Corresponding author e-mail: A.Moerman-1@tudelft.nl

The X-ray variability of AGN: power-spectrum and variance analysis of the *Swift* /BAT light curves

I. E. Papadakis^{1,2} and V. Binas-Valavanis^{1,2}

¹ Department of Physics and Institute of Theoretical and Computational Physics, University of Crete, 71003 Heraklion, Greece
e-mail: jhep@physics.uoc.gr

² Institute of Astrophysics, FORTH, GR-71110 Heraklion, Greece

ABSTRACT

Aims. We study the X-ray power spectrum of Active Galactic Nuclei (AGN) to investigate whether Seyfert I and II power spectra are similar or not, whether the AGN variability depends on black hole mass and accretion rate, and to compare the AGN power spectra with the Galactic X-ray black hole binaries power-spectra.

Methods. We used 14–195 keV band light curves from the 157th *Swift* /BAT hard X-ray survey and we computed the mean power spectrum and excess variance of AGN in narrow black-hole mass/luminosity bins. We fitted a power-law model to the AGN power spectra, and we investigated whether the power spectrum parameters and the excess variance depend on black hole mass, luminosity and accretion rate.

Results. The Seyfert I and Seyfert II power spectra are identical, in agreement with AGN unification models. The mean AGN X-ray power spectrum has the same, power-law like shape with a slope of -1 in all AGN, irrespective of their luminosity and BH mass. We do not detect any flattening to a slope of zero at frequencies as low as 10^{-9} Hz. We detect an anti-correlation between the PSD amplitude and the accretion rate, similar to what has been seen in the past in the 2–10 keV band. This implies that the variability amplitude in AGN decreases with increasing accretion rate. The universal AGN power-spectrum is consistent with the mean, 2–9 keV band Cyg X-1 power spectrum in its soft state. We detect a small difference in amplitude, but this is probably due to the difference in energy.

Conclusions. The mean, low frequency AGN X-ray power spectrum is consistent with the extension of the mean, 0.01–25 Hz Cyg X-1 power spectrum in its soft state to lower frequencies. We cannot prove that the mean AGN PSD is analogous of the mean Cyg X-1 PSD in its soft state, as we do not know the location of the high frequency break in the hard X-ray AGN PSDs. However, if that is the case, then the accretion disc in AGN probably extends to the radius of the innermost circular stable orbit (as is probably the case with the black hole binaries in their soft state). The X-ray corona will then be located on top, illuminating the disc and producing the X-ray reflection and disc reverberation phenomena that are commonly observed in these objects. Furthermore, the agreement between the AGN and the Cyg X-1 power spectrum (either in the soft or the hard state) over many decades in frequency indicates that the X-ray variability process is probably the same in all accreting objects, irrespective of the mass of the compact object. We plan to investigate this issue further in the near future.

Key words. galaxies: active – galaxies: Seyfert – X-rays: galaxies

1. Introduction

Active Galactic Nuclei (AGN) vary at all wavebands, with the variability amplitude increasing with increasing energy. X-rays vary significantly in flux and/or spectral shape on time scales as short as minutes/hours in some cases. This supports the hypothesis that X-rays are emitted in a small region located close to the super-massive black hole (BH), which resides in the center of these objects. X-ray spectral and timing studies are though to be important as their study could help us understand the physical processes that operate in the innermost region of these objects.

AGN variations are stochastic in nature, therefore their study involves the use of statistical tools like the so-called normalized excess variance, σ_{NXV}^2 , and the power-spectral density function (PSD). The former is equal to the integral of the latter, hence it provides limited information on the nature of the variability when compared to the study of the PSD itself. Power spectrum analysis of the X-ray light curves of radio-quiet AGN was first introduced with the use of long, EXOSAT light curve thirty years ago (e.g. Lawrence & Papadakis 1993; Green et al. 1993). De-

tailed characterization of the X-ray power spectra of AGN (in the 2–10 keV band) was later achieved with the combination of RXTE and *XMM-Newton* light curves (e.g. Uttley et al. 2002; Papadakis et al. 2002; Markowitz et al. 2003; McHardy et al. 2004; Uttley & McHardy 2005; Markowitz et al. 2007; Markowitz 2010; González-Martín & Vaughan 2012). The past variability studies have established that the X-ray PSDs in the 2–10 keV band have a featureless, power-law like shape with a slope of ~ -1 over many decades in frequency, which then steepens to a slope of ~ -2 (or even steeper) above a bend-frequency, ν_b . This characteristic frequency depends on BH mass and possibly on the accretion rate as well (McHardy et al. 2006; González-Martín & Vaughan 2012). This power spectrum shape is similar to the shape of the X-ray power spectra of the Galactic X-ray BH binaries (GBHs) in their soft states.

We use the *Swift* /BAT light curves from the 157 month BAT survey (Lien et al, in preparation) of a large sample of AGN, in order to estimate their power spectrum at low frequencies. BAT has been continuously monitoring the sky for ~ 18.5 years, and the 157 month survey provides long, evenly sampled, and high

Updated kinematics of the Radcliffe Wave: non-synchronous, dipole-like vertical oscillations

ZHI-KAI ZHU ¹, MIN FANG ², ZU-JIA LU ^{1,*}, JUNZHI WANG ¹, GUANG-XING LI ³, SHIYU ZHANG ²,
VELI-MATTI PELKONEN ⁴, PAOLO PADOAN ^{4,5} AND EN-WEI LIANG ¹

¹Guangxi Key Laboratory for Relativistic Astrophysics, School of Physical Science and Technology,
Guangxi University, Nanning 530004, China

²Purple Mountain Observatory, Chinese Academy of Sciences, 10 Yuanhua Road, Nanjing 210023, China

³South-Western Institute for Astronomy Research, Yunnan University, Kunming 650500, China

⁴Institut de Ciències del Cosmos, Universitat de Barcelona, IEEC-UB, Martí i Franquès 1, E08028 Barcelona, Spain

⁵Department of Physics and Astronomy, Dartmouth College, 6127 Wilder Laboratory, Hanover, NH 03755, USA

ABSTRACT

The kinematic structure of the Radcliffe Wave (RW) is crucial for understanding its origin and evolution. In this work, we present an accurate measurement of the vertical velocity V_Z by where the radial velocity (RV) measures are taken into consideration. This is achieved in two ways. First, the velocities are measured towards Young Stellar Objects (YSOs), using their RV and proper motion measurements from APOGEE-2 and Gaia DR3. Second, we combine RV measurements toward clouds with proper motion measurements of associated YSOs to determine the vertical velocities of the clouds. The results reveal that the oscillations in V_Z are not synchronous with the vertical coordinate. The difference is caused by a combination of the effect of the radial velocity which we include in this paper, and the difference in models. By supplementing our analysis with additional young star samples, we find a consistent dipole pattern in V_Z . The fact that no significant amplitude differences are found among the analyzed samples indicates that there is no apparent age gradient within the dipole. We propose that RW evolves at a relatively slow rate. The fact that it will take a much longer time for RW to complete a full period compared to the cloud lifetimes challenges its classification as a traditional “wave”. This age discrepancy should explain the phase difference, and non-synchronous oscillation found in kinematic studies.

Keywords: ISM: clouds; ISM: structure; ISM: kinematics and dynamics; stars: kinematics and dynamics

1. INTRODUCTION

The recent discovery of the Radcliffe Wave (RW) has sparked significant interest as it reveals a novel distribution pattern of molecular clouds and dense gas in the solar neighborhood. The RW was first identified by Alves et al. (2020), which belongs to a class of Galactic-scale gas filament reported since Li et al. (2013). Zucker et al. (2020) that had obtained the accurate distances of molecular clouds. It is a coherent molecular cloud structure spanning 2.7 kiloparsecs in length and exhibiting vertical oscillations in the Z direction of the Galactic coordinate system. They described the undulating behavior as a damped sinusoidal mode. Besides, they argued that a part of the well-known Gould Belt, first

described by Benjamin Gould in 1879 and after whom the Belt is named (Gould 1879), is a projection effect of RW.

The nature of the Gould’s belt has been studied for decades after it was first pointed out. Lesh (1972) and Frogel & Stothers (1977) used observation data of O and B stars to separate the Gould’s Belt from the Galactic Belt and to determine the parameters of the velocity field in both belts. They found that within the Gould’s Belt, the young stars form a local irregularity of the velocity field that arises from the superposition of the motion of different local groups of young stars. The kinematics of the Gould’s Belt has been studied considering the spatial distribution and the motion of the stars (e.g. Comeron et al. 1992; Comerón 1999; Moreno et al. 1999; Dunham et al. 2015). Zucker et al. (2022) used Gaia space telescope observation data to analyze

* luzujia@gxu.edu.cn

Physical properties of hyperluminous, dust-obscured quasars at $z \sim 3$: multiwavelength Spectral Energy Distribution analysis and cold gas content revealed by ALMA

WEIBIN SUN (孙卫斌) ^{1,2} LULU FAN (范璐璐) ^{1,2,3} YUNKUN HAN (韩云坤) ^{4,5,6} KIRSTEN K. KNUDSEN ⁷
GUANGWEN CHEN (陈广文) ^{1,2} AND HONG-XIN ZHANG (张红欣) ^{1,2}

¹CAS Key Laboratory for Research in Galaxies and Cosmology, Department of Astronomy, University of Science and Technology of China, Hefei 230026, China

²School of Astronomy and Space Science, University of Science and Technology of China, Hefei 230026, China

³Deep Space Exploration Laboratory, Hefei 230088, China

⁴Yunnan Observatories, Chinese Academy of Sciences, 396 Yangfangwang, Guandu District, Kunming, 650216, P. R. China

⁵Center for Astronomical Mega-Science, Chinese Academy of Sciences, 20A Datun Road, Chaoyang District, Beijing, 100012, P. R. China

⁶Key Laboratory for the Structure and Evolution of Celestial Objects, Chinese Academy of Sciences, 396 Yangfangwang, Guandu District, Kunming, 650216, P. R. China

⁷Department of Space, Earth and Environment, Chalmers University of Technology, Onsala Space Observatory, SE-439 92 Onsala, Sweden

Submitted to AAS Journal

ABSTRACT

We present a UV to millimeter spectral energy distribution (SED) analysis of 16 hyperluminous, dust-obscured quasars at $z \sim 3$, selected by the *Wide-field Infrared Survey Explorer*. We aim to investigate the physical properties of these quasars, with a focus on their molecular gas content. We decompose the SEDs into three components: stellar, cold dust, and active galactic nucleus (AGN). By doing so, we are able to derive and analyze the relevant properties of each component. We determine the molecular gas mass from CO line emission based on Atacama Large Millimeter/submillimeter Array (ALMA) observations. By including ALMA observations in the multiwavelength SED analysis, we derive the molecular gas fractions, gas depletion timescales, and star formation efficiencies (SFEs). Their sample median and 16th-84th quartile ranges are $f_{\text{gas}} \sim 0.33_{-0.17}^{+0.33}$, $t_{\text{depl}} \sim 39_{-28}^{+85}$ Myr, $\text{SFE} \sim 297_{-195}^{+659}$ K km s⁻¹ pc⁻². Compared to main-sequence galaxies, they have a lower molecular gas content and higher SFEs, similar to quasars in the literature. This suggests that the gas in these quasars is rapidly depleted, likely as the result of intense starburst activity and AGN feedback. The observed correlations between these properties and the AGN luminosities further support this scenario. Additionally, we infer the black hole to stellar mass ratio and black hole mass growth rate, which indicate a significant central black hole mass assembly over short timescales. Our results are consistent with the scenario that our sample represents a short transition phase toward unobscured quasars.

Keywords: galaxies: active — galaxies: high-redshift — galaxies: starburst — galaxies: evolution — quasars: general

1. INTRODUCTION

The coevolution between the central supermassive black hole (SMBH) and host galaxy is now widely ac-

knowledged (Kormendy & Ho 2013). This is evidenced by the tight correlation between the mass of central SMBHs and the stellar bulge masses in galaxies (e.g., Magorrian et al. 1998; Ferrarese & Ford 2005). In one of the most popular coevolution scenarios, galaxy gas-rich major galaxy mergers trigger intense starbursts, provide the fuel for central SMBH accretion, and trigger active

Simulation Studies for the First Pathfinder of the CATCH Space Mission

Yiming Huang^{1,2}, Juan Zhang¹, Lian Tao¹, Zhengwei Li¹, Donghua Zhao³, Qian-Qing Yin¹, Xiangyang Wen¹, Jingyu Xiao^{1,2}, Chen Zhang³, Shuang-Nan Zhang^{1,2}, Shaolin Xiong¹, Qingcui Bu⁴, Jirong Cang⁵, Dezhi Cao⁶, Wen Chen⁷, Siran Ding⁷, Min Gao¹, Yang Gao⁷, Shujin Hou⁸, Liping Jia⁵, Ge Jin⁹, Dalin Li¹⁰, Jinsong Li⁷, Panping Li^{1,2}, Yajun Li^{1,2}, Xiaojing Liu¹, Ruican Ma^{1,2}, Xingyu Pan⁵, Liqiang Qi¹, Jinhui Rao^{1,11}, Xianfei Sun⁷, Qingwen Tang¹¹, Ruijing Tang¹², Yusa Wang¹, Yibo Xu⁷, Sheng Yang¹, Yanji Yang¹, Yong Yang⁷, Xuan Zhang^{1,11}, Yueting Zhang⁷, Heng Zhou⁷, Kang Zhao^{1,2}, Qingchang Zhao^{1,2}, Shujie Zhao^{1,2}, Zijian Zhao¹

¹Key Laboratory for Particle Astrophysics, Institute of High Energy Physics, Chinese Academy of Sciences, Beijing, 100149, China.

²University of Chinese Academy of Sciences, Chinese Academy of Sciences, Beijing, 100149, China.

³National Astronomical Observatories, Chinese Academy of Sciences, Beijing, 100101, China.

⁴Institut für Astronomie und Astrophysik, Kepler Center for Astro and Particle Physics, Eberhard Karls Universität, Sand 1, Tübingen, 72076, Germany.

⁵Star Detect CO., LTD., Beijing, 100190, China.

⁶Tsinghua University, Beijing, 100084, China.

⁷Innovation Academy for Microsatellites of Chinese Academy of Sciences, Shanghai, 200135, China.

⁸Nanyang Normal University, Nanyang, 473061, China.

⁹North Night Vision Technology CO., LTD., Nanjing, 211106, China.

¹⁰National Space Science Center, Chinese Academy of Sciences, Beijing, 100190, China.

¹¹Nanchang University, Nanchang, 330031, China.

¹²Beijing Jiaotong University, Beijing, 100044, China.

1

Contributing authors: zhangjuan@ihep.ac.cn; taolian@ihep.ac.cn;

Abstract

The Chasing All Transients Constellation Hunters (CATCH) space mission is an intelligent constellation consisting of 126 micro-satellites in three types (A, B, and C), designed for X-ray observation with the objective of studying the dynamic universe. Currently, we are actively developing the first Pathfinder (CATCH-1) for the CATCH mission, specifically for type-A satellites. CATCH-1 is equipped with Micro Pore Optics (MPO) and a 4-pixel Silicon Drift Detector (SDD) array. To assess its scientific performance, including the effective area of the optical system, on-orbit background, and telescope sensitivity, we employ the Monte Carlo software Geant4 for simulation in this study. The MPO optics exhibit an effective area of 41 cm^2 at the focal spot for 1 keV X-rays, while the entire telescope system achieves an effective area of 29 cm^2 at 1 keV when taking into account the SDD detector's detection efficiency. The primary contribution to the background is found to be from the Cosmic X-ray Background. Assuming a 625 km orbit with an inclination of 29° , the total background for CATCH-1 is estimated to be $8.13 \times 10^{-2} \text{ counts s}^{-1}$ in the energy range of 0.5–4 keV. Based on the background within the central detector and assuming a Crab-like source spectrum, the estimated ideal sensitivity could achieve $1.9 \times 10^{-12} \text{ erg cm}^{-2} \text{ s}^{-1}$ for an exposure of 10^4 s in the energy band of 0.5–4 keV. Furthermore, after simulating the background caused by low-energy charged particles near the geomagnetic equator, we have determined that there is no need to install a magnetic deflector.

Keywords: CATCH, X-ray telescope, Geant4 simulation, effective area, background, sensitivity

1 Introduction

The Chasing All Transients Constellation Hunters (CATCH) space mission is proposed to address the lack of follow-up observation capabilities in the time-domain astronomy era [1]. It will study the dynamic universe via X-ray follow-up observations of various multi-wavelength and multi-messenger transients, such as electromagnetic counterparts of gravitational wave events, X-ray binaries, fast radio bursts, magnetars, and gamma-ray bursts. CATCH plans to consist of 126 X-ray micro-satellites that are controlled by an intelligent system. These satellites work together to perform various observations, including timing, spectroscopy, imaging, and polarization, for numerous transients simultaneously. The mission is composed of three types of satellites, each serving a different scientific purpose. Type-A satellites are used for immediate timing monitoring after target discovery. Based on the results obtained from type-A satellites, type-B satellites are deployed for more in-depth timing, imaging, and spectroscopic follow-up observations, and type-C satellites, on the other hand, are specifically designed for polarization measurements.

2

Exploring Gamma-Ray Burst Diversity: Clustering analysis of emission characteristics of *Fermi* and BATSE detected GRBs

NISHIL MEHTA ^{1,2} AND SHABNAM IYYANI ¹

¹Indian Institute of Science Education and Research, Thiruvananthapuram, Kerala, India, 695551

²Laboratoire Lagrange, Observatoire de la Côte d'Azur, Université Côte d'Azur, Nice, France

ABSTRACT

Gamma-ray bursts (GRBs) are commonly attributed to the demise of massive stars or the merger of binary compact objects. However, their varied emission characteristics strongly imply the existence of multiple GRB classes based on progenitor types, radiation mechanisms, central engines etc. This study utilizes unsupervised clustering with the Nested Gaussian Mixture Model algorithm to analyze *Fermi* and BATSE GRB data, identifying four classes (A, B, C, and D) based on duration, spectral peak, and spectral index, comprising approximately 70%, 10%, 3%, and 17% of the dataset, respectively. Classes A and B consist of long GRBs, C mainly short GRBs, and class D encompasses both short and long GRBs. Using the spectral index, α , for the differentiation of radiation models, it is found that classes B and C align with photospheric emission models, while A and D predominantly show synchrotron radiation characteristics. Short GRBs predominantly exhibit photospheric emission, whereas long GRBs show consistency with synchrotron emission. Overall, 63% of the total bursts exhibit α profiles indicative of synchrotron emission, with the remaining 37% associated with photospheric emission. The classes were further examined for their progenitor origins, revealing that classes A and D demonstrate a hybrid nature, while classes B and C are predominantly associated with collapsar and merger origins, respectively. This clustering analysis reveals distinct GRB classes, shedding light on their diversity in radiation, duration and progenitor.

Keywords: Gamma-ray bursts(629) — Clustering — Multivariate analysis(1913) — Catalogs(205)

1. INTRODUCTION

Gamma ray bursts (GRBs) are the brightest transient phenomenon known in the cosmos. The launch of the Burst Transient Spectrometer Experiment (BATSE) instrument onboard Compton Gamma ray observatory (CGRO) in 1991 led to the discovery and spectral study of 2704 GRBs in the energy range 20 - 2000 keV, during its 9 years of operation (Fishman 2013). The observations were then further enhanced with the launch of *Fermi* gamma ray space telescope in 2008, which observes in a wide energy range from 8 keV to 40 MeV by the Gamma ray Burst Monitor (GBM, Meegan et al. 2009) and from 30 MeV to 300 GeV using the Large Area Telescope (LAT, Atwood et al. 2009).

The immediate emission from the GRBs, dominantly observed in gamma rays is referred to as the prompt emission. The various observational temporal and spectral characteristics of the prompt emission of GRBs are used for exploring the clustering among GRBs. Broadly, the two types of GRB classes (Kouveliotou et al. 1993) refer to two main types of progenitors: merger of binary neutron stars or a neutron star - black hole, which gives rise to largely GRBs of shorter duration ($T_{90} \leq 2$ s) and harder spectra i.e high spectral peak energies; and core-collapse of massive stars which leads to GRBs of longer duration ($T_{90} \geq 2$ s) and softer spectra (MacFadyen & Woosley 1999).

The hypothesis of merger of compact objects was confirmed with the concurrent detection of GRB170817A along with the gravitational waves (Abbott et al. 2017) and the observation of kilonova (Tanvir et al. 2017; McCully et al. 2017). On the other hand, the hypothesis of the progenitor to be a collapsar (MacFadyen & Woosley 1999) is supported

Catalog of Stars with Solar-Type Activity — CSSTA¹

Aleksey A. Shlyapnikov

aas@craocrimea.ru

Introduction

The first lists of flare red dwarfs of UV Cet type appeared in the middle of the past century have comprised 2–3 dozen stars each. The first catalog of such stars was compiled at the Crimean Astrophysical Observatory and presented at the meeting of the International Astronomical Union in 1971. It comprised 53 objects and was placed in the VizieR database at number II/55 (Shakhovskaya, 1971).

At the end of the century, Hawley et al. (1996) carried out a spectral classification of about 2000 M dwarfs that are close to the Sun and found that 105 of them were emission M0–M3 dwarfs and 208 were M4–M8 stars with emission. Taking into account these and other results of those years in the Crimea, the GKL99 catalog was compiled (Gershberg et al., 1999) comprising 462 flare UV Cet stars and related objects in the vicinity of the Sun. In the VizieR database, the catalog is designated as J/A+AS/139/555, whereas in the search system SIMBAD it is represented as GKL99.

The GKL99 catalog was the basis for compiling a new list of stars with solar-type activity. A change of the name from “flare UV Cet stars” into “stars with solar-type activity” has marked certain progress in understanding the physics of activity. This was the GTSh10 catalog comprising 5535 objects. A detailed description of the GTSh10 catalog is given in Issue 1, V. 107 of the *Izvestiya Krymskoi Astrofizicheskoi Observatorii* (Gershberg et al., 2011).

Supplement to the monograph of R. E. Gershberg, N. I. Kleeorin, L. A. Pustilnik, and A. A. Shlyapnikov *Physics of Middle- and Low-Mass Stars with Solar-Type Activity* (M.: FIZMATLIT, 2020, 768 p., ISBN 978-5-9221-1881-1) provides a description of the second version of the catalog of stars with solar-type activity prepared at CrAO in 2019. This catalog has already included 29046 objects.

Below, we provide a description of the third version of the Catalog (CSSTA-3), present its structure and filling with data as at December 03, 2023.

1. Input Catalog

As in the previous version of the Catalog of Stars with Solar-Type Activity, the input list based on which the objects were selected is GAIA² Data Release 2 (GAIA DR2) (GAIA collaboration, 2018).

Interest to the project data in the context of compiling the current Catalog is caused by the following information contained in GAIA DR2. This is the two-color photometry of objects G_{BP} (3300–6800 Å) and G_{RP} (6300–10500 Å) of more than 1×10^9 objects, the detailed characteristic of light curves (~ 400 thousand objects), effective temperature (> 160 million objects), interstellar extinction (> 87 million), color indices (> 87 million), radii and luminosities (> 76 million).

¹ Supplement for book: Gershberg, R.E.; Kleeorin, N.I.; Pustilnik, L.A.; Airapetian, V.S.; Shlyapnikov, A.A. "Physics of mid- and low-mass stars with solar-type activity and their impact on exoplanetary environments", Simferopol: LLC “Forma”, 2024. – 764 p., ISBN 978-5-907548-55-8

² GAIA – https://www.esa.int/Science_Exploration/Space_Science/Gaia

AGN feedback in isolated galaxies with a SMUGGLE multiphase ISM

Aneesh Sivasankaran¹*, Laura Blecha¹, Paul Torrey², Luke Zoltan Kelley³, Aklant Bhowmick¹, Mark Vogelsberger⁴, Lars Hernquist⁵, Federico Marinacci^{6,7} and Laura V. Sales⁸

¹*Department of Physics, University of Florida, Gainesville, Florida 32601, USA*

²*Department of Astronomy, University of Virginia, 530 McCormick Road, Charlottesville, VA 22903, USA*

³*Department of Astronomy, University of California at Berkeley, 501 Campbell Hall, Berkeley, CA 94720, USA*

⁴*Department of Physics, Kavli Institute for Astrophysics and Space Research, Massachusetts Institute of Technology, Cambridge, MA 02139, USA*

⁵*Harvard-Smithsonian Center for Astrophysics, 60 Garden Street, Cambridge, MA 02138, USA*

⁶*Department of Physics & Astronomy “Augusto Righi”, University of Bologna, via Gobetti 93/2, 40129 Bologna, Italy*

⁷*INAF, Astrophysics and Space Science Observatory Bologna, Via P. Gobetti 93/3, I-40129 Bologna, Italy*

⁸*University of California, Riverside, 900 University Ave., Riverside, CA 92521, USA*

Accepted XXX. Received YYY; in original form ZZZ

ABSTRACT

Feedback from active galactic nuclei (AGN) can strongly impact the host galaxies by driving high-velocity winds that impart substantial energy and momentum to the interstellar medium (ISM). In this work, we study the impact of these winds in isolated galaxies using high-resolution hydrodynamics simulations. Our simulations use the explicit ISM and stellar evolution model called Stars and MUltiphase Gas in GaLaxiEs (SMUGGLE). Additionally, using a super-Lagrangian refinement scheme, we resolve AGN feedback coupling to the ISM at ~ 10 -100 pc scales. We find that AGN feedback efficiently regulates the growth of SMBHs. However, its effect on star formation and outflows depends strongly on the relative strengths of AGN vs local stellar feedback and the geometrical structure of the gas disk. When the energy injected by AGN is subdominant to that of stellar feedback, there are no significant changes in the star formation rates or mass outflow rates of the host galaxy. Conversely, when the energy budget is dominated by the AGN, we see a significant decline in the star formation rates accompanied by an increase in outflows. Galaxies with thin gas disks like the Milky Way allow feedback to escape easily into the polar directions without doing much work on the ISM. In contrast, galaxies with thick and diffuse gas disks confine the initial expansion of the feedback bubble within the disk, resulting in more work done on the ISM. Phase space analysis indicates that outflows primarily comprise hot and diffuse gas, with a lack of cold and dense gas.

Key words: methods: numerical – black hole physics – quasars: supermassive black holes – galaxies: ISM – galaxies: interactions

1 INTRODUCTION

It is widely accepted that supermassive black holes (SMBHs) exist at the centers of the majority of massive galaxies. These BHs are thought to start as $\sim 10^2 - 10^5 M_\odot$ seeds and grow in size by many orders of magnitude primarily through gas accretion (Soltan 1982). During accretion, a fraction of the accreted energy is converted into radiation resulting in luminosities as high as $\sim 10^{48} \text{ ergs s}^{-1}$ emanating from milliparsec size regions. These objects are called Active Galactic Nuclei (AGNs) and the coupling of this energy to the surrounding interstellar medium (ISM) of the host galaxy is called AGN feedback. AGN feedback is postulated to play a major role in the evolution of the host galaxy by regulating star formation by expelling cold gas or heating up gas. AGN feedback is also thought to self-regulate the growth of SMBHs by suppressing gas inflows. These postulates are motivated by observational data which show strong correlations between the mass of the SMBHs and the properties of their host galaxies such as bulge mass, stellar velocity dispersion and

luminosity (Kormendy & Richstone 1995; Magorrian et al. 1998; Ferrarese & Merritt 2000; Gültekin et al. 2009; McConnell & Ma 2013; Kormendy & Ho 2013; Reines & Volonteri 2015; Bennert et al. 2015; Savorgnan et al. 2016). Apart from these correlations, there are also observations of strong outflows (with outflow rates $\sim 1000 M_\odot \text{ yr}^{-1}$ and velocities $> 1000 \text{ km s}^{-1}$) emanating from galactic nuclei (Rupke & Veilleux 2011; Sturm et al. 2011; Cicone et al. 2014; Fiore et al. 2017; Fluetsch et al. 2019), supporting the existence of AGN feedback and its importance in the evolution of the host galaxy. Nevertheless, the role of AGN feedback in galaxy evolution is still a debated topic due to the uncertainties in our understanding of how the feedback actually couples to the interstellar medium (ISM). This coupling can happen through various mechanisms such as jets, winds and radiation pressure. Presently, the contributions of these distinct modes and their corresponding coupling efficiencies remain poorly constrained.

Theoretical studies of galaxy formation and evolution using numerical simulations have been very successful at reproducing many observational data (e.g., Vogelsberger et al. 2014b,a; Genel et al. 2014; Schaye et al. 2015; McAlpine et al. 2017; Pillepich et al. 2018;

* E-mail: aneeshs@ufl.edu

Classification of compact radio sources in the Galactic plane with supervised machine learning

S. Riggi^{a,*}, G. Umana^a, C. Trigilio^a, C. Bordiu^a, F. Bufano^a, A. Ingallinera^a, F. Cavallaro^a, Y. Gordon^b, R.P. Norris^{c,d}, G. Gürkan^{e,f}, P. Leto^a, C. Buemi^a, S. Loru^a, A.M. Hopkins^g, M.D. Filipović^c, T. Cecconello^{a,h}

^aINAF - Osservatorio Astrofisico di Catania, Via Santa Sofia 78, 95123 Catania, Italy

^bDepartment of Physics, University of Wisconsin-Madison, 1150 University Ave, Madison, WI 53706, USA

^cWestern Sydney University, Locked Bag 1797, Penrith South DC, NSW 2751, Australia

^dCSIRO Space & Astronomy, P.O. Box 76, Epping, NSW 1710, Australia

^eThüringer Landessternwarte Tautenburg (TLS), Sternwarte 5, D-07778 Tautenburg, Germany

^fCSIRO Space & Astronomy, ATNF, PO Box 1130, Bentley WA 6102, Australia

^gAustralian Astronomical Optics, Macquarie University, 105 Delhi Rd, North Ryde, NSW 2113, Australia

^hDepartment of Electrical, Electronic and Computer Engineering, University of Catania, Viale Andrea Doria 6, 95125 Catania, Italy

Abstract

Generation of science-ready data from processed data products is one of the major challenges in next-generation radio continuum surveys with the Square Kilometre Array (SKA) and its precursors, due to the expected data volume and the need to achieve a high degree of automated processing. Source extraction, characterization, and classification are the major stages involved in this process. In this work we focus on the classification of compact radio sources in the Galactic plane using both radio and infrared images as inputs. To this aim, we produced a curated dataset of $\sim 20,000$ images of compact sources of different astronomical classes, obtained from past radio and infrared surveys, and novel radio data from pilot surveys carried out with the Australian SKA Pathfinder (ASKAP). Radio spectral index information was also obtained for a subset of the data. We then trained two different classifiers on the produced dataset. The first model uses gradient-boosted decision trees and is trained on a set of pre-computed features derived from the data, which include radio-infrared colour indices and the radio spectral index. The second model is trained directly on multi-channel images, employing convolutional neural networks.

Using a completely supervised procedure, we obtained a high classification accuracy (F1-score $>90\%$) for separating Galactic objects from the extragalactic background. Individual class discrimination performances, ranging from 60% to 75%, increased by 10% when adding far-infrared and spectral index information, with extragalactic objects, PNe and HII regions identified with higher accuracies. The implemented tools and trained models were publicly released, and made available to the radioastronomical community for future application on new radio data.

Keywords: Galactic radio sources, Radio source catalogs, Infrared sources, Classification, Astronomy image processing, Convolutional neural networks

1. Introduction

The Square Kilometre Array (SKA) (Dewdney et al., 2016) will open a golden era in radio astronomy due to its anticipated sensitivity, frequency coverage and angular resolution. While the SKA is currently in the construction phase, SKA precursor telescopes have already started their planned survey programs, delivering valuable scientific results even during the commissioning phase. Among them, the Evolutionary Map of the Universe (EMU) program (Norris et al., 2011) of the Australian SKA Pathfinder (ASKAP, Johnston et al. 2008; Hotan et al. 2021) will survey $\sim 75\%$ of the sky at ~ 940 MHz with an angular resolution of $10''$ and a target rms of $15 \mu\text{Jy}/\text{beam}$. As EMU is expected to detect ~ 50 million sources, the cataloguing process will require a significant degree of automation and knowledge extraction

compared to previous surveys. Source finding is a major stage involved in such post-processing of observations.

In the last years, several developments were made within the SKA precursor community, and new tools were produced to improve compact source extraction and measurement capabilities (e.g. completeness, reliability, positional and flux density accuracy) and processing speed, also employing parallel computing methodologies (e.g. see Riggi et al. 2019 and references therein). Fewer efforts, however, has been spent on source classification, particularly for Galactic science targets, as almost all source finders do not provide any information (e.g. labels or tags) on the extracted source class identity. The implication for Galactic plane observations is that, after taking out source classifications made through automated cross-matching to previously classified objects (e.g. $\sim 5\%$ in the Scorpio field in Riggi et al. 2021a), the vast majority of the catalogued sources are unclassified. Of these, more than 90% are typically single-island and single-component

*Corresponding author

Email address: simone.riggi@inaf.it (S. Riggi)

Systematic effects on a Compton polarimeter at the focus of an X-ray mirror

M. Aoyagi^a, R. G. Bose^{b,c}, S. Chun^{b,c}, E. Gau^{b,c}, K. Hu^{b,c}, K. Ishiwata^a,
 N. K. Iyer^{d,e}, F. Kislat^f, M. Kiss^{b,d,e,*}, K. Klepper^{d,e}, H. Krawczynski^{b,c},
 L. Lisalda^{b,c}, Y. Maeda^g, F. af Malmborg^{b,d,e}, H. Matsumoto^{a,h}, A. Miyamotoⁱ,
 T. Miyazawa^{b,j}, M. Pearce^{b,d,e}, B. F. Rauch^{b,c}, N. Rodriguez Caverio^{b,c},
 S. Spooner^{b,f}, H. Takahashi^k, Y. Uchida^l, A. T. West^{b,c,m}, K. Wimalasena^{b,f},
 M. Yoshimoto^{b,a}

^aOsaka University, Department of Earth and Space Science, Graduate School of Science, and Project Research Center for Fundamental Sciences, 1-1 Machikaneyama-cho, Toyonaka, Osaka 560-0043, Japan

^bPhysics Department, Washington University in St. Louis, 1 Brookings Drive, CB 1105, St. Louis, MO 63130, USA

^cMcDonnell Center for the Space Sciences, Washington University in St. Louis, 1 Brookings Drive, CB 1105, St. Louis, MO 63130, USA

^dKTH Royal Institute of Technology, Department of Physics, 106 91 Stockholm, Sweden

^eThe Oskar Klein Centre for Cosmoparticle Physics, AlbaNova University Center, 106 91 Stockholm, Sweden

^fUniversity of New Hampshire, Department of Physics and Astronomy, and Space Science Center, Morse Hall, 8 College Road, Durham, NH 03824, USA

^gInstitute of Space and Astronautical Science, Japan Aerospace Exploration Agency, 3-1-1 Yoshinodai, Sagami-hara, Kanagawa 229-8510, Japan

^hForefront Research Center, Osaka University

ⁱDepartment of Physics, Tokyo Metropolitan University, 1-1 Minami-Osawa, Hachioji, Tokyo 192-0397, Japan

^jOkinawa Institute of Science and Technology Graduate University 1919-1 Tancha, Onna-son, Kunigami-gun Okinawa, Japan 904-0495

^kHiroshima University, 1-3-1 Kagamiyama, Higashi-Hiroshima, Hiroshima 739-8526, Japan

^lTokyo University of Science 2641 Yamazaki, Noda, Chiba 278-8510, Japan

^mCurrently at University of Arizona, Department of Astronomy, Steward Observatory, 933 North Cherry Avenue, Tucson, AZ 85721-0065, USA

Abstract

XL-Calibur is a balloon-borne Compton polarimeter for X-rays in the $\sim 15\text{--}80$ keV range. Using an X-ray mirror with a 12 m focal length for collecting photons onto a beryllium scattering rod surrounded by CZT detectors, a minimum-detectable polarization as low as $\sim 3\%$ is expected during a 24-hour on-target observation of a 1 Crab source at 45° elevation.

*Corresponding author at: KTH Royal Institute of Technology, Department of Physics, 106 91 Stockholm, Sweden

Email address: mozsi@kth.se (M. Kiss)

Primordial black holes as a dark matter candidate - a brief overview

Anne M. Green ^a

^a*University of Nottingham, School of Physics and Astronomy, Nottingham, NG7 2RD, , UK*

Abstract

Historically the most popular dark matter candidates have been new elementary particles, such as Weakly Interacting Massive Particles and axions. However Primordial Black Holes (PBHs), black holes formed from overdensities in the early Universe, are another possibility. The discovery of gravitational waves from mergers of tens of Solar mass black hole binaries by LIGO-Virgo has generated a surge in interest in PBH dark matter. We overview the formation of PBHs, observational probes of their abundance, and some of the key open questions in the field.

Keywords: dark matter, primordial black hole

1. Motivation and history

Primordial Black Holes (PBHs) fulfill all of the necessary requirements to be a good dark matter (DM) candidate. They are cold, non-baryonic and stable, and can be formed in the right abundance to be the DM. Zel'dovich and Novikov (1967) and Hawking (1971) found that Primordial Black Holes may form from overdensities in the early Universe. As they form before nucleosynthesis, PBHs are non-baryonic. PBHs evaporate by emitting Hawking radiation (Hawking, 1975), however a PBH is cosmologically stable (its lifetime is longer than the age of the Universe) if its initial mass is greater than $\sim 10^{15}$ g (Hawking, 1975; Page, 1976). Unlike most other DM candidates (for instance Weakly Interacting Massive Particles, axions, sterile neutrinos,...) PBHs aren't a new particle. However, as we will see in Sec. 2, their formation does typically require 'Beyond the Standard Model' physics, e.g. inflation.

It was realised that PBHs are a DM candidate already in the 1970s (Hawking, 1971; Chapline, 1975). A wave of interest in Solar mass PBH DM occurred in the 1990s, due to the excess of microlensing events observed in the MACHO collaboration's 2 year data set (Alcock et al., 1997). The number of events was larger than expected from known stellar populations, and consistent with roughly half of the Milky Way halo being in Solar mass compact objects. Nakamura et al. (1997) pointed out that if a significant fraction of the DM is in the form of \sim Solar mass PBHs, then PBH binaries would form in the early Universe and (if those binaries survive to the present day) gravitational waves from their coalescence would be detectable by LIGO.

In 2016 LIGO-Virgo announced the discovery of gravitational waves from mergers of tens of Solar mass black holes (BHs) (Abbott et al., 2016). Shortly afterwards several papers appeared (Bird et al., 2016; Clesse and García-Bellido, 2017; Sasaki et al., 2016), suggesting that (some of) these BHs could be primordial, rather than astrophysical, and that these PBHs could also be a significant component of the DM. This has led to another, much larger, wave of interest in PBH DM, with the

number of papers written on PBHs rising to \sim 300 per year.

In Sec. 2 we describe the formation of PBHs, focusing on the collapse of large density perturbations during radiation domination. In Sec. 3 we overview observational probes of the abundance of PBHs. Finally, in Sec. 4, we review some of the key open questions regarding PBH dark matter, before concluding with a summary in Sec. 5.

This brief overview is aimed at readers with knowledge of DM in general, but not PBHs specifically. For longer, more detailed reviews of PBHs as a dark matter candidate with extensive reference lists, see Carr and Kühnel (2020) and Green and Kavanagh (2021). For a 'positivist perspective' on observational evidence for PBHs see Carr et al. (2023), and for future observational searches for PBHs see the Snowmass 2021 white paper (Bird et al., 2023).

2. Formation

We will focus on the most popular, and arguably minimal, PBH formation mechanism, namely the collapse of large density perturbations during radiation domination (Zel'dovich and Novikov, 1967; Hawking, 1971; Carr and Hawking, 1974). These are the same density perturbations that on large scales form galaxies and large scale structure, but on shorter length scales and (if a non-negligible number of PBHs are to form) with a much larger amplitude. If a region is sufficiently overdense then when it enters the horizon (i.e. becomes comparable in length scale to the observable Universe at that time), gravity rapidly overcomes pressure forces and it collapses to form a BH. Other early Universe processes which produce overdensities can also lead to PBH formation. Examples include the collapse of cosmic string loops (Hawking, 1989; Polnarev and Zembowicz, 1991), collisions of bubbles from phase transitions (Hawking et al., 1982), fragmentation of an inflaton scalar condensate (Cotner and Kusenko, 2017) and the collapse of density perturbations during an early period of matter domination (Khlopov and Polnarev, 1980).

How do wavelength correlations affect your transmission spectrum? Application of a new fast and flexible 2D Gaussian process framework to transiting exoplanet spectroscopy

Mark Fortune^{1,*}, Neale P. Gibson¹, Daniel Foreman-Mackey², Thomas Mikal-Evans³, Cathal Maguire¹, Swaetha Ramkumar¹

¹ School of Physics, Trinity College Dublin, University of Dublin, Dublin 2, Ireland

² Center for Computational Astrophysics, Flatiron Institute, New York, NY, USA

³ Max Planck Institute for Astronomy, Königstuhl 17, D-69117 Heidelberg, Germany

Received XXX; accepted XXX

ABSTRACT

The use of Gaussian processes (GPs) is a common approach to account for correlated noise in exoplanet time-series, particularly for transmission and emission spectroscopy. This analysis has typically been performed for each wavelength channel separately, with the retrieved uncertainties in the transmission spectrum assumed to be independent. However, the presence of noise correlated in wavelength could cause these uncertainties to be correlated, which could significantly affect the results of atmospheric retrievals. We present a method which uses a GP to model noise correlated in both wavelength and time simultaneously for the full spectroscopic data set. To make this analysis computationally tractable, we introduce a fast and flexible GP method which can analyse 2D data sets when the input points lie on a (potentially non-uniform) 2D grid - in our case a time by wavelength grid - and the kernel function has a Kronecker product structure. This simultaneously fits all light curves and enables the retrieval of the full covariance matrix of the transmission spectrum. Our new method can avoid the use of a ‘common-mode’ correction which is known to produce an offset to the transmission spectrum. Through testing on synthetic data sets, we demonstrate that our new approach can reliably recover atmospheric features contaminated by noise correlated in time and wavelength. In contrast, fitting each spectroscopic light curve separately performed poorly when wavelength-correlated noise was present. It frequently underestimated the uncertainty of the scattering slope and overestimated the uncertainty in the strength of sharp absorption peaks in transmission spectra. Two archival VLT/FORS2 transit observations of WASP-31b were used to compare these approaches on real observations. Our method strongly constrained the presence of wavelength-correlated noise in both data sets and significantly different constraints on atmospheric features such as the scattering slope and strength of sodium and potassium features were recovered.

Key words. methods: data analysis – methods: statistical – stars: individual (WASP-31) – planets and satellites: atmospheres – techniques: spectroscopic

1. Introduction

Low-resolution transmission spectroscopy has been a powerful technique for probing the atmospheric composition of exoplanets ever since the first detection of an exoplanet atmosphere (Charbonneau et al. 2002). The technique relies upon observing an exoplanet transit - when an exoplanet appears to pass in front of its host star - and analysing the decrease in flux during the transit as a function of wavelength. The resulting transmission spectrum contains information about the planetary atmosphere (Seager & Sasselov 2000; Brown 2001).

The field of exoplanet atmospheres has entered a new era due to the recent launch of JWST. Early Release Science observations of WASP-39b using JWST NIRSpec’s PRISM mode have produced a 33σ detection of H₂O in addition to strong detections of Na, CO and CO₂ (Rustamkulov et al. 2022) - far exceeding what had been achieved with previous ground-based and space-based observations (Nikolov et al. 2016; Sing et al. 2016). As the exoplanet community pushes JWST further to its limits towards smaller terrestrial planets (e.g. Greene et al. 2023; Zieba et al. 2023), the importance of careful treatment of systematics -

astrophysical or instrumental - will become of increasing importance.

Gaussian processes (GPs) were introduced in Gibson et al. (2012b) to account for the uncertainty that correlated noise - also referred to as systematics - produces in the resulting transmission spectrum in a statistically robust way. GPs have been shown to provide more reliable estimates of uncertainties when compared to other common techniques such as linear basis models (Gibson 2014). This difference may help explain contradictory results in the field. For example, WASP-31b was reported to have a strong potassium signal at 4.2σ using data from HST/STIS (Sing et al. 2015) analysed using linear basis models. However, follow-up measurements in Gibson et al. (2017) with the ground-based VLT/FORS2 instrument (Appenzeller et al. 1998) found no evidence of potassium. High-resolution observations in Gibson et al. (2019) using VLT/UVES as well as low-resolution observations from Magellan/IMACS (McGruder et al. 2020) also failed to reproduce this detection. These results are more consistent with the re-analysis of the HST/STIS data using GPs which reduced the significance of the potassium signal to 2.5σ (Gibson et al. 2017), demonstrating the importance of careful treatment of systematics.

* E-mail: fortunma@tcd.ie

Trojan Exoplanets

Philippe Robutel and Adrien Leleu

To be published in: Handbook of Exoplanets, 2nd Edition, Hans Deeg and Juan Antonio Belmonte (Eds. in Chief), Springer International Publishing AG, part of Springer Nature.

Abstract Co-orbital exoplanets are a by-product of the models of formation of planetary systems. However, none have been detected in nature thus far. Although challenging, the observation of co-orbital exoplanets would provide valuable information on the formation of planetary systems as well as on the interactions between planets and their host star. After a brief review of the stability and formation issues of co-orbital systems, some observational methods dedicated to their detection are presented.

Introduction

The existence of Trojans in extrasolar systems has already been discussed in the chapter “Special Cases: Moons, Rings, Comets, and Trojans”. The present chapter generalizes this concept by considering co-orbital planets. This kind of configuration consists of a planet pair trapped in the 1:1 mean motion resonance. Thus, con-

Philippe Robutel
IMCCE, Observatoire de Paris, PSL University, CNRS, Sorbonne Université, 77 avenue Denfert-Rochereau, 75014 Paris, France, e-mail: philippe.robutel@obspm.fr

Adrien Leleu
Observatoire de Genève, Université de Genève, Chemin Pegasi, 51, 1290 Versoix, Switzerland, e-mail: adrien.leleu@unige.ch

On a precessing jet-nozzle scenario with a common helical trajectory-pattern for blazar 3C345

S.J. Qian¹

National Astronomical Observatories, Chinese Academy of Sciences, Beijing 100012, China

Compiled by using A&A latex

ABSTRACT

Context. Based on the possible existence of the jet precession, the kinematics and flux evolution of superluminal components in blazar 3C345 were interpreted in the framework of the precessing jet-nozzle scenario with a precessing common helical trajectory-pattern.

Aims. This study is to show that the jet in 3C345 precesses with a period of 7.3 yr and the superluminal knots move consistently along a precessing common helical trajectory-pattern in their inner jet regions, while in the outer jet regions they follow their own individual tracks. The trajectory-transits can extend to core distances of ~ 1.2 mas, or traveled distances of ~ 300 pc (for example for knots C4 and C9).

Methods. Through model-fitting of the observed kinematic behavior of the superluminal components, their bulk Lorentz factor and Doppler factor are derived as continuous functions of time which were used to investigate their flux evolution.

Results. It is found that the light-curves of the superluminal components observed at 15, 22 and 43 GHz can be well explained by their Doppler boosting effect or model-fitted in terms of their Doppler boosting profiles ($\propto [\delta(t)]^{3+\alpha}$, α -spectral index) associated with their superluminal motion. Additionally, flux fluctuations on shorter time-scales also exist due to variations in knots' intrinsic flux density and spectral index.

Conclusions. The close association of the flux evolution with the Doppler-boosting effect is important, not only firmly validating the precessing jet-nozzle scenario being fully appropriate to explain the kinematics and emission properties of superluminal components in QSO 3C345, but also strongly supporting the traditional common pointview: superluminal components are physical entities (shocks or plasmons) participating relativistic motion towards us with acceleration/deceleration along helical trajectories. Finally, we have proposed both the precessing nozzle scenarios with a single jet and double jets (this paper and Qian [2022b]) to understand the VLBI-phenomena measured in 3C345. VLBI-observations with higher resolutions deep into the core regions (core distances < 0.1 mas) are required to test them.

Key words. galaxies: active – galaxies: nucleus – galaxies: jets – galaxies: individual 3C345

1. Introduction

3C345 ($z=0.595$) is a prototypical quasar emanating emission over the entire electromagnetic spectrum from radio, infrared/optical/UV and X-rays to high-energy γ rays. It is also one of the best-studied blazars. 3C345 is a remarkable compact flat-spectrum radio source which was one of the firstly discovered quasars to have a relativistic jet, emanating superluminal components steadily. Its flaring activities in multifrequency bands (from radio to γ -rays) are closely connected with the jet activity and ejection of superluminal components (Biretta et al. 1986, Hardee 1987, Babadzhantants et al. 1995, Zensus 1997, Klare 2003, Klare et al. 2005, Jorstad et al. 2005, 2013, 2017, Lobanov & Roland 2005, Qian 2009, Schinzel et al. 2010, Schinzel 2011).

Since 1991 (Qian et al. 1991a, 1991b), we have started to interpret the VLBI-phenomenon in QSO 3C345, explaining the kinematics of its superluminal components in terms of a precessing jet-nozzle scenario.

- (1) In the recent work (Qian, 2022a) the kinematics of twenty-seven superluminal components observed during a 38-year period was explained in detail. We proposed the hypothesis that these knots might be possibly di-

vided into two groups (group-A [13knots] and group-B [14 knots]), which were ejected from their precessing nozzles of a double-jet structure (jet-A and jet-B), respectively. Interestingly, it was found that both nozzles precess with the same period 7.3 yr in the same direction (anticlockwise seen in the line of sight). The whole kinematic behaviors of these knots observed by VLBI-observations (including trajectories, coordinates, apparent speed) can be consistently well model-fitted and explained. Their Lorentz and Doppler factor were derived as continuous functions of time. Thus their flux evolution can be investigated.

- (2) In the works of Qian (2022b,2023), the flux evolution of the five knots of group-A (C4, C5, C9, C10 and C22) and the five knots of group-B (C19, C20, C21, B5 and B7) were investigated. It was found that their radio light-curves can be well fitted by their Doppler-boosting profiles. That is, the variability timescales of the knots are consistent with those of their Doppler factor and they light curves are well fitted by Doppler-boosting effect ($\propto [\delta(t)]^{3+\alpha}$; α -spectral index, $S_\nu \propto \nu^{-\alpha}$).
- (3) We also found that the knots of group-A have a precessing common helical trajectory along which they moved according to their precession phases (or ejection

Possible spectral irregularities in the AMS-02 positron spectrum

Xing-Jian Lv,^{1,2,*} Xiao-Jun Bi,^{1,2,†} Kun Fang,^{1,‡} Peng-Fei Yin,^{1,§} and Meng-Jie Zhao^{1,3,¶}

¹Key Laboratory of Particle Astrophysics, Institute of High Energy Physics, Chinese Academy of Sciences, Beijing 100049, China

²University of Chinese Academy of Sciences, Beijing 100049, China

³China Center of Advanced Science and Technology, Beijing 100190, China

(Dated: February 26, 2024)

The excesses in the electron and positron spectra observed by many experiments, such as PAMELA and AMS-02, have sparked significant theoretical investigation. It is not easy to distinguish the two primary hypotheses dark matter annihilation/decay and pulsars from the spectral features. Should pulsars be the source of this excess, the expected variability in their distribution may introduce distinct irregularities in the positron energy spectrum. In this study, we use an irregularity estimator to detect these potential features in the positron energy spectrum of AMS-02. Our analysis of the current AMS-02 data reveals these spectral irregularities with a statistical significance of 1.75σ . However, our projection indicates that, with AMS-02 data collected over a period of 20 years, such irregularities could be identified with a confidence level of 3σ level in 71% of our simulations.

I. INTRODUCTION

Astrophysical evidence overwhelmingly supports the existence of Dark Matter (DM), yet the non-gravitational detection of DM particles remains elusive. The measurements of PAMELA [1] and AMS-02 [2] have reported unexpected excesses in the cosmic ray (CR) positron flux above 10 GeV. These anomalous positron fluxes may originate from DM annihilation or decay within the Galactic halo, e.g. [3–13], or be attributable to nearby astrophysical sources such as pulsars, e.g. [14–25]. Notably, high-energy electrons and positrons undergo substantial energy losses through synchrotron radiation and inverse Compton scattering. The relationship between the maximum energy that electrons and positrons can possess and the source distance R could be estimated by $E_{\max} \approx 100 \text{ GeV} \times (R/2 \text{ kpc})^{-2}$ [26]. Therefore, any potential sources of the positron excess should be nearby, confined to a local volume of approximately $\sim \text{kpc}^3$. The primary objective of this study is to identify an observational signature that could decisively differentiate between these two plausible theoretical propositions.

Pulsars (or pulsar wind nebulae) are established astrophysical accelerators of high-energy electrons and positrons [27], as evidenced by multi-wavelength observations [28]. The discovery of high energy pulsar gamma-ray halos further indicates that the accelerated electrons and positrons can escape from the pulsar wind nebulae and diffuse into the interstellar medium [29–32]. The Milky Way gives rise to pulsars at an approximate rate of one per century [33–37], and these newly formed pulsars

are theorized to impart a significant portion of their rotational energy into electrons and positrons in the initial phase of their life cycle [17, 20, 38]. Due to the necessity

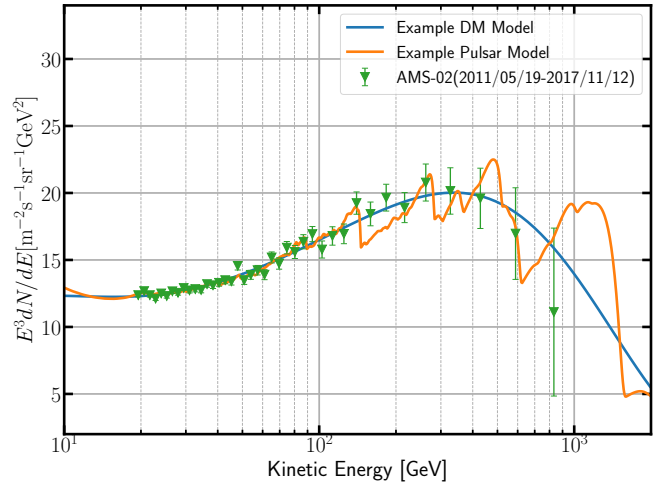


FIG. 1: The AMS-02 positron measurement [2] and two examples of models that fit it well. The orange curve illustrates contributions from a collection of Milky Way pulsars taken from Ref. [38], whereas the purple curve represents a selected DM model. Notably, the DM spectrum manifests as inherently smooth, in contrast to the pulsar spectrum, which reveals discernible contributions from discrete sources.

for any additional sources explaining the positron excess to be nearby, only a limited number of pulsars are in a position to contribute to the positron flux above 10 GeV. This is particularly true when accounting for the slow-diffusion zone surrounding pulsars [39], the scale of which could span tens of parsecs [40, 41]. This scarcity of contributing pulsars may impart discrete features within the CR positron spectra [17, 20, 23, 26, 42, 43], as schematically depicted in Fig. 1. Notably, these characteristics

* lvxj@ihep.ac.cn

† bixj@ihep.ac.cn

‡ fangkun@ihep.ac.cn

§ yinpf@ihep.ac.cn

¶ zhaomj@ihep.ac.cn

The accretion of a solar mass per day by a 17-billion solar mass black hole

Christian Wolf (christian.wolf@anu.edu.au)^{1,2}, Samuel Lai¹,
Christopher A. Onken¹, Neelesh Amrutha¹, Fuyan Bian³, Wei Jeat
Hon⁴, Patrick Tisserand⁵, and Rachel L. Webster⁴

¹Research School of Astronomy and Astrophysics, Australian National
University, Cotter Road Weston Creek, ACT 2611, Australia

²Centre for Gravitational Astrophysics, Australian National University,
Building 38 Science Road, Acton, ACT 2601, Australia

³European Southern Observatory, Alonso de Córdova 3107, Casilla
19001, Vitacura, Santiago 19, Chile

⁴School of Physics, University of Melbourne, Parkville VIC 3010,
Australia

⁵Sorbonne Universités, UPMC Univ Paris 6 et CNRS, Institut
d'Astrophysique de Paris, 98 bis bd Arago, F-75014 Paris, France

draft February 26, 2024

Abstract

Around a million quasars have been catalogued in the Universe by probing deeper and using new methods for discovery. However, the hardest ones to find seem to be the rarest and brightest specimen. In this work, we study the properties of the most luminous of all quasars found so far. It has been overlooked until recently, which demonstrates that modern all-sky surveys have much to reveal. The black hole in this quasar accretes around one solar mass per day onto an existing mass of ~ 17 billion solar masses. In this process its accretion disc alone releases a radiative energy of 2×10^{41} Watts. If the quasar is not strongly gravitationally lensed, then its broad line region (BLR) is expected to have the largest physical and angular diameter occurring in the Universe, and will allow the Very Large Telescope Interferometer to image its rotation and measure its black hole mass directly. This will be an important test for BLR size-luminosity relations, whose extrapolation has underpinned common black-hole mass estimates at high redshift.

Understanding the radio luminosity function of star-forming galaxies and its cosmological evolution

Charles Jose^{1*}, Luke Chamandy^{2,3†}, Anvar Shukurov^{4‡}, Kandaswamy Subramanian^{5,6},
Luiz Felipe S. Rodrigues⁷ and Carlton M. Baugh⁸

¹*Department of Physics, CUSAT, Cochin, 682022, India*

²*National Institute of Science Education and Research, An OCC of Homi Bhabha National Institute, Bhubaneswar 752050, Odisha, India*

³*Department of Physics and Astronomy, University of Rochester, Rochester NY 14627, USA*

⁴*School of Mathematics, Statistics and Physics, Newcastle University, Newcastle upon Tyne, NE1 7RU, UK*

⁵*IUCAA, Post Bag 4, Ganeshkhind, Pune 411007, India*

⁶*Department of Physics, Ashoka University, Rajiv Gandhi Education City, Rai, Sonapat 131029, Haryana, India*

⁷*HAL24K Agri, Uitmeentsestraat 19, 6987 CX Giesbeek, Netherlands*

⁸*Institute for Computational Cosmology, Department of Physics, University of Durham, South Road, Durham DH1 3LE, UK*

Accepted XXX. Received YYY; in original form ZZZ

ABSTRACT

We explore the redshift evolution of the radio luminosity function (RLF) of star-forming galaxies using GALFORM, a semi-analytic model of galaxy formation (SAMGF) and MAGNETIZER, a dynamo model of the magnetic field evolving in a galaxy through its formation history. Assuming energy equipartition between the magnetic field and cosmic rays, we derive the synchrotron luminosity of each sample galaxy. In a model where the turbulent speed is correlated with the star formation rate, the RLF is in fair agreement with observations in the redshift range $0 \leq z \leq 2$. At larger redshifts, the structure of galaxies, their interstellar matter and turbulence appear to be rather different from those at $z \lesssim 2$, so that the turbulence and magnetic field models applicable at low redshifts become inadequate. The strong redshift evolution of the RLF at $0 \leq z \leq 2$ can be attributed to an increased number, at high redshift, of galaxies with large disc volumes and strong magnetic fields. On the other hand, in models where the turbulent speed in galaxies is a constant or assumed to be an explicit function of the redshift, the redshift evolution of the RLF is poorly captured. The evolution of the interstellar turbulence and outflow parameters appear to be major (but not the only) drivers of the RLF changes. We find that both the small- and large-scale magnetic fields contribute significantly to the RLF but the small-scale field dominates at high redshifts. Polarisation observations will therefore be important to distinguish these two components and understand better the evolution of galaxies and their nonthermal constituents.

Key words: galaxies: evolution – galaxies: spiral – radio continuum: galaxies – galaxies: luminosity function – galaxies: magnetic fields – dynamo

1 INTRODUCTION

The galaxy luminosity function (LF) – the comoving number density of galaxies as a function of their magnitude at a given wavelength – is one of the primary observables used to probe the physics of formation and evolution of galaxies. The observed LFs and their redshift evolution have been measured, to various degrees of detail and reliability, for a wide range of wavelengths from the UV to the radio. When assessed in the framework of a theoretical model of galaxy formation, the LFs provide key insights into the evolution of star formation and feedback processes, the nature of and conditions in the ISM (consisting of gas, dust, magnetic fields,

and cosmic rays), and dynamical processes such as galaxy mergers. Two major approaches used to model galaxy formation are: (i) semi-analytic models (SAMGFs) that account for the complex baryonic processes in evolving dark matter (DM) haloes derived from N -body simulations using a combination of analytic approximations and numerical prescriptions, (ii) hydrodynamic or magnetohydrodynamic (MHD) simulations based on fundamental dynamical equations, that include subgrid models to account for unresolved physical processes (often similar to those used in SAMGFs). There are several galaxy formation models (Trayford et al. 2015; Trčka et al. 2022; Croton et al. 2006; Samui et al. 2007; Jose et al. 2013; Lacey et al. 2016) that interpret the ultra-violet (UV) (Wyder et al. 2005; Page et al. 2021), optical (Blanton et al. 2003; Loveday et al. 2012) and infrared (IR) (Dunne et al. 2011; Gruppioni et al. 2013; Marchetti et al. 2016) LFs and shed light on the evolution of obscured star formation rate

* charles.jose@cusat.ac.in

† lchamandy@niser.ac.in

‡ anvar.shukurov@ncl.ac.uk

Magnetic Field at the Galactic Centre from Multi-Wavelength Dust Polarization

M. S. Akshaya^{1*} and Thiem Hoang^{1,2}

¹*Korea Astronomy and Space Science Institute, Daejeon 34055, Republic of Korea*

²*Department of Astronomy and Space Science, University of Science and Technology, 217 Gajeong-ro, Yuseong-gu, Daejeon 34113, Republic of Korea*

Accepted XXX. Received YYY; in original form ZZZ

ABSTRACT

We have mapped the magnetic field (B -field) for a region of about 30 pc around the centre of our Galaxy, which encompasses the circumnuclear disk (CND), the mini-spirals, and the 20 km s^{-1} and 50 km s^{-1} molecular clouds, using thermal dust polarization observations obtained from SOFIA/HAWC+ and JCMT/SCUPOL. We decompose the spectra of ^{12}CO ($J = 3 \rightarrow 2$) transition from this region into individual clustered cloud components and find the polarization observed at different wavelengths might be tracing completely different layers of dust along the line-of-sight (LOS). We use modified Davis–Chandrasekhar–Fermi methods to estimate the B -field from the observations. From our analysis we find the mean strength of the plane-of-sky B -field (B_{pos}) of the CND and the mini-spirals, probed at $53 \mu\text{m}$ to be of the order of $\sim 2 \text{ mG}$. The magnetic field is lowest close to the Galactic Centre, in the region of the ionized mini-cavity within the CND with $B_{\text{pos}} < 1 \text{ mG}$, and increases outwards. However, the longer wavelength polarization at $216 \mu\text{m}$ appears to come from a dust layer that is cooler and behind the CND and has a stronger B -field of about 6 mG . The B -field has the least strength along the Eastern Arm of the mini-spiral, which is also the only region with $\mathcal{M}_A > 1$ and a mass-to-flux ratio of $\lambda \gtrsim 1$. The similarity between the B_{pos} estimates of the $53 \mu\text{m}$ and $850 \mu\text{m}$ observations might indicate them originating from the same depth along the LOS, mostly from the CND and its foreground cloud features, including the negative-longitude extension.

Key words: dust, extinction – Galaxy: centre – infrared: ISM – ISM: magnetic fields – ISM: general – polarization

1 INTRODUCTION

The centre of galaxies play a vital role in their evolution, right from star formation to quenching. A significant fraction of the galactic star formation might be driven by the inflow of material into the galactic centre, whereas the massive outflows from these starburst activities as well as from the supermassive blackhole at the galactic centre (like the Sgr A* in case of the Milky Way) can trigger galactic quenching and hence its evolution (Oort 1977; Kormendy & Kennicutt 2004; Veilleux et al. 2020, and references therein). Only in our Galaxy do we have the capability to study this complex region in great detail at high resolution using various observational techniques like imaging, spectroscopy, and polarimetry. It is well known that the star formation rate (SFR) of the Milky Way is far below what is expected from gravitational collapse of molecular clouds, and the SFR in Galactic Centre (GC) is even lower than the average SFR in the Milky Way, yet the origin for the low SFR in the GC remains elusive (Genzel et al. 2010; Barnes et al. 2017; Bryant & Krabbe 2021; Henshaw et al. 2022, and references therein). Magnetic field (B -field) is one of the popular candidates that can play a role in this suppressed star formation. In order to understand the role of B -fields in star formation and evolution of the GC, it is crucial to map its strength and morphology.

Significant efforts have been made to map the magnetic field of the GC in the past, with most of these studies focused on the circumnuclear disk which is the closest molecular reservoir to Sgr A* (CND; Becklin et al. 1982; Guesten et al. 1987; Jackson et al. 1993). The line-of-sight (LOS) strength of the B -field (B_{LOS}) was estimated from the observations of Zeeman splitting in spectral lines. The average B_{LOS} from the Zeeman measurements at various locations along the CND was about 3 mG (Schwarz & Lasenby 1990; Killeen et al. 1992; Plante et al. 1995; Marshall et al. 1995; Yusef-Zadeh et al. 1996, 1999). Any observed variation between the measurements was attributed to possible changes in the magnetic field orientation.

Aitken et al. (1986) and Aitken et al. (1998) predicted the upper and lower limits of the magnetic field in the region based on the mid-infrared thermal dust polarization observations. They assumed paramagnetic relaxation as the mechanism of grain alignment, and estimate the field to be between $2 - 10 \text{ mG}$ around the GC. However, this assumption no longer holds as recent studies show that paramagnetic relaxation by itself is not strong enough to drive grain alignment (Hoang & Lazarian 2016). Regardless, polarized thermal emission from aligned dust grains is still a popular tool to map the plane-of-sky (POS) magnetic field (B_{pos}). This technique is based on the fact that non-spherical dust grains tend to align with their longest axis perpendicular to the B -fields (Lazarian 2007; Lazarian & Hoang 2007), so that the polarization of thermal emission is perpendicular to the B -fields (Hildebrand 1988). As the result, by observing the

* E-mail: akshayams@kasi.re.kr (MSA)

Investigation of profile shifting and subpulse movement in PSR J0344–0901 with FAST

H. M. TEDILA,^{1,2,3,4,5} R. YUEN,^{3,6} N. WANG,^{3,6} D. LI,^{1,7,8,2,4} Z. G. WEN,^{3,6} W. M. YAN,^{3,6} J. P. YUAN,^{3,6} X. H. HAN,³
P. WANG,^{1,2} W. W. ZHU,^{1,2} S. J. DANG,⁹ S. Q. WANG,³ J. T. XIE,¹⁰ Q. D. WU,^{3,4} SH. KHASANOV,^{11,4,12} AND
FAST COLLABORATION

¹National Astronomical Observatories, Chinese Academy of Sciences, A20 Datun Road, Chaoyang District, Beijing 100101, China

²Key Laboratory of Radio Astronomy and Technology, Chinese Academy of Sciences, A20 Datun Road, Chaoyang District, Beijing, 100101, P.R. China

³Xinjiang Astronomical Observatory, Chinese Academy of Sciences, 150 Science 1-Street, Urumqi, Xinjiang, 830011, People's Republic of China

⁴University of Chinese Academy of Sciences, 19A Yuquan Road, 100049 Beijing, People's Republic of China

⁵Arba Minch University, Arba Minch 21, Ethiopia

⁶Xinjiang Key Laboratory of Radio Astrophysics, 150 Science1-Street, Urumqi, Xinjiang, 830011, People's Republic of China

⁷NAOC-UKZN Computational Astrophysics Centre, University of KwaZulu-Natal, Durban 4000, South Africa

⁸CAS Key Laboratory of FAST, NAOC, Chinese Academy of Sciences, Beijing 100101, People's Republic of China

⁹School of Physics and Electronic Science, Guizhou Normal University, Guiyang, 550001, People's Republic of China

¹⁰Research Center for Intelligent Computing Platforms, Zhejiang Laboratory, Hangzhou, 311100, China

¹¹Institute of Modern Physics, Chinese Academy of Sciences, Lanzhou, 730000, China

¹²Samarkand State University, Samarkand 140104, Uzbekistan

ABSTRACT

We report two phenomena detected in PSR J0344–0901 from two observations conducted at frequency centered at 1.25 GHz using the Five-hundred-meter Aperture Spherical radio Telescope (FAST). The first phenomenon manifests as shifting in the pulse emission to later longitudinal phases and then gradually returns to its original location. The event lasts for about 216 pulse periods, with an average shift of about 0.7° measured at the peak of the integrated profile. Changes in the polarization position angle (PPA) are detected around the trailing edge of the profile, together with an increase in the profile width. The second phenomenon is characterized by the apparent movement of subpulses, which results in different subpulse track patterns across the profile window. For the first time in this pulsar, we identify four emission modes, each with unique subpulse movement, and determine the pattern periods for three of the emission modes. Pulse nulling was not detected. Modeling of the changes in the PPA using the rotating vector model gives an inclination angle of $75.12^\circ \pm 3.80^\circ$ and an impact parameter of $-3.17^\circ \pm 5.32^\circ$ for this pulsar. We speculate that the subpulse movement may be related to the shifting of the pulse emission.

Keywords: profile shifting — pulsars: general — pulsars: individual (PSR J0344–0901)

1. INTRODUCTION

A large diversity of emission variation at different timescales has been observed in radio pulsars. This includes the familiar examples of subpulse drifting, pulse nulling, and profile mode-changing. More than half of the radio pulsars sampled (Weltevrede et al. 2006, 2007)

was found with measurable drift of subpulses from one pulse to the next through the integrated profile window. There is also evidence from both radio and γ -ray observations that a pulsar magnetosphere may exhibit some kind of changes, which affect the subpulse drift pattern (Stairs et al. 2000; Lyne et al. 2010; Kramer et al. 2006; Allafort et al. 2013; Keith et al. 2013). From the observations of pulsars with multiple subpulse drift modes (Smits et al. 2005), each with particular drift rate and pattern, the subpulse drift rate can vary abruptly and then returns to its initial value. In addition, the changes between different subpulse drift modes have been ob-

Corresponding author: R. Yuen, N. Wang

ryuen@xao.ac.cn

na.wang@xao.ac.cn



Magnetar as the Central Engine of AT2018cow: Optical, Soft X-Ray, and Hard X-Ray Emission

Long Li^{1,2} , Shu-Qing Zhong^{1,2} , Di Xiao³ , Zi-Gao Dai^{1,2} , Shi-Feng Huang^{1,2} , and Zhen-Feng Sheng⁴ ¹ Department of Astronomy, University of Science and Technology of China, Hefei 230026, People's Republic of China; lilong1125@ustc.edu.cn, daizg@ustc.edu.cn² School of Astronomy and Space Science, University of Science and Technology of China, Hefei 230026, People's Republic of China³ Purple Mountain Observatory, Chinese Academy of Sciences, Nanjing 210023, People's Republic of China⁴ Institute of Deep Space Sciences, Deep Space Exploration Laboratory, Hefei 230026, People's Republic of China

Received 2023 October 30; revised 2024 January 20; accepted 2024 February 3; published 2024 February 21

Abstract

AT2018cow is the most extensively observed and widely studied fast blue optical transient to date; its unique observational properties challenge all existing standard models. In this paper, we model the luminosity evolution of the optical, soft X-ray, and hard X-ray emission, as well as the X-ray spectrum of AT2018cow with a magnetar-centered engine model. We consider a two-zone model with a striped magnetar wind in the interior and an expanding ejecta outside. The soft and hard X-ray emission of AT2018cow can be explained by the leakage of high-energy photons produced by internal gradual magnetic dissipation in the striped magnetar wind, while the luminous thermal UV/optical emission results from the thermalization of the ejecta by the captured photons. The two-component energy spectrum yielded by our model with a quasi-thermal component from the optically thick region of the wind superimposed on an optically thin synchrotron component well reproduces the X-ray spectral shape of AT2018cow. The Markov Chain Monte Carlo fitting results suggest that in order to explain the very short rise time to peak of the thermal optical emission, a low ejecta mass $M_{ej} \approx 0.1 M_{\odot}$ and high ejecta velocity $v_{SN} \approx 0.17c$ are required. A millisecond magnetar with $P_0 \approx 3.7$ ms and $B_p \approx 2.4 \times 10^{14}$ G is needed to serve as the central engine of AT2018cow.

Unified Astronomy Thesaurus concepts: Magnetars (992); X-ray transient sources (1852); Supernovae (1668); Core-collapse supernovae (304)

1. Introduction

High-cadence surveys over the last decade have discovered a plethora of rapidly evolving transients suggested to have diverse physical origins (see Inserra 2019, for a review). “Fast blue optical transients” (FBOTs; Drout et al. 2014; Arcavi et al. 2016; Tanaka et al. 2016; Pursiainen et al. 2018; Ho et al. 2023) are a subset of those typically characterized by a blue color ($g - r \lesssim -0.2$ mag at peak) and a rapid light curve (time above half-maximum luminosity $t_{1/2} \lesssim 12$ days). AT2018cow (Prentice et al. 2018; Margutti et al. 2019; Perley et al. 2019), the most widely studied FBOT, exhibits peculiar observational properties that challenge all standard models.

AT2018cow boasts the richest set of observations among FBOTs, with emissions ranging from radio to hard X-rays (Prentice et al. 2018; Rivera Sandoval et al. 2018; Ho et al. 2019; Kuin et al. 2019; Margutti et al. 2019; Perley et al. 2019; Nayana & Chandra 2021). The UV+UBV emission from AT2018cow can be aptly modeled using blackbody radiation spectrum, with no evidence of a transition to the nebular phase within 90 days (Margutti et al. 2019). However, the near-infrared+RI emission clearly exceeds the thermal blackbody emission, suggesting that they might stem from a different underlying mechanism or source (Margutti et al. 2019; Perley et al. 2019; Metzger & Perley 2023). Within a few days the bolometric luminosity rises to a peak of $L_{bol} \approx 4 \times 10^{44}$ erg s⁻¹ and then declines with $L_{bol} \propto t^{-2.5}$. AT2018cow also exhibited a luminous and highly variable soft X-ray emission in the

0.3–10 keV range, with a luminosity measured at $L_X \sim 10^{43}$ erg s⁻¹ initially. The soft X-ray flaring shows short variability timescales of a few days, overlaying an initial gradual decay $\propto t^{-1}$ that later steepens to a faster $\propto t^{-4}$ rate (Rivera Sandoval et al. 2018; Kuin et al. 2019; Margutti et al. 2019). Furthermore, a hard X-ray component of emission, spanning 20–200 keV with distinct temporal and spectral properties, was detected at ~ 8 days and dissipated by ~ 17 days (Margutti et al. 2019). The spectra of joint soft and hard X-rays can be described by an absorbed power-law component superposed by an additional absorbed cutoff power-law component (Margutti et al. 2019). The total luminosity from the thermal UV/optical and X-ray emissions decays according to $\propto t^{-2}$ (Margutti et al. 2019). In addition, AT2018cow shows bright radio and millimeter emission, consistent with self-absorbed synchrotron radiation from shock interaction between fast ejecta and dense external medium (Ho et al. 2019; Margutti et al. 2019; Nayana & Chandra 2021).

The optical emission of AT2018cow cannot be powered dominantly by the radioactive decay of ⁵⁶Ni, which is the standard energy source model for normal supernovae (SNe), as its large bolometric peak luminosity and short rise to peak time require a ⁵⁶Ni mass of $\sim 6 M_{\odot}$ but an ejecta mass of $\lesssim 1 M_{\odot}$. There are so many theories and explanations in the literature about the progenitor system and energy source of AT2018cow, including a successful SN with a low-mass ejecta giving birth to a millisecond magnetar as the central engine (Fang et al. 2019; Margutti et al. 2019; Mohan et al. 2020); accretion-induced collapse (AIC) of the product of double white dwarf (WD) merger between ONeMg WD and another WD giving birth to a millisecond magnetar (Lyutikov & Toonen 2019; Lyutikov 2022); AIC of a WD in a binary with a nondegenerate

The use of Specutils by Data Central

James Tocknell¹

¹*Australian Astronomical Optics - Macquarie, Faculty of Science and Engineering, Macquarie University, North Ryde, NSW 2113, Australia;*
james.tocknell@mq.edu.au

Abstract.

Specutils is an Astropy affiliated package which provides a consistent interface to astronomical spectra (primarily 1D). As Specutils can be adapted to parse spectra in many different formats, Specutils plays a key role at Data Central, allowing us to handle the diverse formats provided to us by survey teams. In this poster, I will cover what Specutils is, how it works, how Data Central uses it, and why you too should use and contribute to it.

1. What is Specutils

Specutils (Astropy-Specutils Development Team 2019) is an Astropy coordinated python package, that is, it is centrally maintained by the Astropy Project (Astropy Collaboration et al. 2013, 2018, 2022). Specutils provides three key classes: `Spectrum1D`, `SpectrumCollection`, and `SpectrumList`¹; these are built on core Astropy classes, allowing the usual interaction with arithmetic, slicing and units.

Specutils provides numerous routines that consume these classes, providing such features as: line and continuum fitting; smoothing, convolution and resampling; template matching and uncertainty estimation; and reddening of model spectra.

Specutils also ties into the Astropy IO registry system², providing a user-friendly interface to read and write the various formats spectra are stored in. There is support for more generic formats such as ASCII tables or CSV, but also for more specific formats such as IRAF's FITS, and instrument or survey-specific formats such as HST, Subaru, SDSS and MaNGA. By using the Astropy IO registry system, significant proportions of a codebase can be written to be independent of the underlying file format, reducing its maintenance cost.

¹Documentation for these classes, as well as the rest of Specutils, can be found at <https://specutils.readthedocs.io/>

²Details about the Astropy IO registry system can be found at <https://docs.astropy.org/en/stable/io/registry.html>.

ALMA-IMF XI: The sample of hot core candidates

A rich population of young high-mass proto-stars unveiled by the emission of methyl formate

M. Bonfand^{1,2}, T. Csengeri², S. Bontemps², N. Brouillet², F. Motte³, F. Louvet³, A. Ginsburg⁴, N. Cunningham³, R. Galván-Madrid⁵, F. Herpin², F. Wyrowski⁶, M. Valeille-Manet², A. M. Stutz^{7,8}, J. Di Francesco⁹, A. Gusdorf^{10,11}, M. Fernández-López¹², B. Lefloch², H.-L. Liu^{7,13}, P. Sanhueza^{14,15}, R. H. Álvarez-Gutiérrez⁷, F. Olguin¹⁶, T. Nony⁵, A. Lopez-Sepulcre^{3,17}, P. Dell'Ova^{10,11}, Y. Pouteau³, D. Jeff⁴, H.-R. V. Chen¹⁶, M. Armante^{10,11}, A. Towner¹⁸, L. Bronfman¹⁹, and N. Kessler²

(Affiliations can be found after the references)

Received 1 September 2023; accepted 22 February 2024

ABSTRACT

Context. The star formation process leads to an increased chemical complexity in the interstellar medium. Sites associated with high-mass star and cluster formation exhibit a so-called hot core phase, characterized by high temperatures and column densities of complex organic molecules.

Aims. We aim to systematically search for and identify a sample of hot cores towards the 15 Galactic protoclusters of the ALMA-IMF Large Program and investigate their statistical properties.

Methods. We built a comprehensive census of hot core candidates towards the ALMA-IMF protoclusters based on the detection of two CH₃OCHO emission lines at 216.1 GHz. We used the source extraction algorithm *GExt2D* to identify peaks of methyl formate (CH₃OCHO) emission that is a complex species commonly observed towards sites of star formation. We performed a cross-matching with the catalog of thermal dust continuum sources from the ALMA-IMF 1.3 mm continuum data to infer their physical properties.

Results. We built up a catalog of 76 hot core candidates with masses ranging from $\sim 0.2 M_{\odot}$ to $\sim 80 M_{\odot}$, of which 56 are new detections. A large majority of these objects, identified in methyl formate emission are compact, rather circular, with deconvolved FWHM sizes of ~ 2300 au on average. The central sources of two target fields show more extended methyl formate emission, that is rather circular, with deconvolved FWHM sizes of ~ 6700 au and 13400 au. About 30% of our sample of methyl formate sources have core masses above $8 M_{\odot}$ within sizes ranging from ~ 1000 au to 13400 au, which well correspond to archetypical hot cores. The origin of the CH₃OCHO emission toward the lower-mass cores can be explained by a mixture of contribution from shocks, or may correspond to objects in a more evolved state, *i.e.* beyond the hot core stage. We find that the fraction of hot core candidates increases with the core mass, suggesting that the brightest dust cores are all in the hot core phase.

Conclusions. Our results suggest that most of these compact methyl formate sources are readily explained by simple symmetric models, while collective effects from radiative heating and shocks from compact protoclusters are needed to explain the observed extended CH₃OCHO emission. The large fraction of hot core candidates towards the most massive cores suggests that they rapidly enter the hot core phase and feedback effects from the forming protostar(s) impact their environment on short time-scales.

Key words. stars: formation – stars: massive – stars: formation – stars: protostars – ISM: abundances – ISM: molecules – radio lines: ISM – Line: formation – Line: profiles

1. Introduction

Star formation plays a key role in building the complex inventory of interstellar chemical species in various astronomical sources, which in turn serve as powerful diagnostic tools to study their surrounding environment (see e.g., Jørgensen et al. 2020; Ceccarelli et al. 2022, and references therein). Through the observation of molecular emission lines, it is possible to investigate the still poorly constrained physical conditions and chemical processes that connect the different stages of star formation. In comparison to low-mass stars, the formation process of high-mass stars ($M_{\star} > 8 M_{\odot}$) is still less well-understood (Tan et al. 2013; Motte et al. 2018a). The early evolutionary stage of high-mass star formation is expected to be short. For example, Motte et al. (2007) estimate a pre-stellar phase of $< 10^4$ yr based on the core population in Cygnus-X, Bonfand et al. (2017) estimated a lifetime of 6×10^4 yr for the hot core phase in the Galactic center molecular cloud Sgr B2(N), and Csengeri et al. (2014) estimate $\sim 7.5 \times 10^4$ yr for the phase prior to the emergence

of strong infrared emission, corresponding to stars of type B0 or earlier, based on the statistics of massive clumps uncovered by the ATLASGAL survey. In addition, both mechanical and radiative feedback effects from already formed (proto)stars in a clustered environment complicate the physical and chemical structure of high-mass star-forming regions further. As a consequence, the evolutionary sequence for high-mass star formation remains inadequately tested. Nevertheless, different observational signatures can be used to characterize the deeply embedded protostar, such as hot molecular cores, hyper-, and ultra-compact HII regions that are exclusively associated with sites of high-mass star and cluster formation. Hyper-, and ultra-compact HII regions are characterised by free-free emission from ionised gas pinpointing a (proto)stellar mass $> 8-15 M_{\odot}$ (Hosokawa & Omukai 2009). Free-free emission may also arise from an ionising jet component (for a review see e.g. Anglada et al. 2018). Hot molecular cores (HCs) are identified based on association with a

Multiple Patchy Cloud Layers in the Planetary Mass Object SIMP0136+0933

ALLISON M. MCCARTHY ¹, PHILIP S. MUIRHEAD ¹, PATRICK TAMBURO ², JOHANNA M. VOS ^{3,4},
CAROLINE V. MORLEY ⁵, JACQUELINE FAHERTY ⁴, DANIELLA C. BARDALEZ GAGLIUFFI ^{6,4}, ERIC AGOL ⁷ AND
CHRISTOPHER THEISSEN ⁸

¹*Department of Astronomy & The Institute for Astrophysical Research, Boston University, 725 Commonwealth Ave., Boston, MA 02215, USA*

²*Center for Astrophysics | Harvard & Smithsonian, 60 Garden Street, Cambridge, MA 02138, USA*

³*School of Physics, Trinity College Dublin, The University of Dublin, Dublin 2, Ireland*

⁴*Department of Astrophysics, American Museum of Natural History, New York, NY 10024, USA*

⁵*Department of Astronomy, University of Texas at Austin, Austin, TX 78712, USA*

⁶*Department of Physics & Astronomy, Amherst College, 25 East Drive, Amherst, MA 01003, USA*

⁷*Department of Astronomy & Virtual Planetary Laboratory, University of Washington, Box 351580, U.W., Seattle, WA 98195, USA*

⁸*Department of Astronomy & Astrophysics, University of California, San Diego, 9500 Gilman Drive, La Jolla, CA 92093-0424, USA*

ABSTRACT

Multi-wavelength photometry of brown dwarfs and planetary-mass objects provides insight into their atmospheres and cloud layers. We present near-simultaneous J - and K_s -band multi-wavelength observations of the highly variable T2.5 planetary-mass object, SIMP J013656.5+093347. We reanalyze observations acquired over a single night in 2015 using a recently developed data reduction pipeline. For the first time, we detect a phase shift between J - and K_s -band light curves, which we measure to be $39.9_{-1.1}^{+3.6}$. Previously, phase shifts between near-infrared and mid-infrared observations of this object were detected and attributed to probing different depths of the atmosphere, and thus different cloud layers. Using the Sonora Bobcat models, we expand on this idea to show that at least two different patchy cloud layers must be present to explain the measured phase shift. Our results are generally consistent with recent atmospheric retrievals of this object and other similar L/T transition objects.

Keywords: Brown Dwarfs (185), T dwarfs (1679), Stellar Atmospheres (1584), Exoplanet Atmospheres (487), Exoplanet Atmospheric Variability (2020), Exoplanet Atmospheric Structure (2310)

1. INTRODUCTION

Photometric variability monitoring is a useful tool for understanding the atmospheric structure of brown dwarfs, planetary-mass objects, and exoplanets. The observed variability is attributed to inhomogeneous cloud cover (Radigan 2014), thermochemical instabilities (Tremblin et al. 2016), temperature fluctuations (Robinson & Marley 2014), and/or auroral activity (Hallinan et al. 2015). Cloud structures typically persist for longer than one rotation (Metchev et al. 2015; Apai et al. 2017), and as a result, we can probe the presence of these clouds by measuring the brightness

of a planetary-mass object as it rotates. Past variability surveys in the infrared revealed trends with spectral type (Radigan 2014; Metchev et al. 2015), gravity (Vos et al. 2019, 2022), and inclination (Vos et al. 2017). The objects within the L/T transition, spanning from late-L to early-T, are known for having the largest variability amplitude (e.g. Radigan 2014; Metchev et al. 2015). Recently, Ashraf et al. (2022) found that variable objects can be detected by peculiarities in time-integrated spectra.

While single-wavelength variability monitoring observations have revealed a large population of variable brown dwarfs and planetary-mass objects, multi-wavelength monitoring allows us to study time-dependent effects across the vertical structure of layers within the atmosphere. Additionally, simultaneous mul-

Binary origin of blue straggler stars in Galactic star clusters

M. J., Rain¹, M.S., Pera^{3,4}, G.I., Perren^{2,4}, O.G., Benvenuto^{2,5}, J.A., Panei^{2,5}, M.A. De Vito^{2,5}, G. Carraro⁶, and S. Villanova⁷

¹ European Southern Observatory, Alonso de Córdova 3107, Vitacura, Región Metropolitana, Chile
e-mail: mrainsep@eso.org

² Instituto de Astrofísica de La Plata, IALP (CONICET-UNLP), 1900 La Plata, Argentina

³ Instituto de Física de Rosario, IFIR (CONICET-UNR), 2000 Rosario, Argentina

⁴ Facultad de Ciencias Exactas, Ingeniería y Agrimensura (UNR), 2000 Rosario, Argentina

⁵ Facultad de Ciencias Astronómicas y Geofísicas, Universidad Nacional de La Plata (UNLP), La Plata, Argentina

⁶ Dipartimento di Fisica e Astronomia, Università di Padova, Vicolo Osservatorio 3, I-35122, Padova, Italy

⁷ Departamento de Astronomía, Universidad de Concepción, 160 Casilla, Concepción, Chile

Received September XX, XXXX; accepted March YY, YYYY

ABSTRACT

Building on the recent release of a new *Gaia*-based blue straggler star catalog in Galactic open star clusters (OCs), we explored the properties of these stars in a cluster sample spanning a wide range in fundamental parameters. We employed *Gaia* EDR3 to assess the membership of any individual blue or yellow straggler to their parent cluster. We then made use of the *ASteCA* code to estimate the fundamental parameters of the selected clusters, in particular, the binary fraction. With all this at hand, we critically revisited the relation of the blue straggler population and the latter. For the first time, we found a correlation between the number of blue stragglers and the host cluster binary fraction and binaries. This supports the hypothesis that binary evolution is the most viable scenario of straggler formation in Galactic star clusters. The distribution of blue stragglers in the *Gaia* color-magnitude diagram was then compared with a suite of composite evolutionary sequences derived from binary evolutionary models that were run by exploring a range of binary parameters: age, mass ratio, period, and so forth. The excellent comparison between the bulk distribution of blue stragglers and the composite evolutionary sequences loci further supports the binary origin of most stragglers in OCs and paves the way for a detailed study of individual blue stragglers.

Key words. star clusters and associations: general — stars: blue stragglers — binaries: general

1. Introduction

Defying the traditional single stellar evolution with their position in the optical color-magnitude diagram (CMD), they are bluer and brighter than the main-sequence turn-off (MS-TO) of the system in which they are found, blue straggler stars (BSSs) and recently, yellow straggler stars (YSSs, which may be evolved BSSs) are exotic objects that have fascinated theorists and observers equally for generations. While BSSs were initially discovered in globular clusters (GCs; Piotto et al. 2004; Salinas et al. 2012), they are now known to exist in open clusters (OCs; Ahumada & Lapasset 2007; Rain et al. 2021a), dwarf galaxies (Momany et al. 2007), and even in the field of the Milky Way (e.g., Santucci et al. 2015). Since their detection on the core of globular cluster M3 (Sandage 1953), many formation mechanisms have been proposed. Most of them agree that a main sequence (MS) star has gained mass either through mass transfer (MT) from an evolving primary star via Roche-lobe overflow (RLOF) (McCrea 1964) and/or via collisions involving single, binary, or even triple stars (Hills & Day 1976). The two basic scenarios can be modified by the presence of a third or additional star. Perets & Fabrycky (2009) proposed a scenario in which the inner binary in a hierarchical triple system can coalesce due to perturbations of the outer companion, producing in the end a BSS in a binary system with a long period.

With the advent of the second *Gaia* data release, a renaissance of the study of BSSs on individuals and across a large sample of OCs took recently place (Bhattacharya et al. 2019; Rain et al. 2020; Vaidya et al. 2020; Rain et al. 2021b; Jadhav & Subramaniam 2021; Leiner & Geller 2021; Rain et al. 2021a; Jadhav & Subramaniam 2021; Rao et al. 2023; Rani et al. 2023). It is possible today to accurately identify genuine BSSs candidates while distinguishing them from outliers and field stars by combining *Gaia* parallax measurements, proper motions, and star colors to establish membership with a high degree of certainty. In this study, we use *Gaia* EDR3 to select members of a sample of 12 old (> 9.0 Gyr), relatively nearby ($d < 5000$ parsecs), rich OCs, with the goal of understanding the BS population and their connection with binaries in the host cluster.

The data on BSSs and YSSs allow us to perform a detailed comparison with theoretical predictions. For this purpose, we present detailed calculations of binary evolution to explore whether the hypothesis of a binary origin holds. The quantities necessary to define a particular binary are the stellar masses, the orbital period of the pair, and the type of mass transfer, conservative or nonconservative. Thus, performing a full exploration of the parameter space of the problem represents a major numerical effort that may be warranted in a future study. We restrict ourselves here to a given (fixed) initial mass ratio and conservative MT.

The layout of this study is as follows: We first describe our selection of the sample and the cluster members in § 2, and in § 3,

Correlations between Ca II H&K Emission and the Gaia M dwarf Gap

EMILY M. BOUDREAUX,¹ AYLIN GARCIA SOTO,¹ AND BRIAN C. CHABOYER¹

¹*Department of Physics and Astronomy, Dartmouth College, Hanover, NH 03755, USA*

(Received 02/07/2024; Revised 02/20/2024; Accepted 02/22/2024)

Submitted to ApJ

ABSTRACT

The Gaia M dwarf gap, also known as the Jao Gap, is a novel feature discovered in the Gaia DR2 G vs. BP-RP color magnitude diagram. This gap represents a 17 percent decrease in stellar density in a thin magnitude band around the convective transition mass ($\sim 0.35M_{\odot}$) on the main sequence. Previous work has demonstrated a paucity of Hydrogen Alpha emission coincident with the G magnitude of the Jao Gap in the solar neighborhood. The exact mechanism which results in this paucity is as of yet unknown; however, the authors of the originating paper suggest that it may be the result of complex variations to a star's magnetic topology driven by the Jao Gap's characteristic formation and breakdown of stars' radiative transition zones. We present a follow up investigating another widely used magnetic activity metric, Calcium II H&K emission. Ca II H&K activity appears to share a similar anomalous behavior as H α does near the Jao Gap magnitude. We observe an increase in star-to-star variation of magnetic activity near the Jao Gap. We present a toy model of a stars magnetic field evolution which demonstrates that this increase may be due to stochastic disruptions to the magnetic field originating from the periodic mixing events characteristic of the convective kissing instabilities which drive the formation of the Jao Gap.

Keywords: Stellar Evolution (1599) — Stellar Evolutionary Models (2046)

1. INTRODUCTION

The initial mass requirements of molecular clouds collapsing to form stars results in a strong bias towards lower masses and later spectral classes during star formation. Partly as a result of this bias and partly as a result of their extremely long main-sequence lifetimes, M Dwarfs make up approximately 70 percent of all stars in the galaxy (Winters et al. 2019). Moreover, many planet search campaigns have focused on M Dwarfs due to the relative ease of detecting small planets in their habitable zones (e.g. Nutzman & Charbonneau 2008). M Dwarfs then represent both a key component of the galactic stellar population as well as the most numerous possible set of stars which may host habitable exoplanets. Given this key location M Dwarfs occupy in modern astronomy it

is important to have a thorough understanding of their structure and evolution.

Jao et al. (2018) discovered a novel feature in the Gaia Data Release 2 (DR2) $G_{BP} - G_{RP}$ color-magnitude diagram. Around $M_G = 10$ there is an approximately 17 percent decrease in stellar density of the sample of stars Jao et al. (2018) considered. Subsequently, this has become known as either the Jao Gap, or Gaia M Dwarf Gap. Following the initial detection of the Gap in DR2 the Gap has also potentially been observed in 2MASS (Skrutskie et al. 2006; Jao et al. 2018); however, the significance of this detection is quite weak and it relies on the prior of the Gap's location from Gaia data. The Gap is also present in Gaia Early Data Release 3 (EDR3) (Jao & Feiden 2021). These EDR3 and 2MASS data sets then indicate that this feature is not a bias inherent to DR2.

The Gap is generally attributed to convective instabilities in the cores of stars straddling the fully convective transition mass (0.3 - 0.35 M_{\odot}) known as convective kissing instabilities (Baraffe & Chabrier 2018). These

Corresponding author: Emily M. Boudreaux
emily.m.boudreaux.gr@dartmouth.edu,
emily@boudreauxmail.com

The *Gaia* white dwarf revolution

Pier-Emmanuel Tremblay^a, Antoine Bédard^a, Mairi W. O’Brien^a, James Munday^a, Abigail K. Elms^a, Nicola Pietro Gentillo Fusillo^b, Snehalata Sahu^a

^a*Department of Physics, University of Warwick, Coventry, CV4 7AL, UK*

^b*Università degli studi di Trieste, Via Valerio, 2, Trieste, 34127, Italy*

Abstract

This review highlights the role of the *Gaia* space mission in transforming white dwarf research. These stellar remnants constitute 5-7% of the local stellar population in volume, yet before *Gaia* the lack of trigonometric parallaxes hindered their identification. The mission’s Data Release 2 in 2018 provided the first unbiased colour-absolute magnitude diagram of the local stellar population, identifying 260 000 white dwarfs, with the number later increasing to over 355 000 in Data Release 3. Since then, more than 400 white dwarf studies have made critical use of *Gaia* data, establishing it as a fundamental resource for white dwarf identification, fundamental parameter determination and more recently spectral type characterisation. The review underscores the routine reliance on *Gaia* parallaxes and extensive use of its photometry in white dwarf surveys. We also discuss recent discoveries firmly grounded *Gaia* data, including white dwarf mergers, exotic compact binaries and evolved planetary systems.

Keywords: white dwarfs, astrometry, stars: evolution, stars: statistics, (Galaxy:) solar neighborhood

PACS: 0000, 1111

2000 MSC: 0000, 1111

1. Introduction

At the end of the life cycle of a star less massive than 8–10 M_{\odot} , the remaining core, composed mostly of carbon, oxygen, and in some cases neon, contracts into a white dwarf. These are the most common stellar remnants, accounting for 5-7% of the local stellar population (Gaia Collaboration et al.,

Methods for the detection of stellar rotation periods in individual TESS sectors and results from the Prime mission

ISABEL L. COLMAN ¹ RUTH ANGUS ^{1,2} TREVOR DAVID ^{2,1} JASON CURTIS ³ SOICHIRO HATTORI ^{3,1} AND YUXI (LUCY) LU ¹

¹*Department of Astrophysics, American Museum of Natural History, 200 Central Park West, New York, NY 10024, USA*

²*Center for Computational Astrophysics, Flatiron Institute, 162 5th Avenue, New York, NY 10010, USA*

³*Department of Astronomy, Columbia University, 550 West 120th Street, New York, NY 10027, USA*

(Accepted 2024-02-16)

ABSTRACT

For ongoing studies of the role of rotation in stellar evolution, we require large catalogs of rotation periods for testing and refining gyrochronology. While there is a wealth of data from the Kepler and K2 missions, TESS presents both an opportunity and a challenge: despite its all-sky coverage, rotation periods remain hard to detect. We analyzed individual TESS sectors to detect short-period stellar rotation, using only parameters measured from light curves for a robust and unbiased method of evaluating detections. We used random forest classifiers for vetting, trained on a large corpus of period measurements in KELT data from the Oelkers et al. (2018) catalog and using TESS full-frame image light curves generated by *leanor* (Feinstein et al. 2019). Finally, using data from the first 26 sectors of TESS, we analyzed 432,704 2-minute cadence single-sector light curves for FGKM dwarfs. We detected 16,800 periods in individual sector light curves, covering 10,909 distinct targets, and we present a catalog of the median period for each target as measured by a Lomb-Scargle periodogram.

Keywords: Stellar rotation (1629) — Period determination (1211) — Astronomy data analysis (1858) — Random forests (1935)

1. INTRODUCTION

An understanding of stellar rotation is key to the study of stellar evolution, due to the phenomenon of spin down: the process by which a star gradually rotates more slowly over the course of its main sequence lifetime. The process of determining a precise main sequence stellar age from a star’s rotation period is known as gyrochronology (Barnes 2003). Since the first observation of a power law relation between stellar spin down and age (Skumanich 1972) and the earliest detections to support this from ground-based rotational velocity studies (e.g. Smith 1979; Vaughan & Preston 1980; Vogel & Kuhi 1981), the question of defining gyrochronological relations has only become more complex (Angus et al. 2019; Bouma et al. 2023). To deepen our understanding of these phenomena, we need as many measurements of stellar rotation as possible, from a sample that includes main sequence stars across a wide range of masses, metallicities, and ages. In the spirit of pursuing this goal, our introduction surveys the lineage of the study of stellar rotation using space-based data, to situate our work in its broader context and provide motivation for the refinement of detection, classification, and characterization methods that is undertaken in the larger part of this paper. The Kepler mission (Borucki et al. 2010) represented a massive increase in the volume of available rotation periods, with its high quality time series data spanning four years of continuous observation (e.g. McQuillan et al. 2014; Santos et al. 2021). Rotation is measured in time series data using methods familiar from the detection of exoplanets and other variability: periodicity appears in light curves due to star spots on the surface, dark regions of low magnetic activity, which cause dips in brightness as they pass into our line of sight due to stellar rotation. For the first time

LETTER TO THE EDITOR

Hydrogenated amorphous carbon grains as an alternative carrier of the 9–13 μm plateau feature in the fullerene planetary nebula Tc 1

M. A. Gómez-Muñoz^{1,2}, D. A. García-Hernández^{1,2}, R. Barzaga^{1,2}, A. Manchado^{1,2,3}, and T. Huertas-Roldán^{1,2}

¹ Instituto de Astrofísica de Canarias, E-38205 La Laguna, Tenerife, Spain
e-mail: magm@iac.es, agarcia@iac.es

² Departamento de Astrofísica, Universidad de La Laguna, E-38206 La Laguna, Tenerife, Spain

³ Consejo Superior de Investigaciones Científicas (CSIC), 28006 Madrid, Spain

Received 22 December 2023; Accepted 05 February 2024

ABSTRACT

Fullerenes have been observed in several astronomical objects since the discovery of C₆₀ in the mid-infrared (mid-IR) spectrum of the planetary nebula (PN) Tc 1. It has been suggested that the carriers of the broad unidentified infrared (UIR) plateau features, such as the 9–13 μm emission feature (12 μm hereafter), may be related to the formation of fullerenes. In particular, their carriers have been suggested to be mixed aromatic or aliphatic hydrocarbons such as hydrogenated amorphous carbon (HAC-like hereafter) grains. For this study, we modeled the mid-IR emission of the C₆₀-PN Tc 1 with a photoionization code, including for the first time the laboratory optical constants (n and k indices) of HAC-like dust at 300 K. Interestingly, we find that the broad 12 μm plateau feature in Tc 1 is well reproduced by using a distribution of canonical HAC grains, while at the same time they provide an important fraction of the IR dust continuum emission and are consistent with the other UIR features observed (e.g., the broad 6–9 μm plateau feature). This finding suggests that HAC-like grains may be possible carriers of the 12 μm plateau feature, being likely related to the fullerene formation mechanism in PNe. More laboratory experiments, to obtain the optical constants of HAC-like dust with several structures or a composition at different physical conditions, are strongly encouraged – that is, in order to extend this pilot study to more fullerene PNe, and to unveil the details of fullerene formation and of the potential carriers of the elusive UIR plateau features.

Key words. astrochemistry – circumstellar matter – infrared: stars — planetary nebulae: general – stars: AGB and post-AGB

1. Introduction

Planetary nebulae (PNe) represent the late stages in the evolution of low- and intermediate-mass stars (LIM; $\sim 1\text{--}8 M_{\odot}$), the majority of stars in the Universe. On their way to the PN phase, LIM stars experience a strong mass loss during the preceding asymptotic giant branch (AGB; see e.g., Herwig 2005, for a review) phase and they chemically enrich the surrounding interstellar medium (ISM). The AGB stars are also major suppliers of dust grains and molecular species that are routinely seen in the local Universe (e.g., Ferrarotti & Gail 2006), which makes them (and their subsequent evolutionary stages) very important for our fundamental understanding of the enrichment and chemical composition of the ISM.

Fullerenes, among the most resistant and stable three-dimensional molecules that are only formed by C atoms, such as C₆₀ (first discovered in the laboratory by Kroto et al. 1985), were supposed to be widely spread in space for decades. The presence of fullerenes in astrophysical environments was under debate until the infrared (IR) signatures of the C₆₀ and C₇₀ fullerenes were unambiguously detected in the *Spitzer* mid-IR spectrum of the young PN Tc 1 (Cami et al. 2010). After the first detection of fullerenes in a PN, the presence of C₆₀ was found in several other astrophysical objects such as reflection nebulae (Sellgren et al. 2010), additional PNe (García-Hernández et al. 2010, 2011a, 2012; Otsuka et al. 2014), peculiar R Coronae Borealis (RCB) stars (García-Hernández et al. 2011b), post-AGB stars (Zhang & Kwok 2011; Gielen et al. 2011), and Herbig Ae/Be stars (Arun et al. 2023), among others, by its four strongest mid-IR emission

features at ~ 7.0 , 8.5, 17.4, and 18.9 μm . However, the formation route of fullerenes in such H-rich objects, similar to the majority of PNe, is not well understood. Nowadays, the most suitable routes for the formation of fullerenes are¹: i) the photochemical processing of hydrogenated amorphous carbon (HAC) grains or similar mixed aromatic or aliphatic hydrocarbons (i.e., same chemical composition but a different internal structure; hereafter HAC-like; García-Hernández et al. 2010) and ii) the photochemical processing of large polycyclic aromatic hydrocarbons (PAHs; Berné & Tielens 2012; Murga et al. 2022).

The C₆₀ fullerenes are mainly detected toward PNe, and fullerene PNe are very young low-excitation ($T_{\text{eff}} \sim 30\,000\text{--}45\,000\text{ K}$) C-rich objects, which evolved from low-mass ($\sim 1\text{--}3 M_{\odot}$) progenitors (García-Hernández et al. 2012; Otsuka et al. 2014). Remarkably, the IR *Spitzer* spectra ($\sim 5\text{--}38\mu\text{m}$) of the fullerene-rich PNe are dominated by aliphatic hydrocarbon-rich dust emission features (superimposed on the underlying and featureless dust continuum emission), showing several broad unidentified IR (UIR) plateau emission features at 6–9 (hereafter 7 μm), 9–13 (hereafter 12 μm), 15–20, and 25–35 μm (e.g., García-Hernández et al. 2012). Characteristic aliphatic discrete

¹ We note that, more recently, Bernal et al. (2019) proposed the shock heating and ion bombardment induced processing of SiC grains as an alternative route toward fullerenes in the ISM, but such a strong energetic process seems to be unlikely to happen in the circumstellar environments of fullerene PNe where the atomic nebular emission lines can be well explained by photoionization and shocks seem to be unimportant for fullerene formation (see e.g., García-Hernández et al. 2012).

Properties of the brightest young stellar clumps in extremely lensed galaxies at redshifts 4 to 5

Matteo Messa,^{1,2,3*} Miroslava Dessauges-Zavadsky,² Angela Adamo,¹ Johan Richard⁴
and Adélaïde Claeysens¹

¹The Oskar Klein Centre, Department of Astronomy, Stockholm University, AlbaNova, SE-10691 Stockholm, Sweden

²Observatoire de Genève, Université de Genève, Versoix, Switzerland

³Osservatorio di Astrofisica e Scienza dello Spazio di Bologna, INAF, Bologna, 40129, Italy.

⁴Univ Lyon, Univ Lyon1, ENS de Lyon, CNRS, Centre de Recherche Astrophysique de Lyon UMR5574, Saint-Genis-Laval, France

Accepted XXX. Received YYY; in original form ZZZ

ABSTRACT

We study the populations of stellar clumps in three high-redshift galaxies, at $z=4.92$, 4.88 and 4.03 , gravitationally lensed by the foreground galaxy clusters MS1358, RCS0224 and MACS0940, respectively. The lensed galaxies consist of multiple counter-images with large magnifications, mostly above $\mu > 5$ and in some cases reaching $\mu > 20$. We use rest-frame UV observations from the HST to extract and analyse their clump populations, counting 10, 3 and 11 unique sources, respectively. Most of the clumps have derived effective radii in the range $R_{\text{eff}} = 10 - 100$ pc, with the smallest one down to 6 pc, i.e. consistent with the sizes of individual stellar clusters. Their UV magnitudes correspond to SFR_{UV} mostly in the range $0.1 - 1 M_{\odot}\text{yr}^{-1}$; the most extreme ones, reaching $\text{SFR}_{\text{UV}} = 5 M_{\odot}\text{yr}^{-1}$ are among the UV-brightest compact ($R_{\text{eff}} < 100$ pc) star-forming regions observed at any redshift. Clump masses span a broad range, from 10^6 to $10^9 M_{\odot}$; stellar mass surface densities are comparable, and in many cases larger, than the ones of local stellar clusters, while being typically 10 times larger in size. By compiling published properties of clump populations at similar spatial resolution between redshift 0 and 5, we find a tentative evolution of Σ_{SFR} and $\Sigma_{M_{\star}}$ with redshift, especially when very compact clumps ($R_{\text{eff}} \leq 20$ pc) are considered. We suggest that these trends with redshift reflect the changes in the host galaxy environments where clumps form. Comparisons with the local universe clumps/star clusters shows that, although rare, conditions for elevated clump Σ_{SFR} and $\Sigma_{M_{\star}}$ can be found.

Key words: gravitational lensing; strong – galaxies: high-redshift – galaxies: star formation – galaxies: star clusters: general

1 INTRODUCTION

Since the first deep observations with the Hubble space telescope (HST), galaxy morphology was recognised to change from disk-like or elliptical into more irregular appearance at increasing redshifts (e.g. Abraham et al. 1996; Brinchmann et al. 1998). In addition, galaxies around the cosmic noon ($z \sim 1-3$) are characterised by the presence of bright stellar clumps dominating their rest-frame ultraviolet (UV) morphology (e.g. Cowie et al. 1995; van den Bergh et al. 1996). The James Webb Space Telescope (JWST) is bringing new insight into the properties of high- z galaxies, especially at the epoch of re-ionisation ($z \gtrsim 7$); the first results seem to confirm the overall morphological evolution traced by HST at lower redshifts, with galaxies at redshift 7-12 characterised by irregular (yet compact) structures and in a minor part ($\sim 20\%$) by interaction/mergers (Treu et al. 2023).

One of the current main efforts in the community is understanding the link between clump formation (and evolution) and galaxy growth. Initially observed as large structures, with sizes ~ 1 kpc and masses $\sim 10^8 - 10^9 M_{\odot}$ (e.g. Elmegreen et al. 2007; Förster Schreiber et al.

2011a,b; Guo et al. 2012; Soto et al. 2017), stellar clumps are being recently studied in gravitationally-lensed fields, where lensing allows to reach resolutions down to ~ 10 pc in size and $\sim 10^6 M_{\odot}$ in mass (e.g. Livermore et al. 2012a, 2015; Adamo et al. 2013; Johnson et al. 2017; Cava et al. 2018; Vanzella et al. 2017a,b, 2019, 2021, 2022b; Meštrić et al. 2022; Messa et al. 2022), and thus to investigate clump substructures avoiding overestimates driven by poor resolutions (e.g. Dessauges-Zavadsky et al. 2017; Meng & Gnedin 2020). The exquisite performance of JWST is also contributing to increase the resolution and depth at which clump samples are studied (e.g. Claeysens et al. 2023; Vanzella et al. 2022a,c), and recently proved the possibility of observing the progenitors of local globular clusters (Mowla et al. 2022; Claeysens et al. 2023).

Most of clumps at redshift $z < 3$ may have formed *in-situ* within their host galaxies. This scenario is supported by several observational evidence, such as: (1) the redshift evolution of clumpy galaxies, closely following evolution of the overall star formation rate (SFR) volume density and inconsistent with the evolutionary trends of minor and major mergers (Lotz et al. 2011; Shibuya et al. 2016); (2) the presence of numerous clumpy galaxies (at least up to $z \sim 3$) still dominated by disk-like appearance (Shibuya et al. 2016), with comparable disk scale-heights in case of either presence or absence

* E-mail: matteo.messa@inaf.it

Revisiting thermoelectric effects in the crust of neutron stars

Dionysios Gakis ^{*} and Konstantinos N. Gourgouliatos ^{**}

Department of Physics, University of Patras, Patras, Rio, 26504, Greece

Received ?? ?? 2024; accepted ?? ?? 2024

ABSTRACT

Context. Large thermal variations have been observed in neutron stars that typically are not aligned with density gradients. Such terms may activate the Biermann battery effect, leading to thermo-electric interactions and the generation of electromotive force.

Aims. We aim to identify the impact a temperature anisotropy on a neutron star's crust can have in the evolution of its magnetic field, through the thermo-electric terms.

Methods. We consider a neutron star crust with large temperature gradients, associated with long-lived hot spots, described by a Gaussian-type function localized. We simulate the interplay between the battery term and the Hall and Ohmic evolution numerically, for axisymmetric systems.

Results. The results indicate that for crust temperatures of $\sim 10^9$ K the toroidal field can be amplified up to $\sim 10^{14} - 10^{15}$ G near the points of maximum temperature gradients, and it locally changes the architecture of the poloidal field lines. For internal crustal temperatures around $\sim 10^8$ K, the temperature gradient generates fields of about two orders of magnitude lower. In such cases, saturation is achieved after some hundred thousand years, after which the battery and Ohmic dissipation balance each other.

Conclusions. We conclude that the thermoelectric effect can impact the overall magnetic field evolution, provided that the thermal gradient is maintained for a sufficiently long time. Neutron stars endowed with moderate strength magnetic fields may be affected by the thermoelectric effect if the hotspots survive for timescales of a few kiloyears.

Key words. neutron star – thermoelectric battery mechanism – magnetic field

1. Introduction

Neutron stars are known to sustain the strongest magnetic fields found in the universe, ranging from 10^8 G in the case of millisecond pulsars (e.g. [Possenti et al. 2003](#)) up to 10^{15} G for magnetars (e.g. [Nakagawa et al. 2009](#)). Still, the origin of these fields remains an open question. [Spruit \(2008\)](#) reviews specifically the following two scenarios. The field could be inherited by the progenitor main sequence star through flux conservation (e.g. [Makarenko et al. 2021](#)) or generated by dynamo processes before the supernova explosion. The bottom line is that they appear as plausible explanations only for pulsars but not for magnetars; other interesting theories are suggested for the latter.

Whatever the source is, we have indications that magnetic fields in neutron stars undergo evolution with time. The majority of neutron stars have strong magnetic fields on their surfaces ($\sim 10^{10} - 10^{13}$ G), while the ones with stronger magnetic fields, host high-energy phenomena, like flares and bursts, which are linked to changes of their magnetic field structure (e.g. [Mazets et al. 1999](#); [Turolla et al. 2015](#); [Kaspi & Beloborodov 2017](#); [Coti Zelati et al. 2018](#)). The observed field strengths spanning many orders of magnitude is yet another argument towards the supposed evolution of magnetization in neutron stars.

Broadly speaking, the structure of a typical neutron star may be divided in its crust and core, which in turn are further split into inner and outer parts. The outer crust is physically described by a degenerate relativistic electron gas flowing on a solid crystal Coulomb lattice of protons and ions, whereas matter consisting of neutron-rich nuclei, at densities between nuclear and the neu-

tron drip point, constitute the inner crust. Moving deeper, the outer core is a superconductive superfluid of protons and neutrons with only a few free electrons. Regarding the innermost part of a neutron star, the inner core, the extremely high dominating densities restrict us to only speculations about exotic forms of matter, such as free quarks or other unknown particles (e.g. [Baym et al. 2018](#)). The part of a neutron star between the crust and the magnetosphere (governed by plasma) is the atmosphere, containing the ocean (sometimes called envelope). Although it might be possible that the magnetic field permeates both crust and core of a neutron star, simulations typically consider solely the crustal magnetic field, and only a handful of recent studies include the core as well (e.g. [Ciolfi & Rezzolla 2013](#); [Moraga et al. 2023](#); [Skiathas & Gourgouliatos 2024](#)). In our paper, we will also assume that the magnetic flux in the core is frozen, and deal with its evolution in the crust.

The main processes governing the magnetic field evolution in neutron stars are typically three ([Goldreich & Reisenegger 1992](#)). The Hall drift is the transport of magnetic flux by a moving electron fluid rising electric currents and is conservative. The conversion of magnetic energy into heat because of the crust's finite conductivity is called Ohmic dissipation. Thirdly, the ambipolar diffusion, another dissipative process, is caused by the relative movement of magnetic field and charged particles to neutrons (e.g. [Shalybkov & Urpin 1995](#)). The latter effect is important only in the core and inner crust of neutron stars though, where neutrons are abundant, and hence is disregarded in the context of this study. The inner battle between Hall and Ohmic terms in neutron star crusts has been thoroughly analyzed in literature (e.g. [Hollerbach & Rüdiger 2002](#); [Cumming et al. 2004](#); [Pons & Geppert 2007](#); [Kojima & Kisaka 2012](#); [Gourgouliatos &](#)

* dgakis@upnet.gr

** kngourg@upatras.gr

Dark no more: The low luminosity stellar counterpart of a dark cloud in the Virgo cluster*

MICHAEL G. JONES ¹, STEVEN JANOWIECKI ², SWAPNANEEL DEY ¹, DAVID J. SAND ¹, PAUL BENNET ³,
DENIJA CRNOJEVIĆ ⁴, CATHERINE E. FIELDER ¹, ANANTHAN KARUNAKARAN ^{5,6}, BRIAN R. KENT ⁷,
NICOLAS MAZZIOTTI ¹, BURÇIN MUTLU-PAKDIL ⁸, AND KRISTINE SPEKKENS ^{9,10}

¹Steward Observatory, University of Arizona, 933 North Cherry Avenue, Rm. N204, Tucson, AZ 85721-0065, USA

²University of Texas, Hobby–Eberly Telescope, McDonald Observatory, TX 79734, USA

³Space Telescope Science Institute, 3700 San Martin Drive, Baltimore, MD 21218, USA

⁴Department of Physics & Astronomy, University of Tampa, 401 West Kennedy Boulevard, Tampa, FL 33606, USA

⁵Department of Astronomy & Astrophysics, University of Toronto, Toronto, ON M5S 3H4, Canada

⁶Dunlap Institute for Astronomy and Astrophysics, University of Toronto, Toronto ON, M5S 3H4, Canada

⁷National Radio Astronomy Observatory, 520 Edgemont Road, Charlottesville, VA 22903, USA

⁸Department of Physics and Astronomy, Dartmouth College, Hanover, NH 03755, USA

⁹Department of Physics and Space Science, Royal Military College of Canada P.O. Box 17000, Station Forces Kingston, ON K7K 7B4, Canada

¹⁰Department of Physics, Engineering Physics and Astronomy, Queen’s University, Kingston, ON K7L 3N6, Canada

ABSTRACT

We have discovered the stellar counterpart to the ALFALFA Virgo 7 cloud complex, which has been thought to be optically dark and nearly star-free since its discovery in 2007. This ~ 190 kpc long chain of enormous atomic gas clouds ($M_{\text{HI}} \sim 10^9 M_{\odot}$) is embedded in the hot intracluster medium of the Virgo galaxy cluster but is isolated from any galaxy. Its faint, blue stellar counterpart, BC6, was identified in a visual search of archival optical and UV imaging. Follow-up observations with the Green Bank Telescope, Hobby-Eberly Telescope, and Hubble Space Telescope demonstrate that this faint counterpart is at the same velocity as the atomic gas, is actively forming stars, and is metal-rich ($12 + (\text{O}/\text{H}) = 8.58 \pm 0.25$). We estimate its stellar mass to be only $\log(M_{*}/M_{\odot}) \sim 4.4$, making it one of the most gas-rich stellar systems known. Aside from its extraordinary gas content, the properties of BC6 are entirely consistent with those of a recently identified class of young, low-mass, isolated, and star-forming clouds in Virgo, that appear to have formed via extreme ram pressure stripping events. We expand the existing discussion of the origin of this structure and suggest NGC 4522 as a likely candidate, however, the current evidence is not fully consistent with any of our proposed progenitor galaxies. We anticipate that other “dark” gas clouds in Virgo may have similarly faint, star-forming counterparts. We aim to identify these through the help of an ongoing citizen science search of the entire cluster.

Keywords: Star formation regions (1565); Ram pressure stripped tails (2126); HI line emission (690); Galaxy interactions (600); Virgo Cluster (1772)

1. INTRODUCTION

Surveys of atomic gas (HI) have a long history of identifying apparently dark structures made up of large quantities of neutral gas and (almost) no stars (e.g. Giovanelli & Haynes 1989; Chengalur et al. 1995; Verdes-Montenegro et al. 2001; Davies et al. 2004; Minchin et al. 2005; Haynes et al. 2007; Kent et al. 2007; Taylor et al. 2012; Wong et al. 2021; Józsa et al. 2022; Jones et al. 2023). HI is prone to forming such structures as it is typically the most loosely bound baryonic component of a galaxy’s disk and is thus the most easily removed by

Corresponding author: Michael G. Jones
jonesmg@arizona.edu

* Based on observations obtained with the Hobby-Eberly Telescope (HET), which is a joint project of the University of Texas at Austin, the Pennsylvania State University, Ludwig-Maximilians-Universitaet Muenchen, and Georg-August Universitaet Goettingen. The HET is named in honor of its principal benefactors, William P. Hobby and Robert E. Eberly.

Radial halo substructure in harmony with the Galactic bar

Adam M. Dillamore,^{1*} Vasily Belokurov,¹ and N. Wyn Evans¹

¹*Institute of Astronomy, University of Cambridge, Madingley Road, Cambridge CB3 0HA, UK*

Accepted XXX. Received YYY; in original form ZZZ

ABSTRACT

Overdensities in the radial phase space (r, v_r) of the Milky Way’s halo have previously been associated with the phase-mixed debris of a highly radial merger event, such as *Gaia* Sausage-Enceladus. We present and test an alternative theory in which the overdense ‘chevrons’ are instead composed of stars trapped in resonances with the Galactic bar. We develop an analytic model of resonant orbits in the isochrone potential, and complement this with a test particle simulation of a stellar halo in a realistic barred Milky Way potential. These models are used to predict the appearance of action space (J_ϕ, J_r) and radial phase space in the Solar neighbourhood. They are able to reproduce almost all salient features of the observed chevrons. In particular, both the analytic model and simulation predict that the chevrons are more prominent at $v_r < 0$ when viewed near the Sun, as is observed by *Gaia*. This is inconsistent with formation by an ancient merger event. We also associate individual chevrons with specific resonances. At a bar pattern speed of $\Omega_b = 35 \text{ km s}^{-1} \text{ kpc}^{-1}$, the two most prominent prograde chevrons align very closely with the corotation and outer Lindblad resonances. The former can be viewed as a highly eccentric extension of the Hercules stream. Finally, our model predicts that the v_r asymmetry changes sign as a function of Galactic radius and azimuth, and we find evidence that this is indeed the case in the Milky Way.

Key words: Galaxy: kinematics and dynamics – Galaxy: halo – Galaxy: structure

1 INTRODUCTION

In the days of the old quantum theory, Max Born developed perturbation theory to cope with the effects of resonances. This is summarized in his 1926 book *‘The Mechanics of the Atom’*. When there are commensurable frequencies in a dynamical problem, Born showed how to perform a canonical transformation to a new set of action-angle coordinates – the so-called fast and slow action-angles. The basic idea is then to average over the rapid variations in the fast coordinates, keeping the slow variables fixed. Hamilton’s equations then show that the fast action is constant or adiabatically invariant. This powerful technique was introduced into galactic dynamics by Lynden-Bell (1973) and exploited in the struggle to understand the origin of spiral structure and bar formation (e.g., Lynden-Bell 1979; Contopoulos 1979; Earn & Lynden-Bell 1996; Collett et al. 1997). It has also been widely used to model the capture of planets and planetesimals in solar system dynamics (e.g., Yoder 1979; Henrard 1982; Borderies & Goldreich 1984).

The influence of the Galactic bar on stars in the stellar disc has been long realised as substantial. Kalnajs (1991) made the pioneering suggestion that, if the Sun were located near a resonance, then there may be two stellar streams, one moving inward and the other outward. Resonant capture is an important mechanism for generating substructure in the stellar disc (e.g., Debattista & Sellwood 2000; Sellwood 2010; Gerhard 2011; McMillan 2013; Binney 2020; Chiba et al. 2021; Chiba & Schönrich 2021). With the advent of *Gaia* data, the ridges and features in the phase space distribution of disc stars

have been subjected to scrutiny and often attributed to bar or spiral arm resonances (e.g., Fragkoudi et al. 2019; Khoperskov et al. 2020; Trick et al. 2021; Trick 2022; Khoperskov & Gerhard 2022; Wheeler et al. 2022).

By contrast, the effect of bar resonances in the halo has not received as much attention. Debattista & Sellwood (1998, 2000) demonstrated that dynamical friction from dark matter haloes acts to spin down bars. The phenomenon of dynamical friction is driven by the trapping of dark matter particles by the bar. This showed that resonances due to bars affect the dynamics of stars and dark matter in the halo, though the emphasis of the work was on implications for bar evolution and dark matter density. This has been further explored by Athanassoula (2002); Weinberg & Katz (2002); Ceverino & Klypin (2007); Collier et al. (2019); Chiba & Schönrich (2022); and Hamilton et al. (2023). The possibility of bar resonances creating substructures in the stellar halo was first suggested by Moreno et al. (2015, 2021). They showed that the trapping can extend several kpc above or below the Galactic plane and suggested that it may be the origin of some known moving groups. The first demonstration that this effect is present in the data on stellar halo stars was provided in Myeong et al. (2018) who noted the presence of a possible resonance in halo stars at all metallicities.

The *Gaia* Data Release 3 (DR3; Gaia Collaboration et al. 2023) provided a large sample of halo stars with full phase space coordinates around the Sun. Belokurov et al. (2023) exploited this to identify prominent chevrons in the space of radial position and velocity (r, v_r). These are the tell-tale signatures of shells, which are known to form in nearly radial mergers (e.g., Fillmore & Goldreich 1984; Quinn 1984; Amorisco 2017; Dong-Páez et al. 2022; Davies et al. 2023b). A natural conclusion was that the chevrons were caused

* E-mail: amd206@cam.ac.uk (AMD)

A perspective on the Milky Way Bulge-Bar as seen from the neutron-capture elements Cerium and Neodymium with APOGEE

J. V. SALES-SILVA,¹ K. CUNHA,^{2,1} V. V. SMITH,³ S. DAFLON,¹ D. SOUTO,⁴ R. GUERÇO,¹ A. QUEIROZ,⁵ C. CHIAPPINI,⁶ C. R. HAYES,⁷ T. MASSERON,^{8,9} STEN HASSELQUIST,¹⁰ D. HORTA,¹¹ N. PRANTZOS,¹² M. ZOCCALI,^{13,14} C. ALLENDE PRIETO,^{8,9} B. BARBUY,¹⁵ R. BEATON,¹⁰ D. BIZYAEV,^{16,17} J. G. FERNÁNDEZ-TRINCADO,¹⁸ P. M. FRINCHABOY,¹⁹ J. A. HOLTZMAN,²⁰ J. A. JOHNSON,²¹ HENRIK JÖNSSON,²² S. R. MAJEWSKI,²³ D. MINNITI,^{24,25,26} D. L. NIDEVER,²⁷ R. P. SCHIAVON,²⁸ M. SCHULTHEIS,²⁹ J. SOBECK,³⁰ G. S. STRINGFELLOW,³¹ AND G. ZASOWSKI³²

¹Observatório Nacional/MCTI, R. Gen. José Cristino, 77, 20921-400, Rio de Janeiro, Brazil

²Steward Observatory, University of Arizona, 933 North Cherry Avenue, Tucson, AZ 85721-0065, USA

³NOIRLab, Tucson AZ 85719

⁴Departamento de Física, Universidade Federal de Sergipe, Av. Marechal Rondon, S/N, 49000-000 São Cristóvão, SE, Brazil

⁵Instituto de Astrofísica de Canarias, E-38200 La Laguna, Tenerife, Spain

⁶Leibniz-Institut für Astrophysik Potsdam (AIP), An der Sternwarte 16, 14482 Potsdam, Germany

⁷NRC Herzberg Astronomy and Astrophysics Research Centre, 5071 West Saanich Road, Victoria, B.C., Canada, V9E 2E7

⁸Instituto de Astrofísica de Canarias (IAC), E-38205 La Laguna, Tenerife, Spain

⁹Universidad de La Laguna (ULL), Departamento de Astrofísica, 38206 La Laguna, Tenerife, Spain

¹⁰Space Telescope Science Institute, Baltimore, MD, USA

¹¹Center for Computational Astrophysics, Flatiron Institute, 162 Fifth Avenue, New York, NY 10010, USA

¹²Institute d'Astrophysique de Paris, UMR 7095 CNRS & Sorbonne Université, 98 bis Blvd Arago, Paris 75014 France

¹³Instituto de Astrofísica, Pontificia Universidad Católica de Chile, Vicuña Mackenna 4860, Macul, Casilla 306, Santiago 22, Chile

¹⁴Millennium Institute of Astrophysics (MAS), Nuncio Monseñor Sótero Sanz 100, Providencia, Santiago Chile

¹⁵Universidade de São Paulo, IAG, Rua do Matão 1226, Cidade Universitária, São Paulo 05508-090, Brazil

¹⁶Apache Point Observatory and New Mexico State University, P.O. Box 59, Sunspot, NM 88349-0059, USA

¹⁷Sternberg Astronomical Institute, Moscow State University, Moscow, Russia

¹⁸Instituto de Astronomía, Universidad Católica del Norte, Av. Angamos 0610, Antofagasta, Chile

¹⁹Department of Physics & Astronomy, Texas Christian University, TCU Box 298840, Fort Worth, TX 76129, USA

²⁰New Mexico State University, Las Cruces, NM 88003, USA

²¹The Department of Astronomy and Center of Cosmology and Astro Particle Physics, The Ohio State University, Columbus, OH 43210, USA

²²Materials Science and Applied Mathematics, Malmö University, SE-205 06 Malmö, Sweden

²³Department of Astronomy, University of Virginia, Charlottesville, VA 22904-4325, USA

²⁴Departamento de Física, Universidade Federal de Santa Catarina, Trindade 88040-900, Florianópolis, Brazil

²⁵Instituto de Astrofísica, Facultad de Ciencias Exactas, Universidad Andres Bello, Avenida Fernández Concha 700, Santiago, Chile

²⁶Vatican Observatory, I-V00120 Vatican City State, Italy

²⁷Department of Physics, Montana State University, P.O. Box 173840, Bozeman, MT 59717-3840

²⁸Astrophysics Research Institute, Liverpool John Moores University, Liverpool, L3 5RF, UK

²⁹Université Côte d'Azur, Observatoire de la Côte d'Azur, CNRS, Laboratoire Lagrange, Bd de l'Observatoire, CS 34229, 06304 Nice Cedex 4, France

³⁰Department of Astronomy, University of Washington, Box 351580, Seattle, WA 98195, USA

³¹Center for Astrophysics and Space Astronomy, University of Colorado at Boulder, 389 UCB, Boulder, CO 80309-0389, USA

³²Department of Physics and Astronomy, University of Utah, Salt Lake City, UT 84105, USA

(Received; Revised; Accepted 2024 February 11)

Submitted to ApJ

ABSTRACT

This study probes the chemical abundances of the neutron-capture elements cerium and neodymium in the inner Milky Way from an analysis of a sample of ~ 2000 stars in the Galactic Bulge/bar spatially

Novelty Detection on Radio Astronomy Data using Signatures

Paola Arrubarrena*, Maud Lemerrier*, Bojan Nikolic, Terry Lyons, and Thomas Cass

Abstract—We introduce SigNova, a new semi-supervised framework for detecting anomalies in streamed data. While our initial examples focus on detecting radio-frequency interference (RFI) in digitized signals within the field of radio astronomy, it is important to note that SigNova’s applicability extends to any type of streamed data. The framework comprises three primary components. Firstly, we use the signature transform to extract a canonical collection of summary statistics from observational sequences. This allows us to represent variable-length visibility samples as finite-dimensional feature vectors. Secondly, each feature vector is assigned a novelty score, calculated as the Mahalanobis distance to its nearest neighbor in an RFI-free training set. By thresholding these scores we identify observation ranges that deviate from the expected behavior of RFI-free visibility samples without relying on stringent distributional assumptions. Thirdly, we integrate this anomaly detector with Pysegments, a segmentation algorithm, to localize consecutive observations contaminated with RFI, if any. This approach provides a compelling alternative to classical windowing techniques commonly used for RFI detection. Importantly, the complexity of our algorithm depends on the RFI pattern rather than on the size of the observation window. We demonstrate how SigNova improves the detection of various types of RFI (e.g., broadband and narrowband) in time-frequency visibility data. We validate our framework on the Murchison Widefield Array (MWA) telescope and simulated data and the Hydrogen Epoch of Reionization Array (HERA).

Index Terms—Novelty detection, anomaly detection, semi-supervised learning, radio frequency interference.

1 INTRODUCTION

RADIO astronomy provides a unique perspective on the universe by observing the celestial radiation at radio frequencies (50 MHz up to 950 GHz). Lower parts of the radio spectrum (50 MHz to about 5 GHz) are of particular current scientific interest and with the Square Kilometer Array (SKA) [1] there is substantial international investment in making it possible to make very sensitive, large-field observations at these frequencies. Amongst the goals are investigation of the very earliest galaxies through the impact they have on the primordial intergalactic neutral hydrogen by observing the red-shifted hyperfine transition

of hydrogen ($\lambda_{\text{rest}} = 21 \text{ cm}$).

One of the major challenges for observations at these lower frequencies is radio-frequency interference (RFI), which refers to any unwanted electromagnetic signal that contaminates the radio observations. RFI can seriously degrade the quality of radio observations and can even render them unusable. In this paper we present a technique to identify sections of data from interferometric telescopes that is contaminated by RFI. Since radio observations combine information from a range of frequencies, times and antennas, if only sections of data are contaminated by RFI they can be excluded from further combination allowing high fidelity and sensitivity final measurements or images.

Radio interferometers work by measuring the correlated signal in the electric field received by pairs of separated antennas, $\gamma_{i,j} = \langle E_i(t)E_j^*(t) \rangle$, which because of similarity to optical interferometry is called the *visibility*. If there are N_A antennas the telescope’s digital correlator will calculate correlations between each pair of antennas (including each antenna with itself), giving $N_B := N_A(N_A + 1)/2$ measurements of visibilities. Each visibility between antenna pair (i, j) is a complex-valued signal indexed on a time-frequency domain $I \times \Omega$,

$$\gamma_{i,j} : I \times \Omega \rightarrow \mathbb{C}, (t, \nu) \mapsto \gamma_{i,j}(t, \nu).$$

The digital correlator performs this correlation at regular time intervals. At each time the interferometer outputs a sample of the visibility in the frequency domain. Much research has gone into the design of automated RFI detection techniques to flag corrupted visibility samples $\gamma_{i,j}(t_m, \nu_n)$.

- Paola Arrubarrena* is with the Department of Mathematics at Imperial College London, London SW7 2AZ, UK, and also with The Alan Turing Institute, London NW1 2DB, UK. E-mail: p.arrubarrena@imperial.ac.uk.
- Maud Lemerrier* is with the Mathematical Institute at University of Oxford, Oxford OX2 6GG, UK, and also with The Alan Turing Institute, London NW1 2DB, UK. E-mail: maud.lemerrier@maths.ox.ac.uk.
- Bojan Nikolic is with The Cavendish Laboratory of the Department of Physics at University of Cambridge, Cambridge CB3 0HE, UK. E-mail: bn204@cam.ac.uk.
- Terry Lyons is with the Mathematical Institute at University of Oxford, Oxford OX2 6GG, UK, and also with The Alan Turing Institute, London NW1 2DB, UK. E-mail: terry.lyons@maths.ox.ac.uk.
- Thomas Cass is with the Department of Mathematics at Imperial College London, London SW7 2AZ, UK, also with The Alan Turing Institute, London NW1 2DB, UK, and with the Institute for Advance Study, New Jersey 08540, USA. E-mail: thomas.cass@imperial.ac.uk.

This work was supported in part by EPSRC (NSFC) under Grant EP/S026347/1, in part by The Alan Turing Institute under the EPSRC grant EP/N510129/1, the Data Centric Engineering Programme (under the Lloyd’s Register Foundation grant G0095), the Defence and Security Programme (funded by the UK Government) and the Office for National Statistics & The Alan Turing Institute (strategic partnership) and in part by the Hong Kong Innovation and Technology Commission (InnoHK Project CIMDA), in part by the Programme Grant, and in part by the Erin Ellentuck Fellowship at the Institute for Advanced Study.

*Equal contribution and corresponding author.



Policy Brief

REGIONAL AND GLOBAL COLLABORATIONS IN ASTRONOMY

Discussed and drafted during S20 Policy Webinar on Astroinformatics for Sustainable Development held on 6-7 July 2023

Contributors: Kazuhiro Sekiguchi, Jess McIver, Annapurni Subramaniam, Eswar Reddy, R Srianand, Reinaldo Rosa, Stefano Andreon, Tarun Souradeep, Bernard Fanaroff, Rafael Santos, Paula Coelho, Pranav Sharma, Ashish Mahabal

INDIAN NATIONAL SCIENCE ACADEMY – CENTRE FOR SCIENCE POLICY AND RESEARCH

Introduction

Astronomy brings together advanced scientific research, state-of-the-art technology, and educational initiatives, all while captivating and stimulating people of all ages. By doing so, it possesses the potential to serve as a powerful catalyst for sustainable global development and the resolution of global societal issues. It attracts a diverse range of scientists and experts from various fields, fostering collaboration and innovation.

By leveraging their resources, influence, and diplomatic initiatives, S20 academies can foster an enabling environment for international collaborations in astronomy, facilitate knowledge exchange, and drive scientific advancements that benefit humanity. This policy brief explores the opportunities and challenges presented by regional and global collaborations in astronomy.

Opportunities

Regional and global collaborations in astronomy offer a wide range of opportunities to advance scientific knowledge, foster international cooperation, and contribute to the betterment of society through scientific discoveries, technological advancements, and public engagement. Some of these opportunities include:

1. Sharing knowledge and expertise

Data Sharing and Knowledge Exchange: Collaboration in astronomy fosters knowledge sharing and education, particularly in STEM fields. It enables the exchange of expertise, best practices, and research findings, allowing scientists and educators to learn from one another. This knowledge dissemination and transfer contribute to developing skilled scientists and researchers worldwide. Additionally, astronomy's inherent interdisciplinary nature encourages cross-disciplinary collaboration, which can lead to innovative solutions for sustainable development challenges.

Access to Diverse Expertise: Collaborations bring together scientists from different regions, institutions, and backgrounds, creating opportunities for interdisciplinary research and access to diverse expertise. This enhances the quality of research and fosters innovative approaches to solving complex astronomical problems.

2. Resources and Infrastructure Sharing

Shared Access to Facilities: Collaborations facilitate shared access to astronomical facilities and resources. Researchers from participating regions can access telescopes, observatories, and data archives they might not have in their home countries, broadening their observational capabilities and enabling new scientific investigations.

Large-scale projects and cost-sharing: Regional and global collaborations enable large-scale projects that require significant resources and infrastructure. Examples include building and operating large telescopes, observatories, and space missions. These projects can lead to groundbreaking discoveries and advancements in our understanding of the universe.

3. Training and Capacity Building

Collaborations provide training and capacity-building opportunities, especially for scientists and students from regions with limited resources. Participating researchers can gain knowledge, skills, and exposure to advanced research techniques through



Policy Brief

LARGE PROJECTS IN ASTRONOMY: AN INDIAN ENDEAVOUR

Discussed and drafted during S20 Policy Webinar on Astroinformatics for Sustainable Development held on 6-7 July 2023

Contributors: Yogesh Wadadekar, Shriharsh Tendulkar, Sanjit Mitra, Eswar Reddy, A N Ramaprakash, Timo Prusti, Juna Kollmeier, Pranav Sharma, Ashish Mahabal

INDIAN NATIONAL SCIENCE ACADEMY – CENTRE FOR SCIENCE POLICY AND RESEARCH

Introduction

Cutting-edge astronomy initiatives often entail substantial investment and require a high level of expertise. Even the most technologically advanced nations recognize the value of establishing international partnerships to secure both financial resources and talent for these ambitious endeavours. Key examples of such collaborations include groundbreaking projects like the Ground-based Next-Generation Optical and Infrared Telescopes (GMT, TMT, and E-ELT), the Square Kilometre Array (SKA) for radio astronomy, and the Laser Interferometer Gravitational-Wave Observatory (LIGO) for gravitational astronomy. These ventures hold immense promise for catalysing transformative scientific discoveries, driving technological innovation, provide training opportunities for the next generation of scientists and engineers, and expanding our understanding of the cosmos that surrounds us.

Crucially, large-scale multilateral collaborations serve as powerful agents for promoting unity and peace among the global population. Participants from various nations share a vested interest in the success of these projects and the wealth of knowledge they yield, fostering a sense of common purpose and shared goals.

By utilizing astroinformatics capabilities, these initiatives are not merely enhancing our comprehension of the universe but are also actively contributing to the attainment of sustainable development objectives. They are accomplishing this by fostering international cooperation, education, and technological progress. In this discussion, we delve into the challenges faced, accomplishments achieved, and prospective avenues for substantial astronomical undertakings. Additionally, we present recommendations aimed at guaranteeing their effectiveness and optimizing their influence on both scientific advancement and society.

LIGO and LIGO-India

LIGO-India is an Astronomy mega-science project on Indian soil. The project recently received approval from the Union Cabinet of India and aims to start observing by 2030. LIGO-India aims to operate at the same sensitivity as the two LIGO detectors in the US at the time of operation. It will significantly boost precise localisation of astrophysical events on the sky, which will, in turn, vastly improve the chances of following up those events using electromagnetic telescopes and the Astrophysics that we learn from those observations.

The observatory will be built by the Department of Atomic Energy (DAE) and the Department of Science and Technology (DST), Government of India, with a Memorandum of Understanding (MoU) with the National Science Foundation (NSF), USA, along with several national and international research and academic institutions. The project is being led by four institutions, Directorate of Construction Services and Estate Management (DCSEM), Institute of Plasma Research (IPR), Inter-University Centre for Astronomy and Astrophysics (IUCAA), and Raja Ramanna Centre for Advanced Technology (RRCAT). Being multidisciplinary in nature, a mega-science project like LIGO-India fosters collaborations across various expertise and creates a common platform for exchanging knowledge and expertise. Such platforms can immensely help in building foundations for sustainable development. The scientific requirement for LIGO-India demanded a site which is remote. This provides the opportunity to bring a major boost in education and awareness, especially the excitement for science, in the neighbouring areas, especially to the underprivileged population.